STRUCTURAL PROPERTIES OF GLASSES: AN INTRODUCTION

Dr. Giorgio F. SIGNORINI, PhD
Dipartimento di Chimica, Università di Firenze
via della Lastruccia, 3
I-50019 Sesto F. (Firenze), Italy
giorgio.signorini@unifi.it

Contents

Chapter 1

Introduction

1.1 A glass has a structure -but not only

When dealing with glasses from a physico-chemical perspective, we first need to clarify what scientists mean with the term “glass”.

In a broad sense, a glass is often defined as a “solid with no long-range order”, sometimes with some additional requirement. See for example Varshneya (1994):

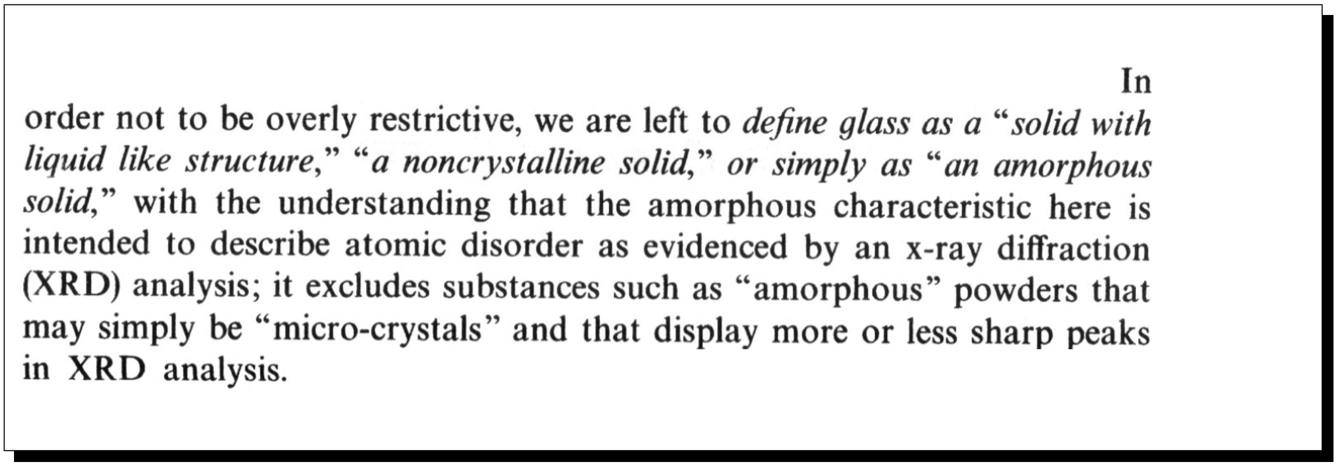

In order not to be overly restrictive, we are left to *define glass as a* “*solid with liquid like structure,*” “*a noncrystalline solid,*” *or simply as* “*an amorphous solid,*” with the understanding that the amorphous characteristic here is intended to describe atomic disorder as evidenced by an x-ray diffraction (XRD) analysis; it excludes substances such as “amorphous” powders that may simply be “micro-crystals” and that display more or less sharp peaks in XRD analysis.

This view comes from the observation that the glassy state closely resembles the liquid in terms of their generic response to diffraction (see figure 1.1):

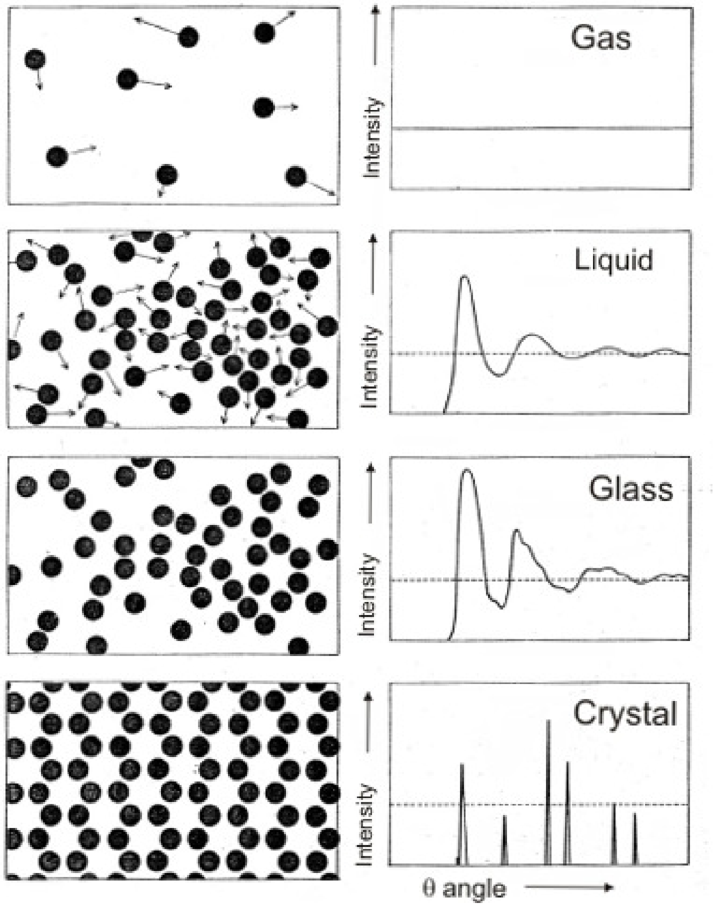

Figure 1.1: schematic of structure and diffraction from a monoatomic substance in different states

It should be noted, however, that the definition we just introduced also encompasses systems that have no direct relation to the liquid state, a point that, instead, many physicist consider central. In their view, a glass has a "liquid-like" structure because it *originates* from a liquid: it is a supercooled liquid that is no longer capable of rearranging in the laboratory time scale. In fact, a more generally accepted definition is that of Shelby Shelby (2005):

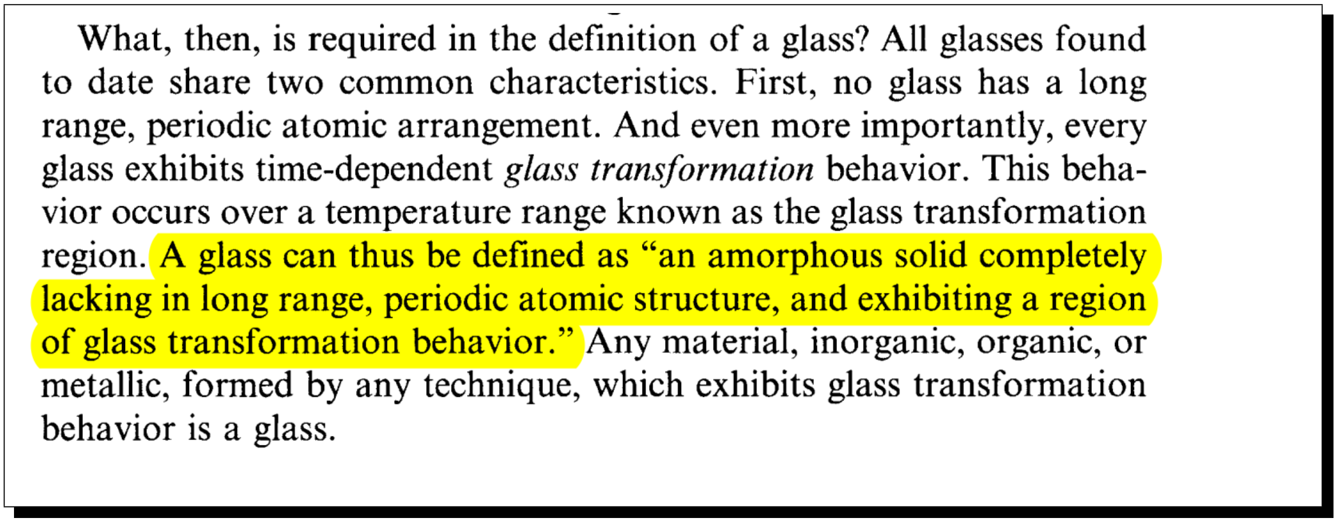

> What, then, is required in the definition of a glass? All glasses found to date share two common characteristics. First, no glass has a long range, periodic atomic arrangement. And even more importantly, every glass exhibits time-dependent *glass transformation* behavior. This behavior occurs over a temperature range known as the glass transformation region. A glass can thus be defined as "an amorphous solid completely lacking in long range, periodic atomic structure, and exhibiting a region of glass transformation behavior." Any material, inorganic, organic, or metallic, formed by any technique, which exhibits glass transformation behavior is a glass.

The dynamical (as opposed to structural) properties of a glass manifest themselves in time-dependent phenomena. In the transition from liquid to glass, the substance's structure loses its ability to relax or *de-correlate* (figure 1.2); the diffusion of the particles comes to an arrest (figure 1.3); and the viscosity approaches infinity (figure 1.4).

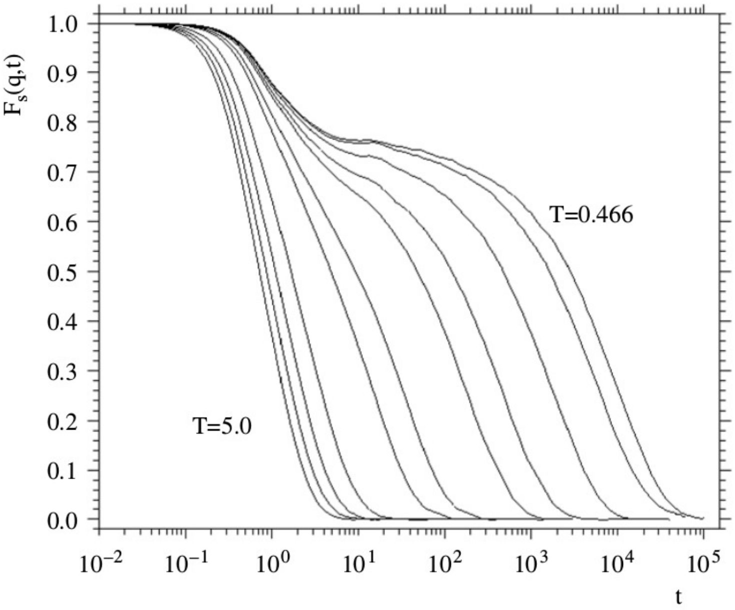

Figure 1.2: *Time self-correlation function of particles in a model system (the Lennard-Jones liquid), at different temperatures around the liquid-glass transition. At low T, decorrelation times are of the order of days.*

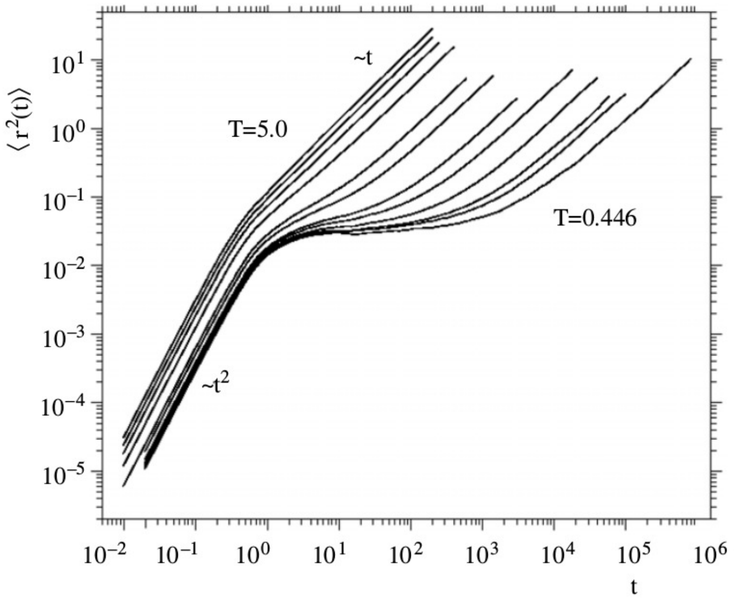

Figure 1.3: *mean squared displacements of particles in the Lennard-Jones liquid, at different temperatures around the liquid-glass transition.*

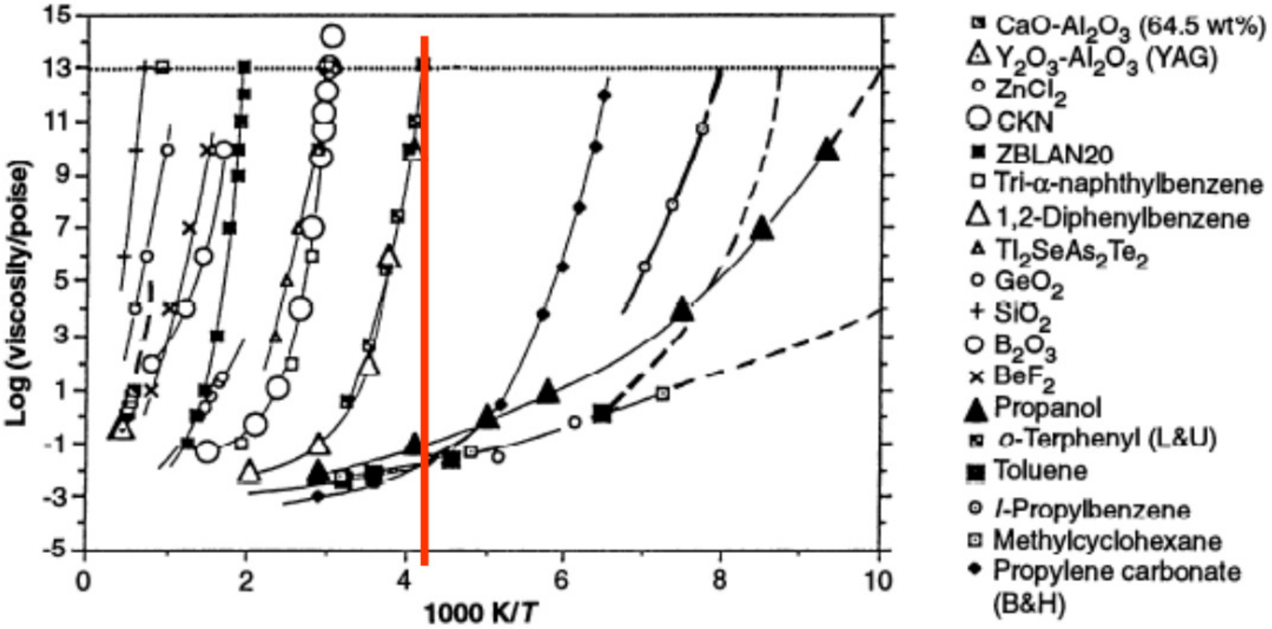

Figure 1.4: viscosity (η) of various substances near the liquid-glass transition. By convention, the transition temperature is where $\eta = 10^{13} Poise$

We will not be treating the dynamical properties of glasses here; however, it should be kept in mind that they are an essential feature of the glassy state.

Lastly, note that structure and dynamics are not completely independent in a system. This can be readily understood by considering that in order for an atom to move to a different environment, that is to diffuse, there are structural requirements that have to be realized, at least instantaneously (see figure 1.5).

More specifically, the ability to diffuse is determined by collective moves and by their time scale as compared to single particle velocities; see Royall and Williams (2015).

1.2 Description of glass structure

Limiting ourselves to the structure, the central point is how it can be described; that is, which structural parameters or functions are best suited to describe the glassy state.

The structure of systems with long range order, such as crystals, can be defined exactly by few physical quantities: three vectors to define the unit cell, and a limited number of atom positions within the cell. On the contrary, there cannot be any *exact* description of atom positions in a glass; only a *statistical* description is possible, perhaps through some order parameters.

1.2.1 *order* in a *disordered* structure?

One could wonder if it even makes any sense to look for some *order* in a *disordered* system.

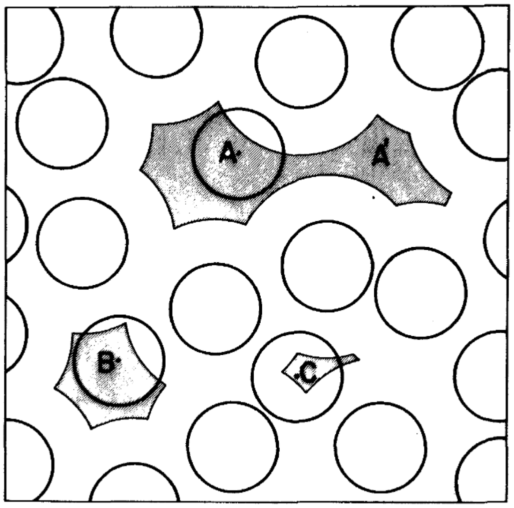

Figure 1.5: The *free volume* available for movement allows atom A, but not atoms B and C, to diffuse

However, as in the liquid state, glasses do not exhibit a *completely* disordered structure, that is the condition where atom positions are totally random, as in a perfect gas. Indeed, in liquids and glasses there are some preferred atom arrangements, due to the particles impenetrability, on one side, and to their tendency to be in close or near-close contact, on the other. Thus, moving from a certain atom in the origin, there is a zero probability of finding a second atom at distances less than the contact distance (the sum of the atom radii, 2σ), while there is a higher probability of finding it at 2σ than at a longer distance.

In systems where directional bonds impose additional structural constraints, there may be an increased probability of finding a third atom at a distance dictated by bond length and angle. Correlation with atoms further apart are expected to vanish rapidly.

In summary, while they have **no long range order**, glasses exhibit **partial short-range order**.

1.2.2 the pair distribution function, $g\left(r\right)$

The most useful parameter, and by far the most used one, containing structural information of a glass is the **pair distribution function** $g\left(r\right)$[1].

The pair distribution function (in short PDF) measures the relative probability of finding an atom at distance r from an other atom, scaled by the same probability if atom positions were totally random, or uncorrelated:

---

[1] many authors give $g\left(r\right)$ the name *radial distribution function*; we will use this term for a different function, closely related to $g\left(r\right)$ -see below

$$g\left(\mathbf{r}\right) \;=\; \frac{\left\langle n\left(\mathbf{r}\right)\right\rangle}{\left\langle n\left(\mathbf{r}\right)\right\rangle_{unc}}$$

where

$\left\langle n\left(\mathbf{r}\right)\right\rangle d\mathbf{r} =$ (conditioned) probability of finding an atom in a small volume $d\mathbf{r}$ around position $\mathbf{r}$ with respect to a given atom (A)

$\left\langle n\left(\mathbf{r}\right)\right\rangle_{unc} d\mathbf{r} =$ the same, in an uncorrelated system (such as an ideal gas), and

$\langle\rangle =$ represents a thermodynamic average

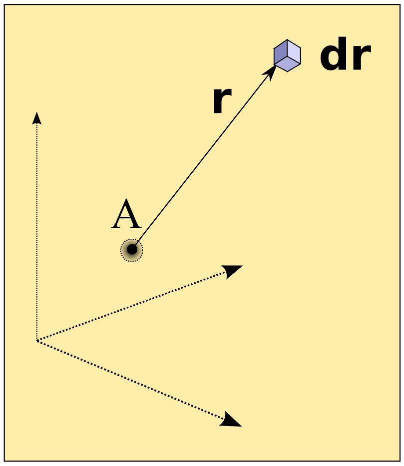

Thus, $g\left(\mathbf{r}\right)$ tells us how much, on average, the presence of one atom influences the presence of another atom at a certain distance, with $g\left(\mathbf{r}\right) = 1$ for no influence.

Also note that $\left\langle n\left(\mathbf{r}\right)\right\rangle$ is a *probability density*: it has dimensions of $\frac{\text{number of particles}}{\text{volume}}$. If integrated over some spatial domain D, it gives the number of atoms in that domain:

$$\int_D \left\langle n\left(\mathbf{r}\right)\right\rangle d\mathbf{r} = N_D \tag{1.1}$$

The integral over the total volume V of the systems equals the total number N of particles[2]:

$$\int_V \left\langle n\left(\mathbf{r}\right)\right\rangle d\mathbf{r} = N$$

We now consider two important simplifications on $g\left(\mathbf{r}\right)$.

In principle, in a disordered system, the arrangement of atoms around one origin atom -which is the property represented by $g\left(\mathbf{r}\right)$- may be different when measured in different points of the system; think, for example, of a material that has a density gradient along some direction. This is not the case in a glass, which is ***homogeneous***: that is, its properties are (on average) the same in every point. In such a system, $g\left(\mathbf{r}\right)$ does not depend on the position of the origin atom, but only on the vector distance $\mathbf{r}$ from it.

In a homogeneous system the uncorrelated probability density $\left\langle n\left(\mathbf{r}\right)\right\rangle_{unc}$ is constant, and equals the number density ρ_0:

$$g\left(\mathbf{r}\right) = \frac{\left\langle n\left(\mathbf{r}\right)\right\rangle}{\rho_0}$$

with

$$\begin{aligned} \rho_0 &= \frac{N}{V} \\ N &= \text{total number of atoms} \\ V &= \text{total volume} \end{aligned}$$

Second, we note that, unlike crystals, glasses are also ***isotropic***: their physical properties do not change with sample orientation. As a consequence, $g\left(\mathbf{r}\right)$ does not depend on the direction of $\mathbf{r}$, but only on its absolute value.

---

[2] more precisely, it yields $N-1$, since one particle lies in the origin; but in macroscopic samples, where $N \gg 1$, this distinction is irrelevant

In conclusion, the pair distribution function of glasses is a function of a scalar value:

$$\boxed{g\left(\mathbf{r}\right) \quad \rightarrow \quad g\left(r\right)}$$

and

$$\boxed{g\left(r\right) \quad = \quad \frac{\langle n(r)\rangle}{\rho_0}} \tag{1.2}$$

1.2.3 properties of $g\left(r\right)$ and the radial distribution function

In agreement with its definition, the pair distribution function of a glass features a first peak at the first neighbours shell, then a few rapidly fading peaks at higher values, before getting to its limiting value (see figure 1.6).

As the interparticle distance r increases, correlations vanish, and accordingly

$$\lim_{r\rightarrow\infty} g(r) = 1$$

The space differential in equation (1.1) is best expressed in polar coordinates $\{r, \theta, \phi\}$

$$d\mathbf{r} = r^{\mathbf{2}} \sin\theta dr d\theta d\phi$$

-which is the volume of an element of spherical shell- and the expression 1.1 for the number of atoms in domain D in this reference

$$N_D = \int_D \langle n\left(r\right)\rangle\, r^{\mathbf{2}} \sin\theta dr d\theta d\phi$$

can be integrated over all θ and ϕ values, as $\langle n\left(r\right)\rangle$ is independent from angular coordinates, giving

$$\begin{aligned} N_D &= \int_D 4\pi r^{\mathbf{2}} \langle n\left(r\right)\rangle\, dr \\ &= \int_D 4\pi r^{\mathbf{2}} \rho_0 g\left(r\right) dr \end{aligned}$$

As the last equation suggests, the function $4\pi r^{\mathbf{2}}\rho_0 g\left(r\right)$, which is called by many authors the *radial distribution function* or RDF, is of some interest in itself: its differential

$$\rho_0 4\pi r^2 g\left(r\right) dr$$

represents the number of atoms contained in a spherical shell of thickness dr (figure 1.8), while the integral

$$\int_0^R \rho_0 4\pi r^2 g\left(r\right) dr \tag{1.3}$$

is the number of atoms in a sphere of radius R; for example, the average number of nearest neighbours, or **coordination number**, of an atom can be estimated from the area under the first peak of the RDF (see figure 1.7).

Note also that the limit of the RDF for no correlation, at longer distances, is not a constant value as in $g\left(r\right)$ but the parabola $4\pi r^{\mathbf{2}}\rho_0$ (compare figure 1.9 to figure 1.1).

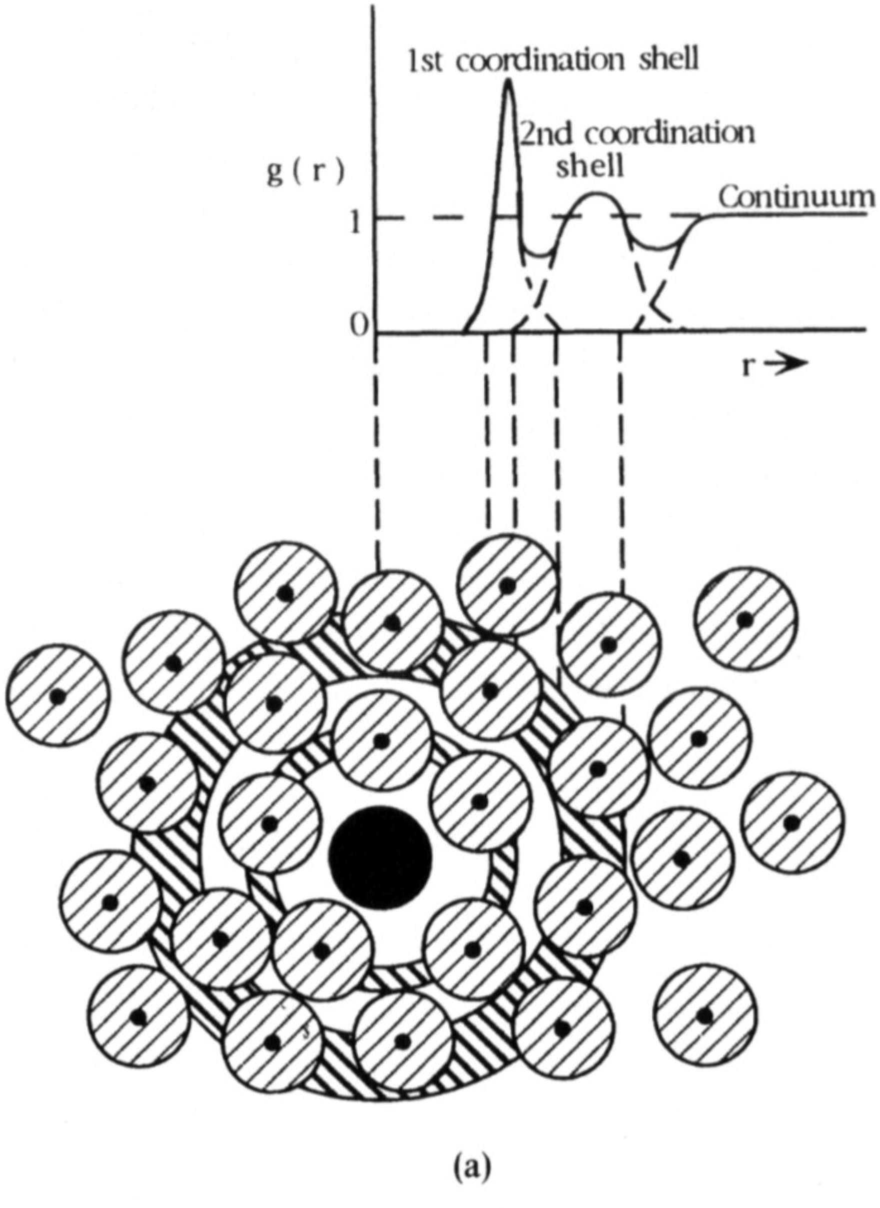

Figure 1.6: (From Varshneya (1994)) schematic illustration of the configuration of a glass around an origin atom (in black) with the corresponding $g\left(r\right)$

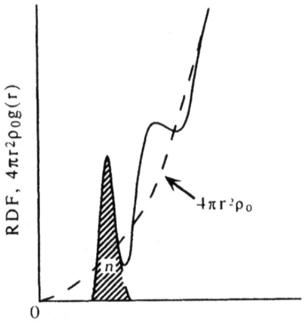

Figure 1.7: radial distribution function $4\pi r^{2}\rho_0 g\left(r\right)$. The number of nearest neighbours n can be evaluated from the area under the first peak

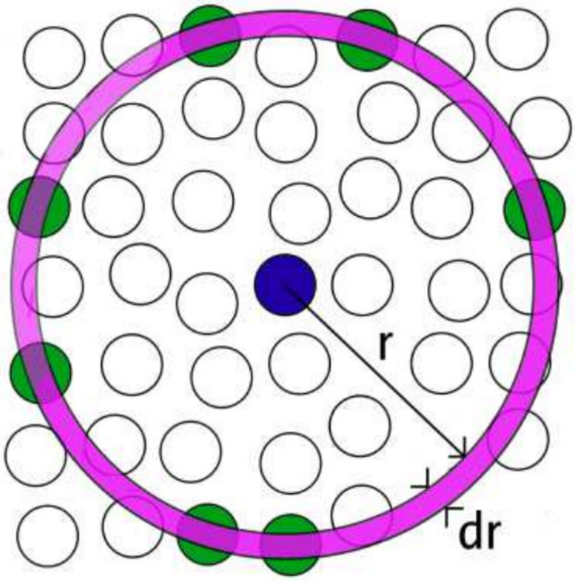

Figure 1.8: number of atoms in a spherical shell of radius dr

1.2.4 extension to binary systems

In a system with two components, A and B, partial distribution functions can be defined. If

$$\begin{aligned} \left\langle n_{AB}\left(r\right)\right\rangle d\boldsymbol{r} &= \begin{array}{l}\text{probability of finding a B atom in volume } d\boldsymbol{r}\\ \text{placed at distance } r \text{ from a given A atom}\end{array} \\ \left\langle n_{AB}\left(r\right)\right\rangle_{nonc} d\boldsymbol{r} &= \text{the same, in an uncorrelated system} \end{aligned}$$

then the partial distribution function $g_{AB}\left(r\right)$ is

$$g_{AB}\left(r\right) \equiv \frac{\left\langle n_{AB}\left(r\right)\right\rangle}{\left\langle n_{AB}\left(r\right)\right\rangle_{nonc}} = \frac{\left\langle n_{AB}\left(r\right)\right\rangle}{\rho_B} \tag{1.4}$$

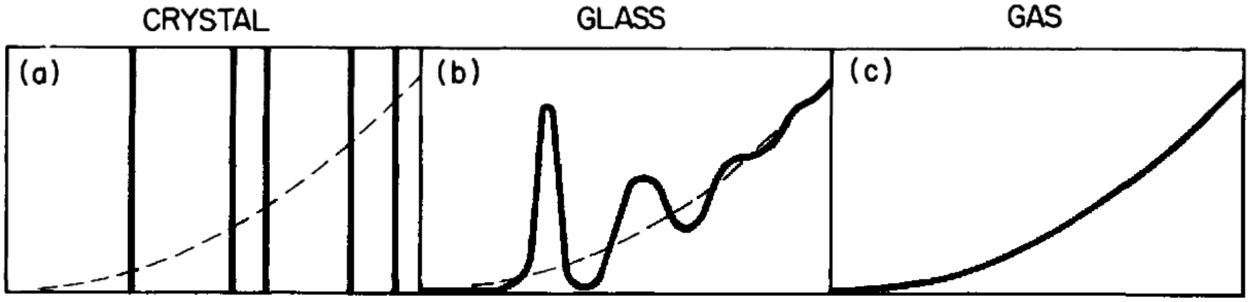

Figure 1.9: sketch of RDF in different systems

Note that

$$g_{AB}(r) \quad = \quad g_{BA}(r) \tag{1.5}$$

In fact, the number of A-B and B-A contacts with a distance value between r e $r + dr$ must be the same:

$$\rho_A \langle n_{AB}(r) \rangle 4\pi r^2 dr = \rho_B \langle n_{BA}(r) \rangle 4\pi r^2 dr$$

From this equality, 1.5 can be recovered through the definition of $g_{ij}(r)$.

Coordination numbers of B atoms around A atoms and *vice versa* are proportional to their respective densities. For example, the number of B atoms whose distance from an A atom is less than R is (compare 1.3)

$$N_{AB} = \int_0^R \rho_B 4\pi r^2 g_{AB}(r)\, dr$$

and similarly

$$N_{BA} = \int_0^R \rho_A 4\pi r^2 g_{BA}(r)\, dr$$

Now recalling that $g_{BA} = g_{AB}$ we verify that

$$\frac{N_{BA}}{\rho_A} = \frac{N_{AB}}{\rho_B}$$

1.2.5 information contained in $g(r)$

The function $g(r)$ carries information about distances between **two atoms**; it doesn't say anything about the mutual positions of **three atoms**, such as the **angle** they form.

This can be illustrated by an example (see figure 1.10). Suppose we have a binary AB compound and we know, from $g^{AB}(r)$, that atom A's first and second neighbors, B and B', are placed at distances r_1^{AB} and r_2^{AB}; note that B' may be anywhere on a spherical surface of radius r_2^{AB}.

We know, additionally, that there is a second B atom also at a distance r^{BB} from B, where r^{BB} is the first peak in $g^{BB}(r)$. However, **in no way can we know whether this atom is the same as** B'! it could as well be in position B^{III} while A's second neighbour is in B^{II}, see the figure**. Only if** B^{III} e B^{II} are the same, triangle ABB' is univocally determined, including the angle $\widehat{ABB'}$.

Careful analysis of the peaks in the PDF will help here:

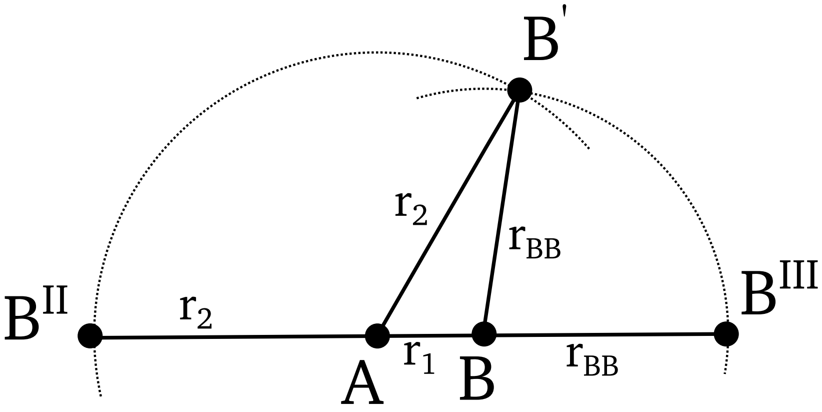

Figure 1.10: mutual positions of three atoms A, B and B^I (or B^{II}, or B^{III}) with first neighbour distances r_1, r_2, and r_{BB}

- if $B^{II} \neq B^{III}$, there must be a third peak in the $g^{AB}(r)$ at a distance between r_2 and $\left(r_1 + r^{BB}\right)$ -not at a shorter distance than r_2, since in this case it would have appeared before!- and a second peak between r^{BB} e $(r_1 + r_2)$ in the $g^{BB}(r)$ (both of which with coordination number 1).
- if the three atoms are equal and B^{III} e B^{II} coincide in B', then A,B and B' form an isosceles triangle with sides r_1, r_1, r_2 where the "bonding" angle $\widehat{BAB'} = \theta$ is given by

  $$\sin\frac{\theta}{2} = \frac{r_2}{2r_1}$$

  (Elliott (1984) p.63, table at p.74; Rao et al. (1998))
- similarly, if $r_2 = r_1$, with $N_{AB} = 2$ (such as in an AB$_2$ molecule), the bonding angle $\widehat{BAB'} = \phi$ is given by:

  $$\sin\frac{\phi}{2} = \frac{r_{BB}}{2r_1}$$

1.2.6 geometry of the atom surroundings (Voronoi polyhedra)

The $g(r)$ gives information about the average distances from an origin atom, but, due to the assumption of (average) spherical symmetry, it does not say anything about the *shape* of the atom surroundings. However, even in a disordered material, neighbouring atoms may be arranged following preferential geometries; for instance, in many metal alloys it has been observed that the first contacts tend to assume an "approximately" icosahedral shape.

There are different ways of partitioning the space in a disordered arrangement of atoms (figure 1.11, left), into geometrical figures (polyhedra) that add up to the whole space. A natural choice is considering the polyhedra whose vertices are the atoms themselves and whose edges are the connection lines between atoms; this is what is commonly done when representing crystal structures. If we add the requirement that these elemental volumes contain no atoms, we obtain a "lattice" like the one illustrated by red lines in the right panel of the same figure 1.11

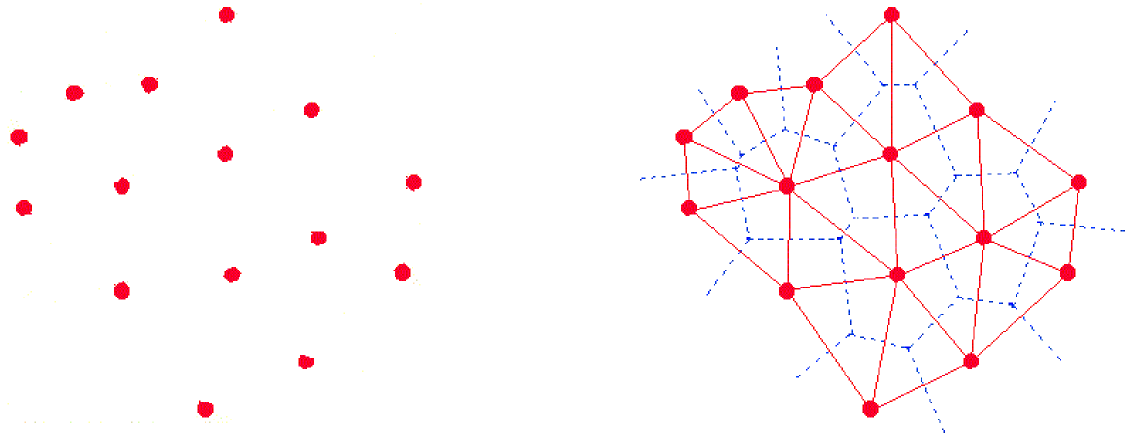

Figure 1.11: Left: a disordered array of points. Right: the same points connected in a lattice (red lines), and their Voronoi polyhedra (blue dashed lines)

Note that the choice of these minimal polyhedra is a purely geometrical abstraction and does not imply the existence of real (chemical) bonds between connected atoms. Indeed, the choice is to some extent arbitrary, like the choice of a primitive cell in crystallography.

There is an alternative method of partitioning the space, in which the atoms are placed at the *center* rather than at the vertices of the polyhedra. This partitioning is illustrated in two dimensions by the dashed blue lines in the figure. The elemental units of space delimited by the blue lines are called Voronoi polyhedra and are defined as follows:

the Voronoi polyhedron of an atom is the *locus* of all points that are closer to that atom than to any other

The recipe for drawing the Voronoi polyhedron of atom A is

- draw all the lines connecting A to its neighbours
- cut each of these lines in the middle point with the normal plane

- the planes delimit a convex figure around A that is its Voronoi polyhedron[3]

The Voronoi subdivision of space finds an ever-increasing number of applications. Among the most obvious: associating each point in a map to the nearest fire station!

As a direct consequence of its definition, the Voronoi partition, or *tessellation*, of an ensemble of points is **unique**. As we have seen, this is not so for the lattice that connects atoms; however, a unique lattice can be derived from the Voronoi partition[4] with the so-called Delauney triangulation:

in the Delauney lattice two atoms are connected if they share one face of their Voronoi polyhedra

The red network in figure 1.11 (right) is the Delauney lattice of the points.

Clearly, the Delauney and Voronoi partitioning are duals of each other.

It can be shown that in 2D the cells of the Delauney lattice are triangles (hence the term "Delauney triangulation"), while in 3D the cells are tetrahedra; Voronoi cells, on the contrary, can be any kind of polygons and polyhedra, respectively. The vertices of the Voronoi polygons (polyhedra) are the circumcenters of the Delauney triangle (tetrahedron) that contains them; thus, each Delauney cell contains only one Voronoi vertex, in the same way as each Voronoi cell contains only one vertex of the Delauney lattice (one atom).

Given a certain array of atoms, Voronoi cells describe the geometry of the space *around atoms*; Delauney cells describe the dimension of the empty spaces, or *holes*, between atoms.

If the array has translational symmetry, as a crystal lattice, Voronoi polyhedra are termed Wigner-Seitz cells: they are primitive cells whose symmetry properties are the same as the non-translational properties of the lattice (for example, the dashed hexagons in the regular triangular lattice in figure 1.12).

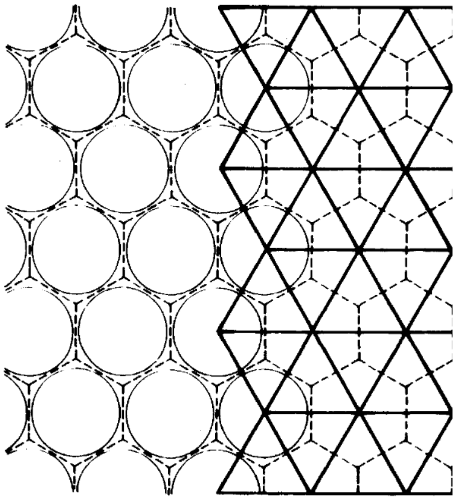

Figure 1.12: (from Zallen (1998)) A regular hexagonal 2D lattice of atoms (the circles, or the nodes of the heavy line network). The dashed hexagons are Voronoi cells, called in this case Wigner-Seitz cells

In a disordered array, instead, there is a whole ensemble of different Voronoi polyhedra. They can be grouped according to several properties, such as their volume, number of faces, number of edges per face,

---

[3] to understand this, consider that all points on the same side of the plane as A are closer to it than to the neighbour

[4] in fact, in special cases, called *degenerate*, the lattice is not uniquely determined

etc. In a totally disordered system (figure 1.13, left) these properties are distributed over a wide range of values; partially disordered systems (figure 1.13, right) exhibit less diversity. In figure 1.14 distributions of Voronoi cell volumes for a simulated solid, liquid and gas are reported.

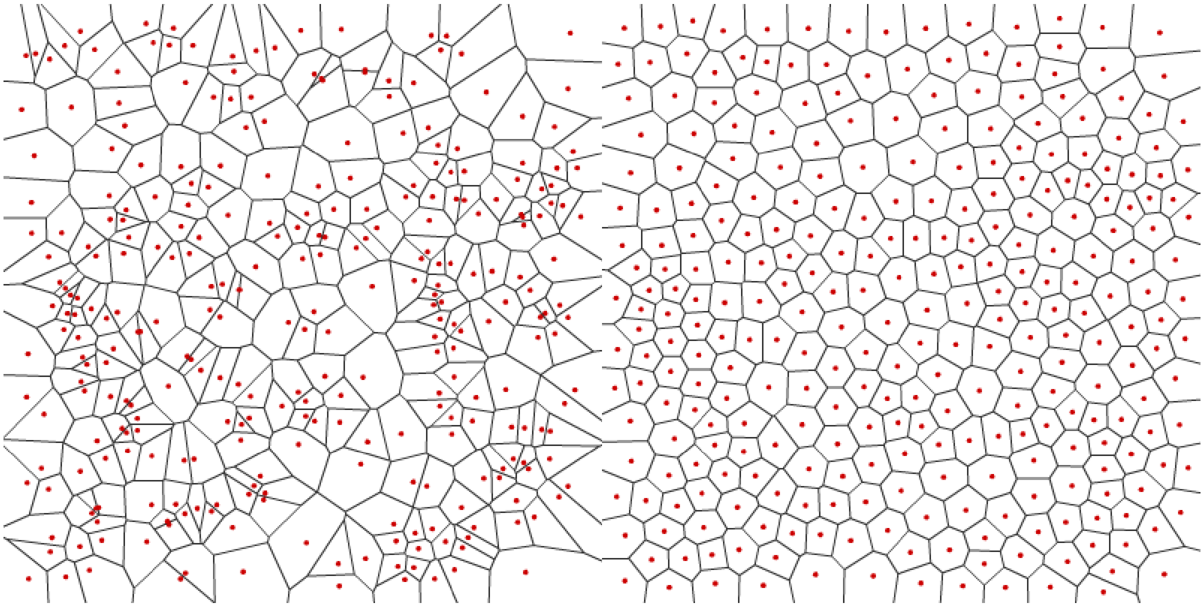

Figure 1.13: Voronoi polyhedra of a highly disordered system (left) and in a less disordered system (right)

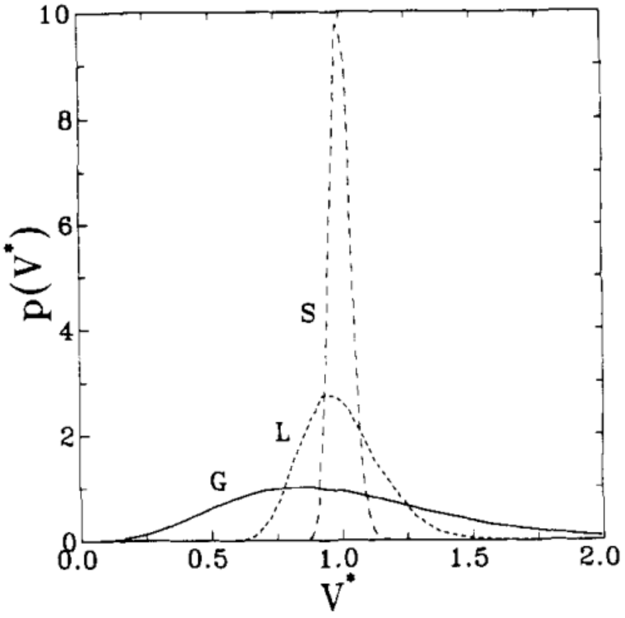

Voronoi polyhedra volume distribution functions about the mean for the solid (S), liquid (L), and gas (G) systems.

Figure 1.14: (from Montoro and Abascal (1993))

The next figure (figure 1.15) shows the statistics of the number of faces and number of edges per face of Voronoi polyhedra in a random close-packed structure (which will be treated in detail in section 3.3).

The number of faces of the Voronoi cell of an atom represents the number of adjacent cells, which can be taken as definition of the number of neighbours of the atom. Note that in real aggregates where atoms have non-zero radius, these *geometrical neighbours* (the atoms whose Voronoi polyhedra are in contact) may be not the same as the *first neighbours* (atoms that are themselves in direct contact).

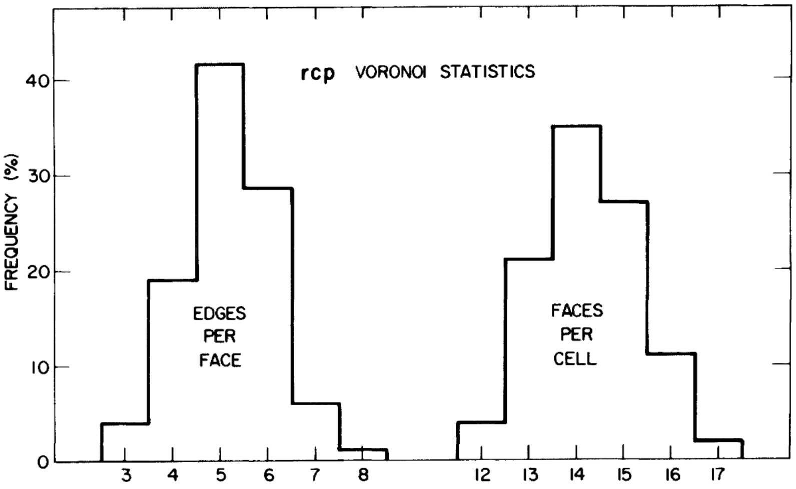

Figure 1.15: Frequency distribution of number of faces and number of edges per face of Voronoi polyhedra of a simulated random close-packed structure

1.2.7 more structural parameters

In addition to the $g(r)$ and the Voronoi analysis and pair correlation quantities, such as the coordination numbers, that can be derived from them, there are other quantities, useful in the description of glass structure, that can be obtained from computer simulations and -at least in principle- from experiments. We briefly review them here, in order of atom correlations involved (2, 3, and more atoms); some will be discussed in more detail below.

1.2.7.1 atom connectivity

In many glassy substances, there is a network of chemical (covalent) bonds connecting neighbouring atoms. In some cases (silicate glasses, chalcogenide glasses) the number of bonds that one atomic species can form is variable. For example, in silicate glasses, oxygen atoms can link to two silicon atoms, thus acting as bridges between them, or can carry a negative charge and be bound to one silicon atom only: this is illustrated in figure 1.16, a 2-D reduction of a sodium silicate glass . In real space silicate glasses, of the four oxygens surrounding one silicon atom, the number of “bridging” atoms ranges from zero to four.

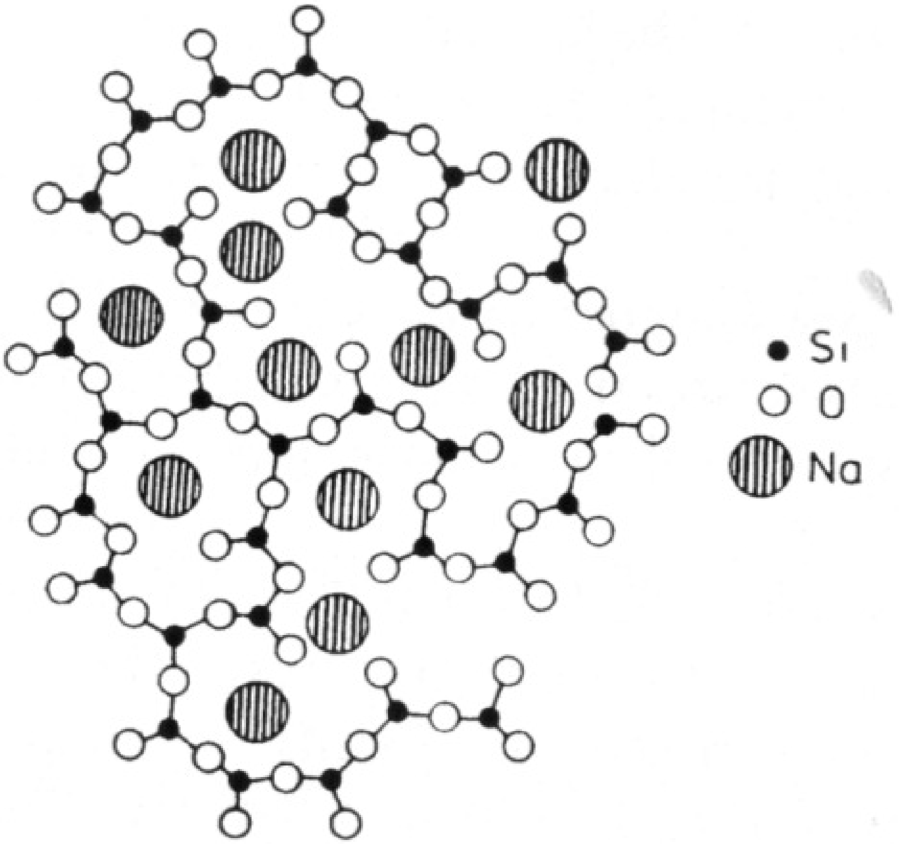

Figure 1.16: (from Varshneya (1994)) 2-D example of bridging and non-bridging atoms in a sodium silicate glass

1.2.7.2 bond angles

As we have seen, structure models that respect observed atom distances can differ as to bond angles. Figure 1.17 shows two models for silica glass that predict a median $Si-O-Si$ angle of $\sim -180°$ and $\sim -140°$, respectively.

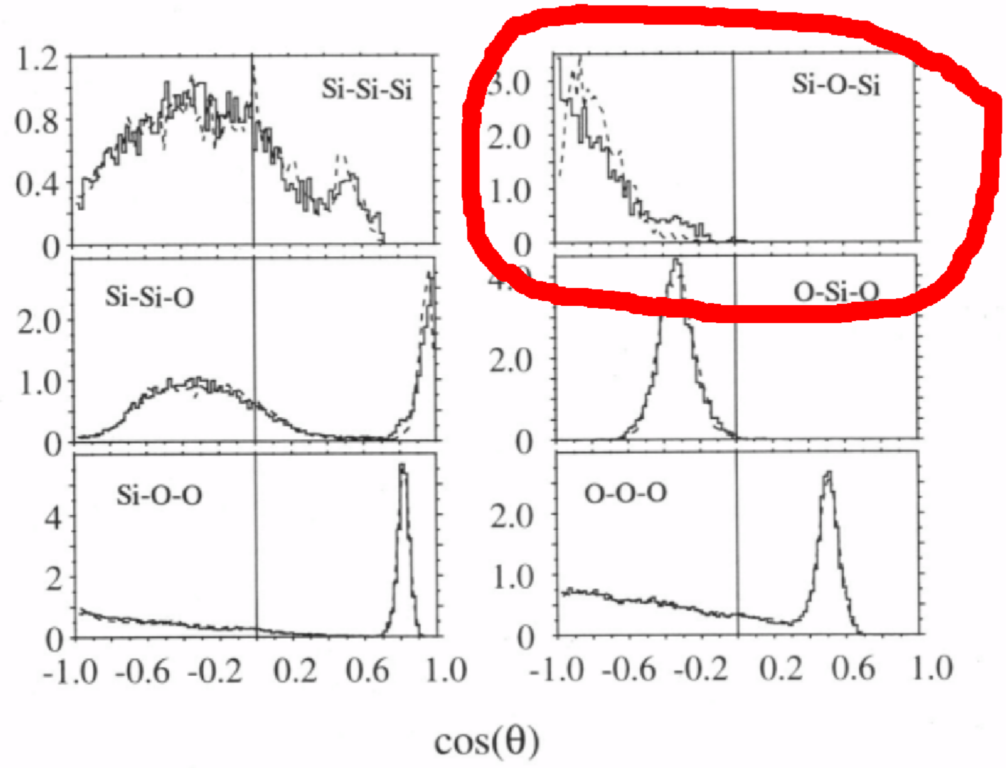

Bond angle distributions for glassy silica calculated from the starting model (dashed line) and the RMC refined model (full line)[21] (arbitrary units).

Figure 1.17: (from Keen (1998)) Two different $Si-O-Si$ bond angle distributions (circled in red) in silica glass

1.2.7.3 medium-range structures (rings)

Chemical bonds in a covalent glass form ring structures of varying sizes. The relative abundance of rings composed of n atoms (see figure 1.18) is a property that can be evaluated with computer simulations and in some cases be inferred from experimental data.

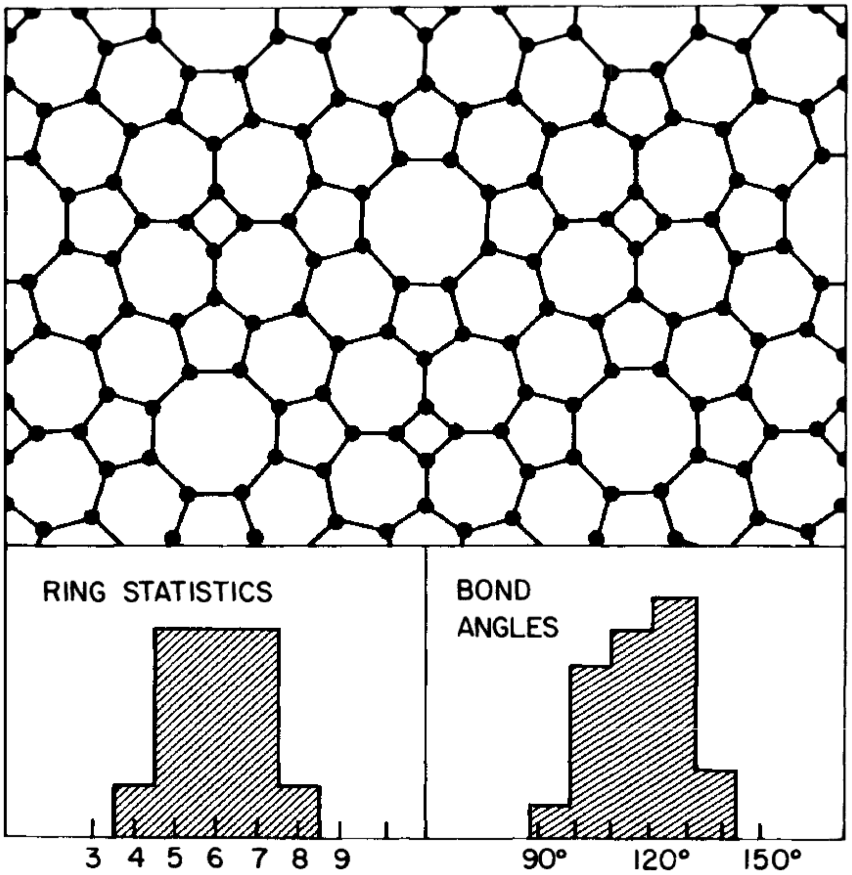

Figure 1.18: ring size statistics (lower left histogram) in a 2-D covalent glass (from Zallen (1998))

1.3 reference texts

Two texts, Varshneya (1994) and Shelby (2005), although a little outdated, are still considered standard textbooks in the general subject of glasses from an experimentalist's point of view; specific chapters are devoted to structural properties and to methods for the description of glass structure. A more theoretical description, not limited to glasses but covering the broader subject of disordered matter, is in Zallen (1998).

Chapter 2

Methods for the investigation of glass structure

In this section we will briefly review the methods for analyzing the structure of a glass. They are divided into experimental and computational methods; to each one will be devoted one of the following subsections.

2.1 Experimental methods

Traditionally, the techniques of choice for investigating the atomic structure of substances have been techniques based on diffraction. There is a one-to-one correspondence between the prevalence of this kind of measurements and the prevalence of $g\left(r\right)$ as structure descriptor; in fact, diffraction methods probe interactions between pairs of scattering centers, so the main output is a pair distribution function. Other experimental techniques are based on the response produced by three or more atoms, so they provide information about more complex atomic environments; we will touch vibrational and NMR spectroscopy.

2.1.1 methods based on diffraction

In a typical diffraction experiment, the incident beam of particles (the wave) is scattered by individual centers of the sample with different phases; the scattered rays interfere with each other, either positively or negatively, and the resulting wave is collected at some angle with the incident beam by a distant detector. The signal at a certain angle depends on the phase difference between scattered waves, which in turn depend on the angle and the atomic distances.

First, a review of essential quantities.

A **plane wave** travelling in the $\boldsymbol{k}$ direction has the equation:

$$A = A_0 \sin\left(\boldsymbol{k} \cdot r - \omega t\right)$$

or, more generally,

$$A = A_0 e^{i\left(\boldsymbol{k} \cdot r - \omega t\right)}$$

where

$$\begin{aligned} \omega &= \text{frequency} \\ \boldsymbol{k} &= \text{wave vector} \\ |\boldsymbol{k}| &= \frac{2\pi}{\lambda} \\ \frac{\omega}{|\boldsymbol{k}|} &= \text{velocity} \end{aligned}$$

Energy and momentum of an **electromagnetic wave** are

$$\begin{aligned} E &= \hbar\omega \\ \boldsymbol{p} &= \hbar\boldsymbol{k} \end{aligned}$$

and are connected by the velocity expression $\frac{\omega}{|\boldsymbol{k}|} = c$.

Interference of waves of equal frequency. The interference of two waves of equal frequency is conveniently evaluated with the *rotating vectors method* (see for example Alonso and Finn (1982))*:*

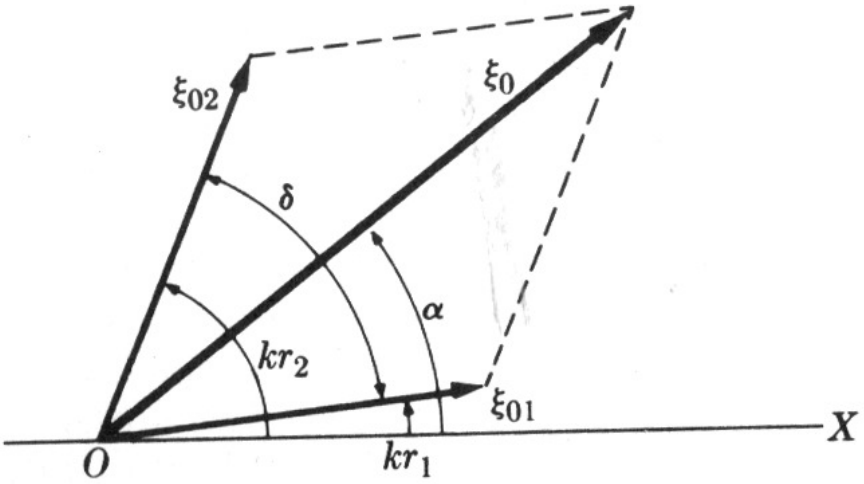

Two waves of equal amplitude, A_0, and frequency, ω, but different spatial phase $\boldsymbol{kr_1}$, $\boldsymbol{kr_2}$, with

$$\delta = \boldsymbol{k}\cdot(\boldsymbol{r_1} - \boldsymbol{r_2})$$

superimpose giving rise to a wave of amplitude

$$\xi_0 = A_0\sqrt{2\,(1 + cos\delta)}$$

The amplitude has a maximum (constructive interference) for $\cos\delta = +1$, that is for

$$\delta = 2n\pi \tag{2.1}$$

with $n = 0, \pm1, \pm2, ...$

Geometry of the scattering experiment. We want to study the interference between the wave scattered by an origin center O and a generic point P, when collected at an angle θ.

Let

$$\hbar \boldsymbol{k_i}, \hbar \boldsymbol{k_f} \quad = \quad \text{momentum of incident and final (scattered) wave}$$

The phase difference between the wave scattered by O and P is

$$\boldsymbol{k_i} \cdot \boldsymbol{R_P} - \boldsymbol{k_f} \cdot \boldsymbol{R_P} = \boldsymbol{Q} \cdot \boldsymbol{R_P} \tag{2.2}$$

with

$$\boldsymbol{Q} \equiv \boldsymbol{k_i} - \boldsymbol{k_f}$$

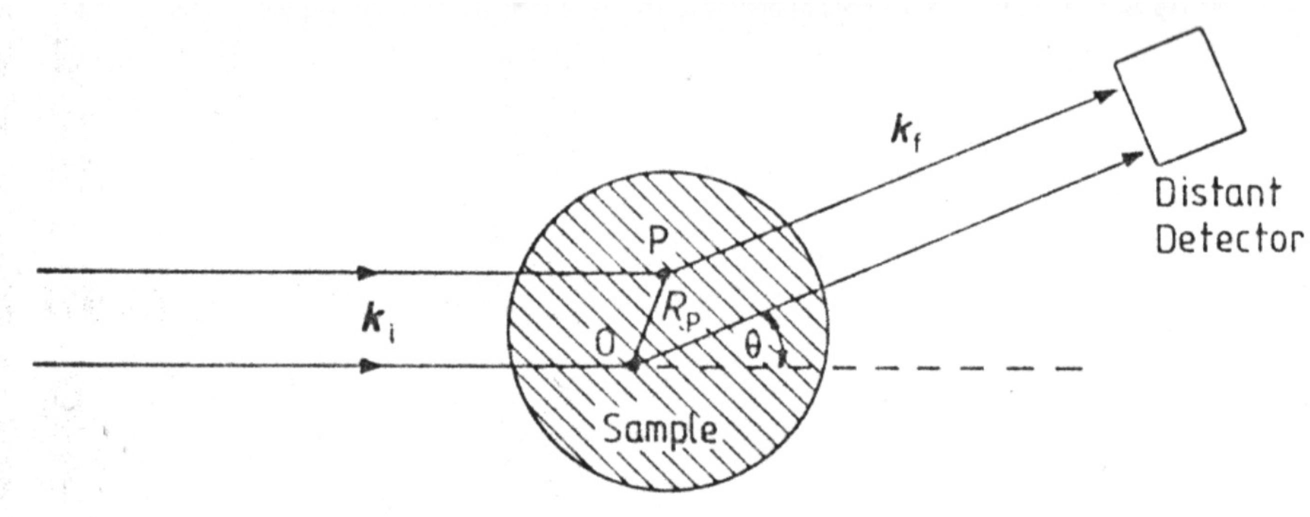

For better clarity, in the following figure, the two spatial phases $\boldsymbol{k_i} \cdot \boldsymbol{R_P}$, $\boldsymbol{k_f} \cdot \boldsymbol{R_P}$ are marked by colors:

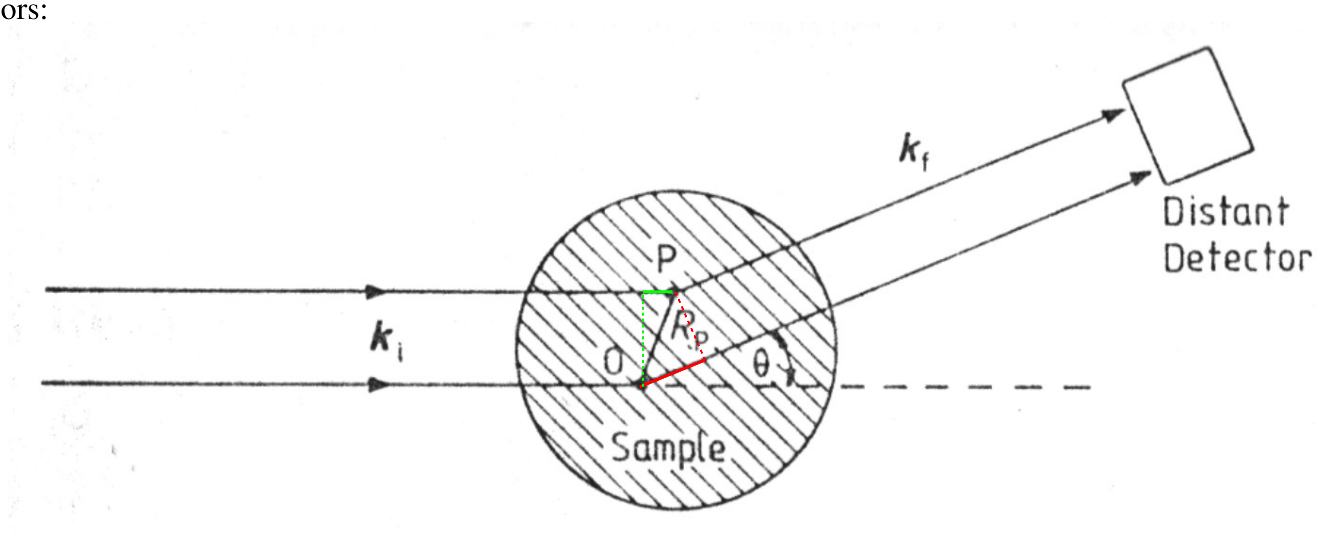

If scattering is *elastic,* kinetic energy of the incident wave is conserved, and so is the modulus of its momentum (since $\frac{\omega}{|\boldsymbol{k}|} = c$; see above)

$$|\boldsymbol{k_i}| = |\boldsymbol{k_f}| = k$$

so that for a given k the modulus of $\boldsymbol{Q}$ depends only on the scattering angle:

$$|\boldsymbol{Q}| = Q = 2k \sin\left(\frac{\theta}{2}\right)$$

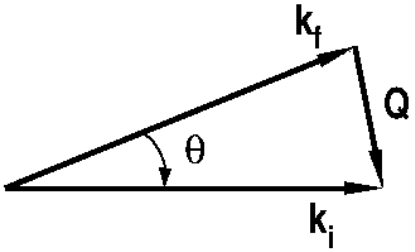

and substituting λ for k (recall $k = \frac{2\pi}{\lambda}$):

$$Q = \frac{4\pi}{\lambda}\sin\left(\frac{\theta}{2}\right) \tag{2.3}$$

The latter is the modulus of the scattering vector at angle θ.

The intensity will be maximum at angles that realize the constructive interference condition on the phase difference (equation (2.1)), that is,

$$\boldsymbol{Q} \cdot \boldsymbol{R_P} \quad = \quad 2n\pi$$

It is useful to write $\boldsymbol{Q}$ as its modulus times its direction:

$$\boldsymbol{Q} = \frac{4\pi}{\lambda}\sin\left(\frac{\theta}{2}\right)\boldsymbol{u_Q}$$

(where $\boldsymbol{u_Q}$ is a unit vector in the direction of $\boldsymbol{Q}$); now the condition becomes

$$\frac{4\pi}{\lambda}\sin\left(\frac{\theta}{2}\right)\boldsymbol{u_Q} \cdot \boldsymbol{R_P} \quad = \quad 2n\pi$$

or

$$\boxed{\boldsymbol{u_Q} \cdot \boldsymbol{R_P} = \frac{n\lambda}{2\sin\left(\frac{\theta}{2}\right)}} \tag{2.4}$$

Maximum constructive interference with radiation scattered by O is given by points whose distance from O, projected in the direction of $\boldsymbol{Q}$, equals $\frac{n\lambda}{2\sin\left(\frac{\theta}{2}\right)}$

The maximum interference condition is illustrated in the following figure:

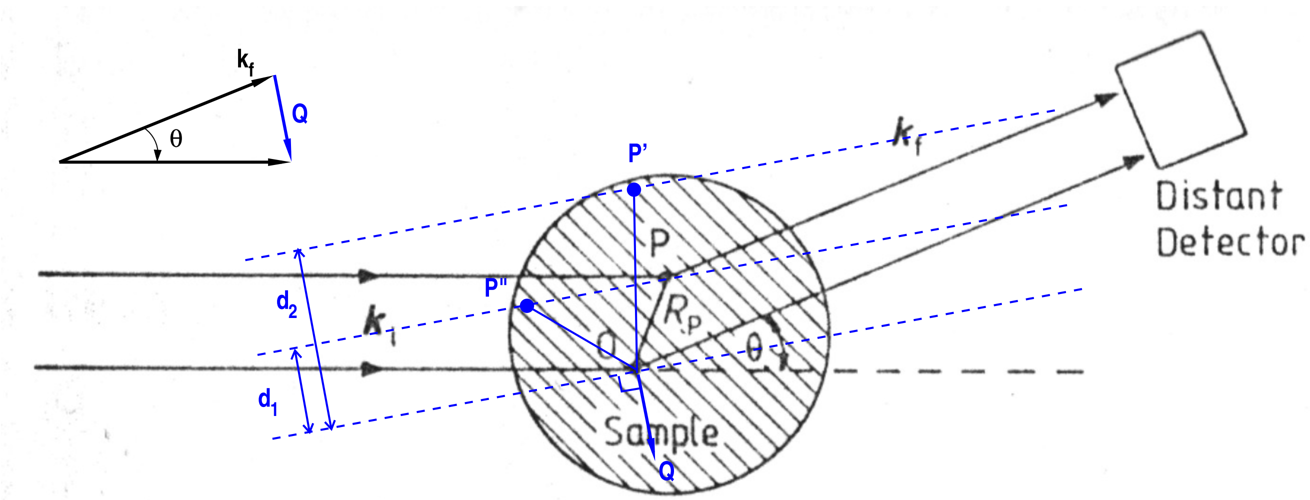

Figure 2.1: scattering planes are a manifold of parallel planes spaced $d = \frac{\lambda}{2\sin\left(\frac{\theta}{2}\right)}$

All points (P, P', P") lying on the series of planes $\perp$ $\boldsymbol{Q}$ and whose distance from O is $d_n = \frac{n\lambda}{2\sin\left(\frac{\theta}{2}\right)}$ contribute to the maximum interference.

A few comments on the important relation of 2.4.

1. Bragg's law. Equation (2.4) is just a different form of the well-known *Bragg's law* of crystal scattering

$$2d\sin\left(\frac{\theta}{2}\right) = n\lambda$$

which is illustrated in standard textbooks with sketches like the following[1]:

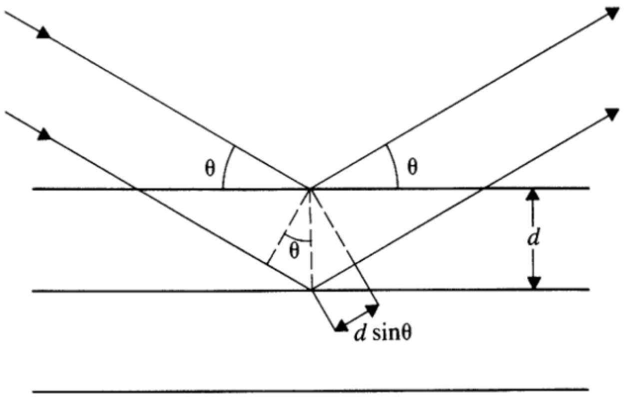

Illustration of the Bragg scattering law $n\lambda = 2d\sin\theta$.

Figure 2.2: Bragg's law (from Elliott (1984))

---

[1] note that in this figure $\frac{\theta}{2} \to \theta$

However, similar representations are somehow misleading, since they do not show that positive interference with the point on the lower plane is given by *any* point on the plane above, not just the one that is on the perpendicular: compare our figure 2.1.

2. Measurement resolution. The smallest distances that can be measured with a diffraction method are of the order of the spacing between planes

$$d_1 = \frac{\lambda}{2\sin\left(\frac{\theta}{2}\right)}$$

The point on the first plane that is closest to O is the one for which $\boldsymbol{R_P}$ is closest to the direction of $\boldsymbol{Q}$, so that $\boldsymbol{u_Q}\cdot\boldsymbol{R_P} \sim |\boldsymbol{R_P}|$; if the scattering angle is not too small, that is $\sin\left(\frac{\theta}{2}\right) \sim 1$, we have

$$|\boldsymbol{R_P}| \sim \lambda$$

which shows that **the wavelength λ of the radiation involved must be of the order of $|\boldsymbol{R_P}|$,** the minimum distance between two centers that we want to detect (of the order of Å -like X-rays- for the short range atomic distances).

3. Angle dependence. Note also that at constant λ the angle θ of the first diffraction peak and the distance $|\boldsymbol{R_P}|$ between the two centers are inversely proportional:

$$\sin\left(\frac{\theta}{2}\right) \sim \frac{\lambda}{2\,|\boldsymbol{R_P}|}$$

that is, **interference between centers at a larger distance than λ can be seen at small angles**

In Small Angle X-ray Scattering (SAXS), for example, X-rays ($\lambda \sim 10^{-10}m$) are used to detect particles of dimension scale of nm at angles of the order of $1°$

We now consider the cumulative effect of interference between many (pairs of) centers.

When there is an ensemble of scattering points P, each one interferes with the radiation scattered by O, and the total radiation is the sum of the single superimposed waves. The resulting intensity is proportional to the square of this amplitude:

$$I\left(\boldsymbol{Q}\right) = A\left|\sum_{P} f_P\left(\boldsymbol{Q}\right)\exp\left(i\boldsymbol{Q}\cdot\boldsymbol{R_P}\right)\right|^2$$

where

$$f_P\left(\boldsymbol{Q}\right) \quad = \quad \text{scattering length of a single site}$$

(and A is some proportionality constant).

The intensity depends on

- the type of incident wave
- the type of scattering center
- the direction of scattering

2.1.1.1 X-ray scattering (XRS)

X-rays are scattered by *electrons* in matter. Within a good approximation, in a polyatomic sample (made up of heavy atoms) the electronic density is concentrated in the close vicinity of the atomic nuclei. This allows us to first consider scattering from an isolated atom, then sum up all single atom contributions. The derivation we will follow is, to some extent, general.

The intensity of radiation scattered by one atom, expressed as a function of the radiation scattered by one electron ("in electron units"), is

$$I_{eu}(\boldsymbol{Q}) \propto \left| \int n_e(\boldsymbol{r}) \exp(i\,\boldsymbol{Q}\cdot\boldsymbol{r})\, d\boldsymbol{r} \right|^2$$

with

$$n_e(\boldsymbol{r})\, d\boldsymbol{r} \quad = \quad \text{fraction of electron in volume } d\boldsymbol{r}$$

In a system of N atoms, contributions from each atom must be cumulated. If we define:

$$\begin{aligned} \boldsymbol{R}_i &= \text{position of atom } i \text{ (nucleus)} \\ \boldsymbol{r}' &= \text{distance \textit{within the atom} (from nucleus)} \end{aligned}$$

it can be shown (Cusack (1987)) that (for a collection of equal atoms) the resulting intensity can be written

$$I_{eu}(\boldsymbol{Q}) = \left| \sum_{i=1}^{N} \exp(i\,\boldsymbol{Q}\cdot\boldsymbol{R}_i) \right|^2 \cdot |f_a(\boldsymbol{Q})|^2 \tag{2.5}$$

with

$$f_a(\boldsymbol{Q}) \equiv \int_{atom} n_e(\boldsymbol{r}') \exp(i\,\boldsymbol{Q}\cdot\boldsymbol{r}')\, d\boldsymbol{r}' \tag{2.6}$$

representing the scattering from a single atom.

N.B.: By means of equation (2.5), which is general, $I_{eu}(\boldsymbol{Q})$ is partitioned into two factors, of which one depends on atoms and one on their positions.

Accordingly, one can consider each factor separately.

The factor dependent on atoms, or **atomic form (or scattering) factor** $f_a(\boldsymbol{Q})$, expresses the total interference between infinitesimal elements of the space around one atom; it is known and tabulated for each atomic species and for each type of incident wave.

In the X-ray case, electronic density of the atom has an approximately spherical symmetry, and thus the atomic form factor does not depend on the direction of the incident wave with respect to the atom, but only on the scattering angle:

$$f_a(\boldsymbol{Q}) \to f_a(Q) = f_a\left(\frac{sin\theta}{\lambda}\right)$$

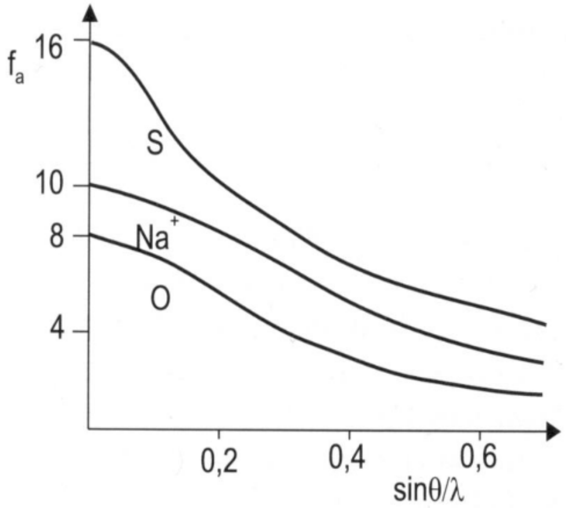

Clearly, f_a is larger for heavier atoms (which contain more electrons), while the hydrogen atom ^{1}H gives a negligible scattering. At $\theta = 0$ there is total scattering and f_a is simply the number of electrons of the atom(recall equation (2.6) with $Q = 0$)

We may note that $f_a(Q)$ has a roughly Gaussian shape; this is not unexpected, since equation (2.6) defines it as the spatial Fourier transform of electron density which is approximately Gaussian itself[2].

As for the factor that contains atom positions, it is called the *structure factor $S(\boldsymbol{Q})$*

$$NS(\boldsymbol{Q}) \equiv \left| \sum_{i=1}^{N} \exp\left(i\,\boldsymbol{Q}\cdot\boldsymbol{R}_i\right) \right|^2 \qquad (2.7)$$

It depends on the distribution of interatomic *distances* $(\boldsymbol{R}_i - \boldsymbol{R}_j)$.

It is therefore reasonable to expect it to be connected to $g(\boldsymbol{r})$. Indeed, it can be proved (Cusack (1987)) that its thermodynamic average is

$$\langle S(\boldsymbol{Q})\rangle = 1 + \rho_0 \int \left(g(\boldsymbol{r}) - 1\right) \exp\left(i\,\boldsymbol{Q}\cdot\boldsymbol{r}\right) d\boldsymbol{r}$$

In an *isotropic* medium, such as a liquid or a glass, $g(\boldsymbol{r}) \to g(r)$ so $S(\boldsymbol{Q}) \to S(Q)$. Omitting brackets $\langle\rangle$ for clarity:

$$S(Q) = 1 + \rho_0 \int_0^\infty \left(g(r) - 1\right) \frac{\sin Qr}{Qr} 4\pi r^2 dr$$

The last formula shows that $S(Q)$ is directly connected to the Fourier transform of $g(r)$, or that of the radial distribution function $\rho_0 4\pi r^2 g(r)$

2.1.1.2 neutron scattering (NS)

Neutron beams from a nuclear reactor have a wavelength of $0.1 \div 1$ Å, which is suitable for atomic structure investigation, like X-rays.

Neutron scattering (NS) can be treated in much the same way as XRS (Cusack (1987)), with some important differences.

First, neutrons are scattered by nuclei (as opposed to electrons); so it is the atom positions that will be detected, rather than the (centre of) electronic density.

Differently from XRS, the atomic form factor for NS, named b, is isotropic and does not depend on Q (see figure 2.3). The atomic form factor, indeed, is the Fourier transform of a Dirac δ function in this case, and consequently it has a constant value (compare the corresponding argument for X-rays).

Also, b does not increase with the atomic number Z of the element: light nuclei scatter as efficiently as heavier ones. This is a major difference from XRD, and explains why when we are interested in the position of small atoms, such as hydrogen atoms, which are not seen in XRS, we must resort to NS.

---

[2] see for example Bracewell (1986)

Different isotopes of the same element can have different form factors; this fact is exploited in the technique of isotopic substitution, by which binary pair distribution functions, $g_{AB}(r)$, are obtained.

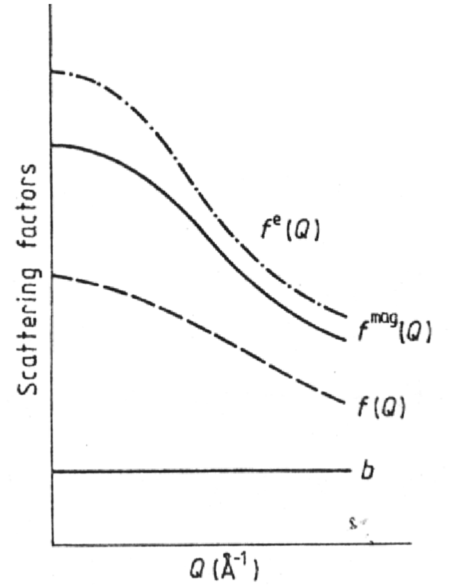

Single-centre scattering factors for: electrons by atoms (f^e), neutrons by magnetic ions (f^{mag}), x-rays by atoms (f), and neutrons by nuclei (b)

Figure 2.3: (from Cusack (1987))

Inelastic neutron scattering, where some energy and momentum are transferred to the substance, can be used for studying its vibrational states. In this case the experimental quantity of interest is

$$S(Q) \rightarrow S(Q,\omega)$$

where

$$\hbar\omega \quad = \quad \text{energy lost to the system}$$

From $S(Q,\omega)$ the *vibrational density of states* can be measured. Also, it gives information about the time relaxation of the structure, which is an important topic in the glass transition.

2.1.1.3 Electron scattering (ES)

Electrons from an electron microscope, for which $\lambda_{min} = 0.05$Å, are also employed for scattering.

Electrons interact with both nuclei and electrons of the sample. One way to see this is that they are scattered by the screened Coulomb field of the atoms, which is reflected in the electronic atomic scattering factor $f_e(Q)$ being connected to the X-ray atomic form factor $f_a(Q)$ (Cusack (1987)):

$$f_e(Q) \propto \frac{Z - f_a(Q)}{Q^2}$$

Because of the strong interactions with the charge density of the sample, $f_e(Q) > f_a(Q)$ (see figure 2.3 again)

Strong Coulombic interactions also prevent electrons from reaching the inner parts of a substance. Thin samples must be prepared to be examined with ES.

2.1.1.4 Comparison of different scattering methods

A useful comparison of the different scattering techniques we have just mentioned is reported in table 2.1 below:

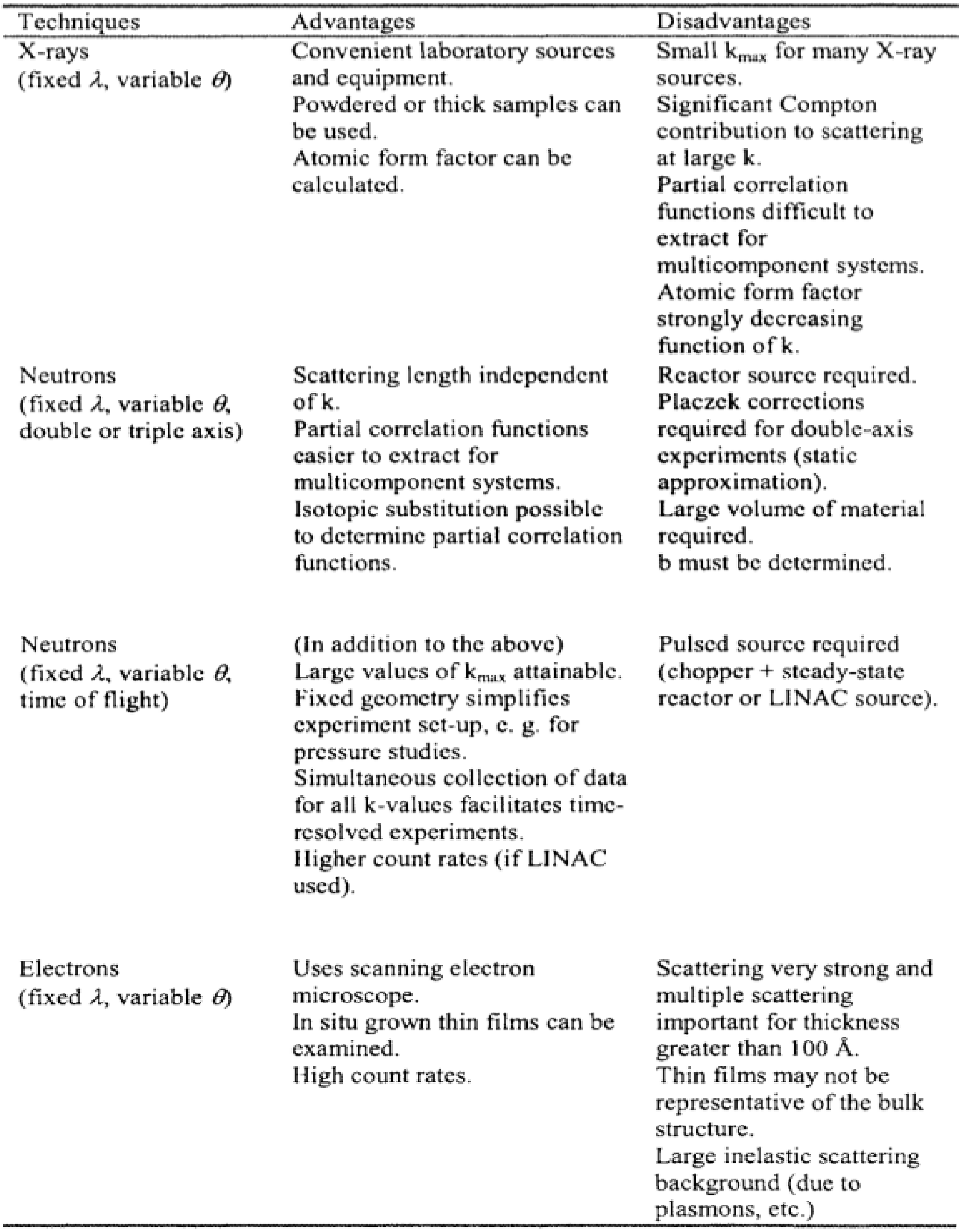

Techniques	Advantages	Disadvantages
X-rays (fixed λ, variable θ)	Convenient laboratory sources and equipment. Powdered or thick samples can be used. Atomic form factor can be calculated.	Small k_{max} for many X-ray sources. Significant Compton contribution to scattering at large k. Partial correlation functions difficult to extract for multicomponent systems. Atomic form factor strongly decreasing function of k.
Neutrons (fixed λ, variable θ, double or triple axis)	Scattering length independent of k. Partial correlation functions easier to extract for multicomponent systems. Isotopic substitution possible to determine partial correlation functions.	Reactor source required. Placzek corrections required for double-axis experiments (static approximation). Large volume of material required. b must be determined.
Neutrons (fixed λ, variable θ, time of flight)	(In addition to the above) Large values of k_{max} attainable. Fixed geometry simplifies experiment set-up, e. g. for pressure studies. Simultaneous collection of data for all k-values facilitates time-resolved experiments. Higher count rates (if LINAC used).	Pulsed source required (chopper + steady-state reactor or LINAC source).
Electrons (fixed λ, variable θ)	Uses scanning electron microscope. In situ grown thin films can be examined. High count rates.	Scattering very strong and multiple scattering important for thickness greater than 100 Å. Thin films may not be representative of the bulk structure. Large inelastic scattering background (due to plasmons, etc.)

Table 2.1: Advantages and disadvantages of different scattering techniques (from Rao (2002))

2.1.1.5 Examples

X-Ray Scattering is the method of choice for studying monoatomic liquids or glasses:

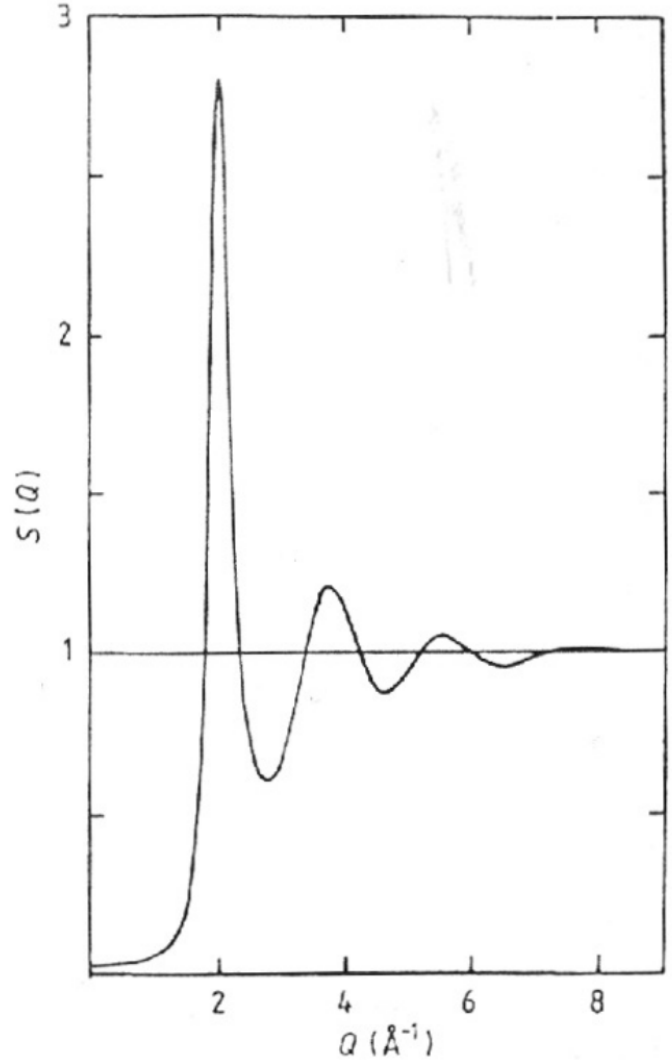

$S(Q)$ from Greenfield *et al* (1971) for liquid Na.

Figure 2.4: (from Cusack (1987))

With Neutron Scattering, partial structure factors of binary compounds can be obtained, using isotopic substitution (figure 2.5)

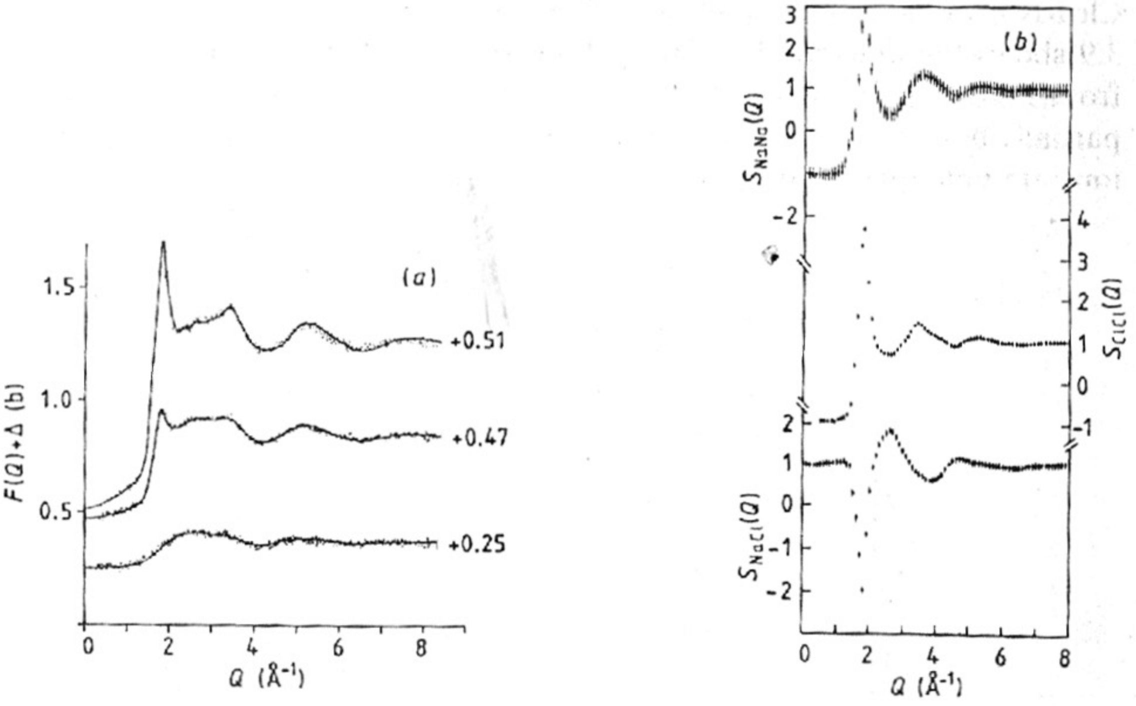

Figure 2.5: (from Cusack (1987)) Neutron scattering of liquid NaCl with isotopic substitution. (a) from top: $\mathrm{Na^{35}Cl}$,NaCl,$\mathrm{Na^{37}Cl}$; (b) partial structure factors

Partial structure factors give the binary PDFs (figure 2.6)

Note that layers of positive and negative charge alternate; and that $g\left(r\right)_{\mathrm{Na-Na}}$ superimposes with $g\left(r\right)_{\mathrm{Cl-Cl}}$

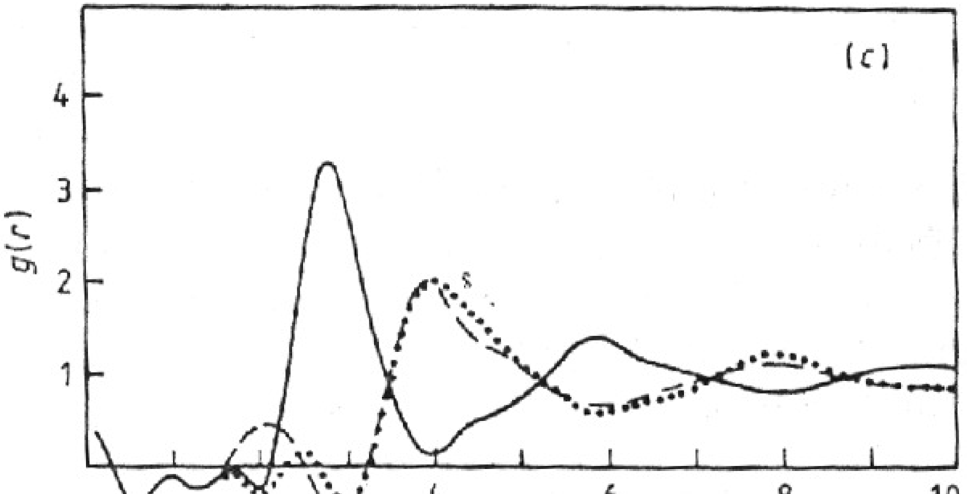

Figure 2.6: (from Cusack (1987)) PDF of liquid NaCl from NS with isotopic substitution. Solid line: $g\left(r\right)_{\mathrm{Na-Cl}}$. Broken: $g\left(r\right)_{\mathrm{Na-Na}}$. Dotted: $g\left(r\right)_{\mathrm{Cl-Cl}}$

In the case of $\mathrm{BaCl_2}$, instead, the $\mathrm{Ba-Ba}$ curve differs from $\mathrm{Cl-Cl}$[3]:

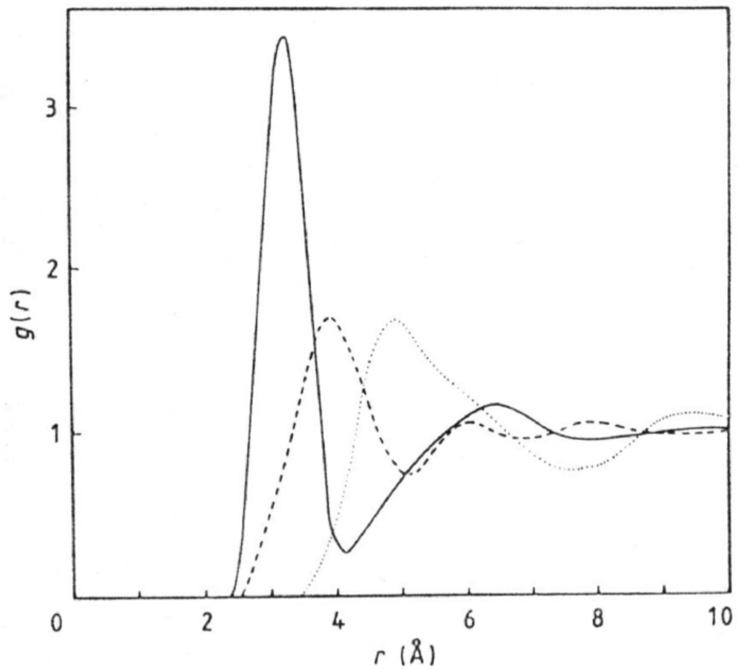

$g_{ij}(r)$ for $\mathrm{BaCl_2}$ from Edwards *et al* (1978). Full curve, $g_{\mathrm{BaCl}}(r)$; broken curve, $g_{\mathrm{ClCl}}(r)$; dotted curve, $g_{\mathrm{BaBa}}(r)$.

Figure 2.7: (from Cusack (1987)) PDF of liquid $\mathrm{BaCl_2}$.

As we have seen, coordination numbers can be estimated from the Radial Distribution Function RDF= $\rho_0 4\pi r^2 g\left(r\right)$, equation (1.3). The number of atoms contained in a sphere of radius D is given by $N_D = \rho_0 \int_0^D g\left(r\right) 4\pi r^2 dr$. In vitreous silica (figure 2.8), the area under the first peak gives $N_{Si-O} \approx 4$.

---

[3] The different first-neighbour peaks might well be due only to the different Cl and Ba densities. Assuming complete disorder, since $\rho_{Cl} = 2\rho_{Ba}$ the volume that contains 1 neighbour is $v_{Cl} = \frac{1}{2} v_{Ba}$ and consequently the corresponding sphere radius is $\frac{r_{Ba}}{r_{Cl}} = 2^{\frac{1}{3}} = 1.26$, and this is the ratio of average distances. From the $g\left(r\right)$ curves one can compute $\frac{r_{Ba}}{r_{Cl}} \approx \frac{5}{4} = 1.25$. Does this make any sense to the reader?

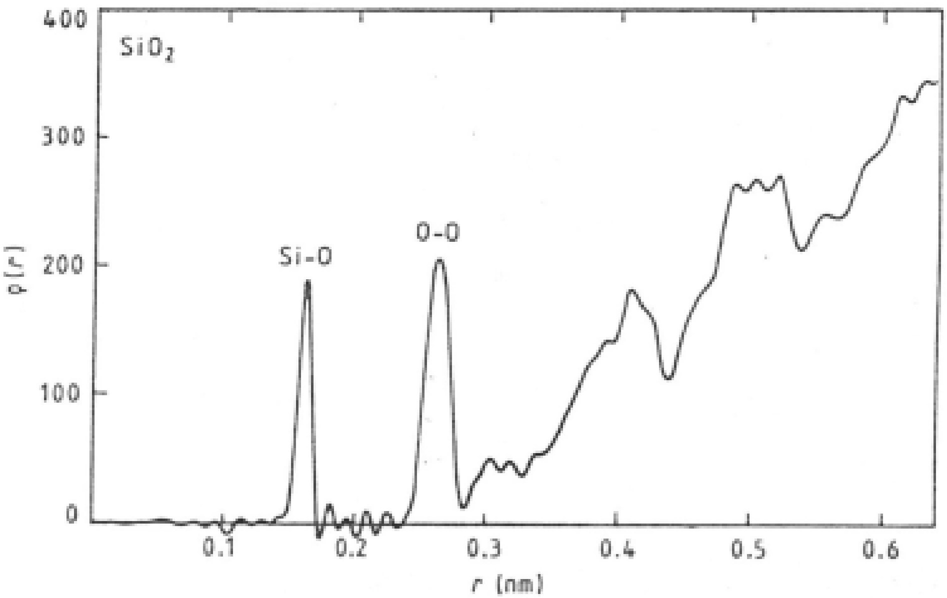

The radial distribution junction of vitreous silica derived from the scattering of neutrons from a spallation source (from Misawa *et al* 1980).

Figure 2.8: (from Cusack (1987)) RDF $\rho_0 4\pi r^2 g\left(r\right)$ of vitreous $\mathrm{SiO_2}$ from NS.

The RDF can be extracted also from Electron Scattering. Like XRS, and contrary to NS, ES gives no access to partial structure factors (figure 2.9)

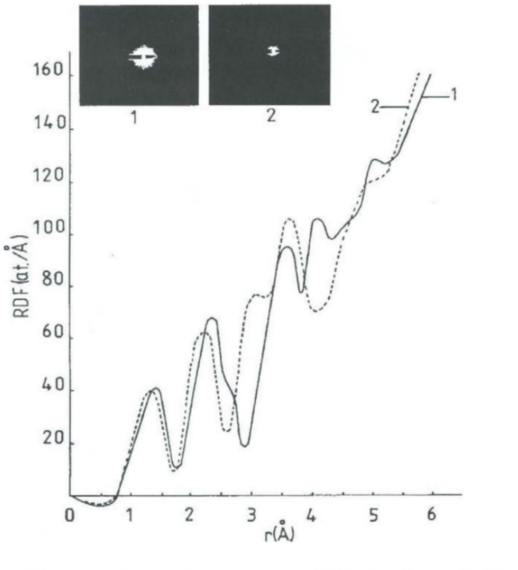

RDF curves for powdered samples of (1) B_2O_3 glass and (2) B_2O_3. 4 TeO_2 glass (After Bursukova et al, 1995).

Figure 2.9: (from Rao (2002)) RDF $\rho_0 4\pi r^2 g\left(r\right)$ of vitreous $\mathrm{B_2O_3}$ from ES.

2.1.2 NMR and vibrational spectroscopy

We mention here, for completeness, two other basic experimental methods that have been traditionally used in the investigation of the structure of glasses: NMR and optical vibrational (IR) spectroscopy. The physical principles and experimental setup of apparatus of each are treated in standard physical chemistry textbooks. Here we will only show some examples of how they are exploited for deriving other glass structural parameters than $g(r)$, such as bond angles or rings.

2.1.2.1 NMR

In a nutshell:

- Nuclei that are active in NMR (^{13}C, ^{31}P, ^{29}Si, ^{77}Se, ...) have a magnetic momentum
- Interaction of this momentum with an external magnetic field, and with momentum of neighbouring atoms, causes a splitting of energy levels which is probed with electromagnetic radiation
- *Chemical shift*s, which represent the perturbation due to neighbouring atoms, give information about the molecular environment of active nuclei.
- In a liquid or disordered solid an *isotropic shift*, an average scalar value, is observed

E. g. in silica the hexacoordinate group $\mathrm{SiO}_6 \rightarrow -180 \div -220$ ppm; while the tetracoordinate $\mathrm{SiO}_4 \rightarrow -65 \div -120$ ppm (Source: Leonova (2009)).

The following slides have been borrowed from a seminar by Micoulaut (2013)

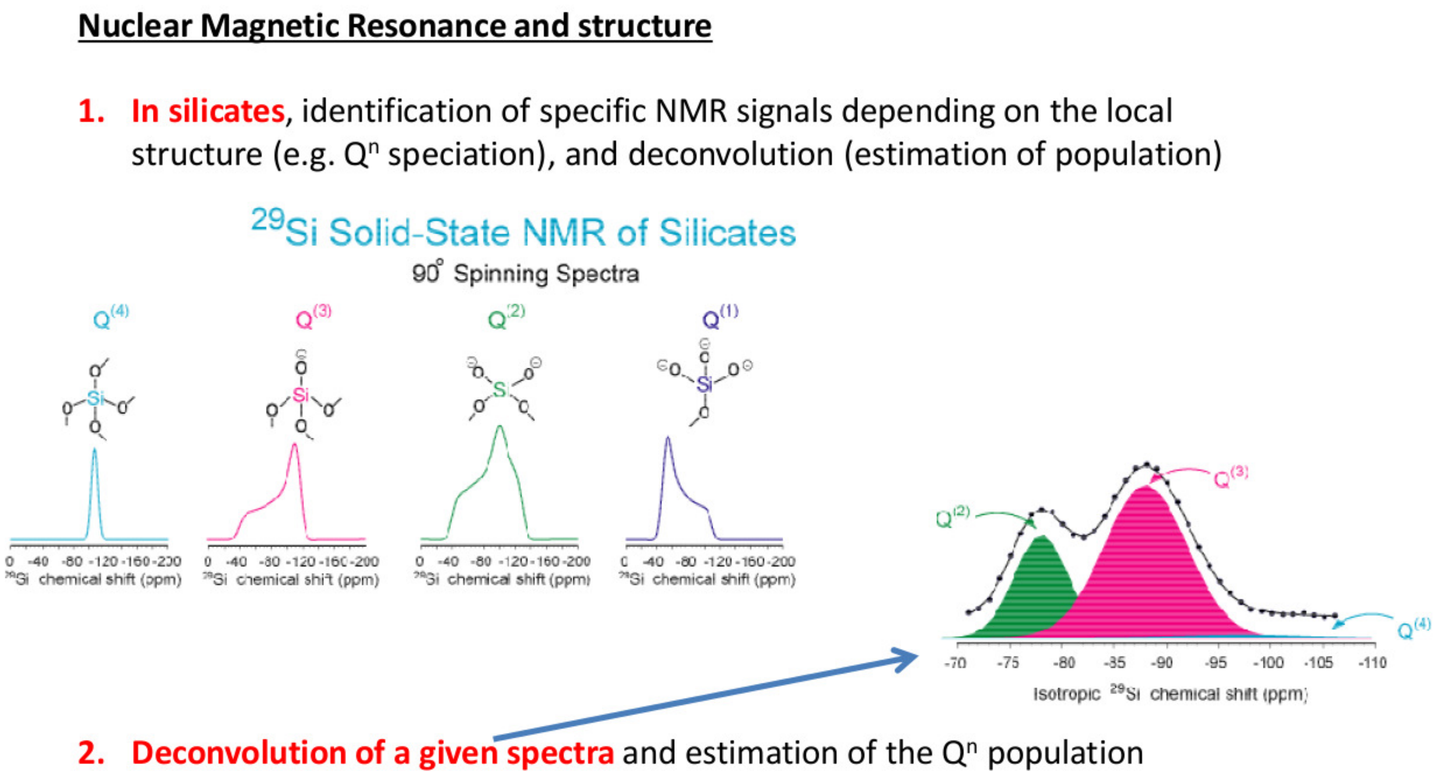

Nuclear Magnetic Resonance and structure

1. **In silicates**, identification of specific NMR signals depending on the local structure (e.g. Q^n speciation), and deconvolution (estimation of population)

2. **Deconvolution of a given spectra** and estimation of the Q^n population

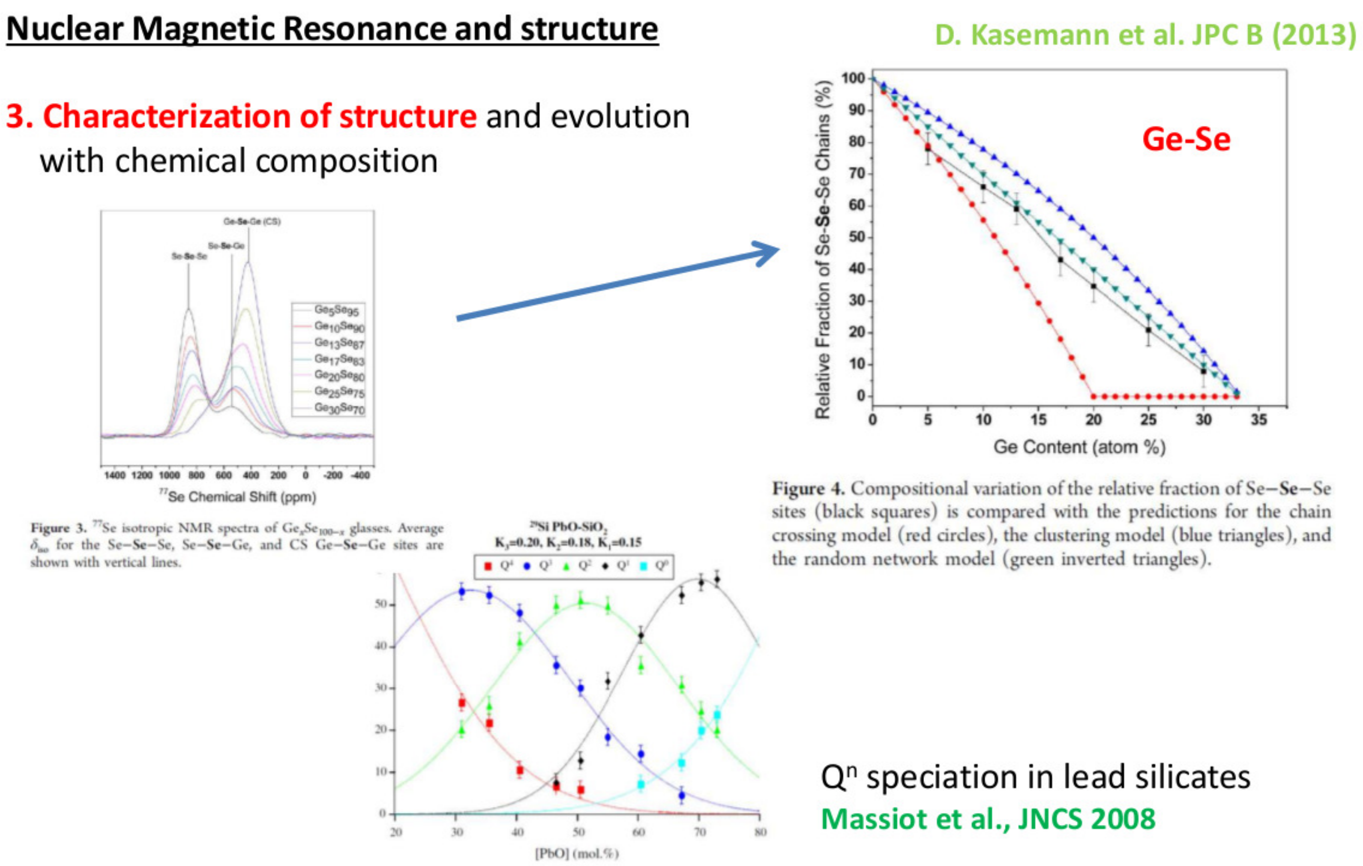

Nuclear Magnetic Resonance and structure

D. Kasemann et al. JPC B (2013)

3. Characterization of structure and evolution with chemical composition

Figure 3. ^{77}Se isotropic NMR spectra of Ge_xSe_{100-x} glasses. Average δ_{iso} for the Se−**Se**−Se, Se−**Se**−Ge, and CS Ge−**Se**−Ge sites are shown with vertical lines.

Figure 4. Compositional variation of the relative fraction of Se−**Se**−Se sites (black squares) is compared with the predictions for the chain crossing model (red circles), the clustering model (blue triangles), and the random network model (green inverted triangles).

Q^n speciation in lead silicates

Massiot et al., JNCS 2008

2.1.2.2 Vibrational spectroscopy

There are two main types of optical vibrational spectroscopy:

- InfraRed (IR) is due to the interaction between electromagnetic radiation and the change in the *electric dipole* of a molecule associated to a vibration
- Raman is due to interaction between electromagnetic radiation and the change of molecular *polarizability* associated to a vibration

Both techniques reveal the *nature* and *geometry* of chemical bonds in the system. Molecular vibrations commonly involve a small group of neighbouring atoms, the arrangement of which can be inferred from the spectra.

Again, we borrow a few examples from Micoulaut (2013):

Raman spectroscopy and probe of glass structure

Raman spectra of vitreous SiO_2 (silica)

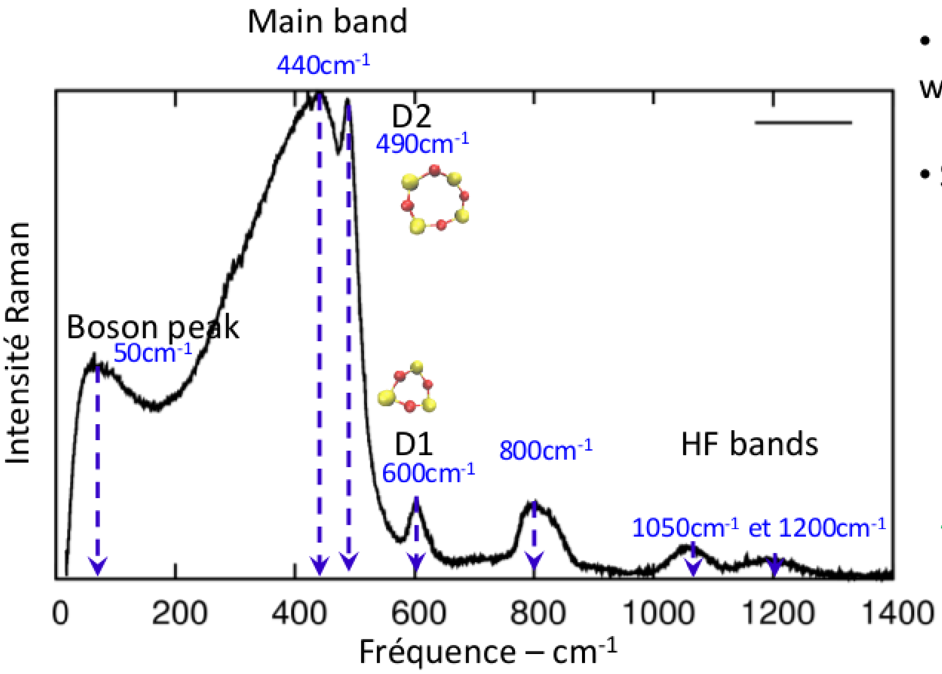

- « *Boson peak* » at low frequency.
- Main band at 440 cm^{-1} together with a shoulder peak D2
- Shoulder at D1 (600 cm^{-1}).

T. Deschamps, 2009

Raman spectroscopy and probe of glass structure

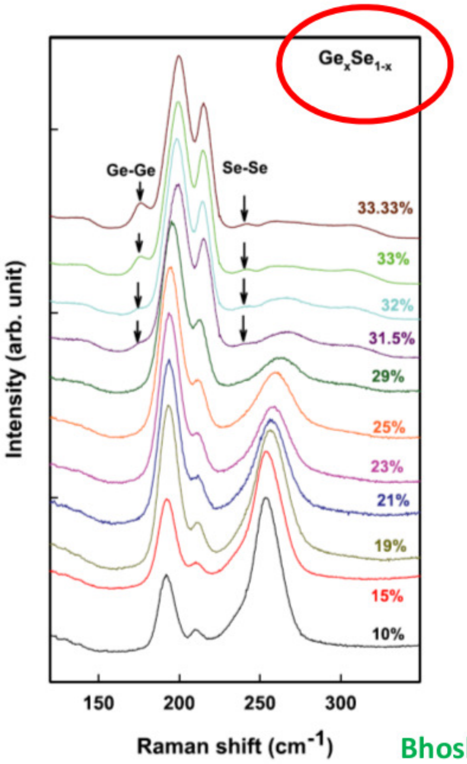

Bhosle et al. IJAGS 2012

☐ Measure of spectral changes with composition

☐ Gaussian decomposition of the main lines

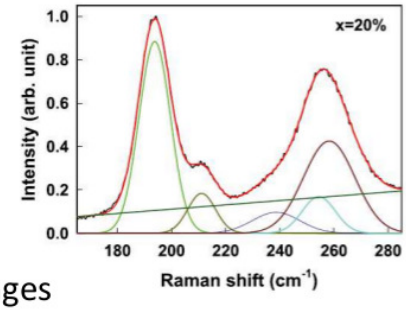

☐ Analysis of structural changes

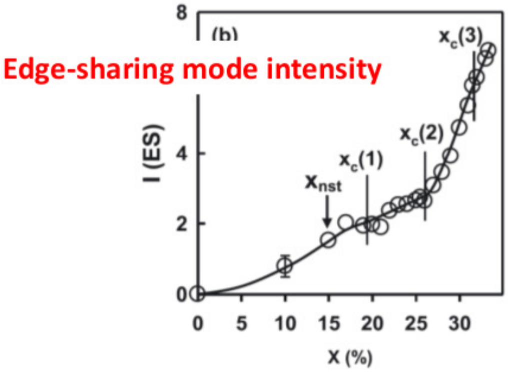

2.1.3 Reference texts for section §2.1

This section is based on Cusack (1987), chapter 3 "Investigation of disordered structures", with additions from Rao (2002), chapter 4 "Structural Techniques". Examples are taken from the same books; from a lesson by Matthieu Micoulaut (Micoulaut (2013), lesson 2); and from Leonova (2009). A good description of diffraction geometry -though one limited to crystals- is also in Alonso and Finn (1982), section 23.8.

2.2 Computational methods

2.2.1 Empirical force fields

The simulation methods whose main features we will describe in the next two sessions[4] share a common foundation: a reasonably accurate, and computationally accessible, representation of the forces acting on particles.

When modelling the interaction field in a solid, two approaches can be taken:

- The system can be treated within the framework of quantum mechanics (QM), using *ab initio* or semiempirical methods. Although these are the most accurate methods available, they are extremely demanding in terms of computational resources; the more so, if the simulated system is made up a large number (tens of thousands at least) of atoms, as is necessarily the case with an intrinsically disordered system like a liquid or glass.

- Or, the interactions can be represented in a simple analytical form, which is a function of the particles' classical dynamical variables, coordinates and velocities, and contains partially adjustable parameters that can be fitted to *ab initio* results and/or to measured properties. In addition to being less resource-consuming, this *empirical field* approach is also more readily understood by researchers, who can picture the meaning of the functions and parameters used and possibly adjust them.

It is useful to review some aspects of the latter approach, the empirical field.

If we consider two rare gas atoms, their interaction can be modelled with a function depending on the (scalar) interatomic separation r, that approaches infinity at small distance, and whose limit is zero at high values of r (figure 2.10). There is an energy minimum at the atom-atom contact distance r^*_{AB}; for $r > r^*_{AB}$ the force is attractive, while it is increasing repulsive for $r < r^*_{AB}$. There are a number of analytical forms for this, for example the Lennard-Jones function

$$V\left(r\right) = 4\epsilon\left(\left(\frac{\sigma}{r}\right)^{12} - \left(\frac{\sigma}{r}\right)^{6}\right) \tag{2.8}$$

where ϵ is the minimum depth and σ corresponds to the zero of the potential energy function (see figure 2.10). (Also sketched in the figure is the oversimplified *hard sphere* model, mainly employed in theoretical models, which includes no attraction term).

The parameters in equation (2.8) depend on the atomic species involved. To each couple of atom species (i, j) a set of parameters is associated: in the Lennard-Jones expression $(\epsilon_{ij}, \sigma_{ij})$.

---

[4] but not the Reverse Monte Carlo method that will be presented at the end of the chapter

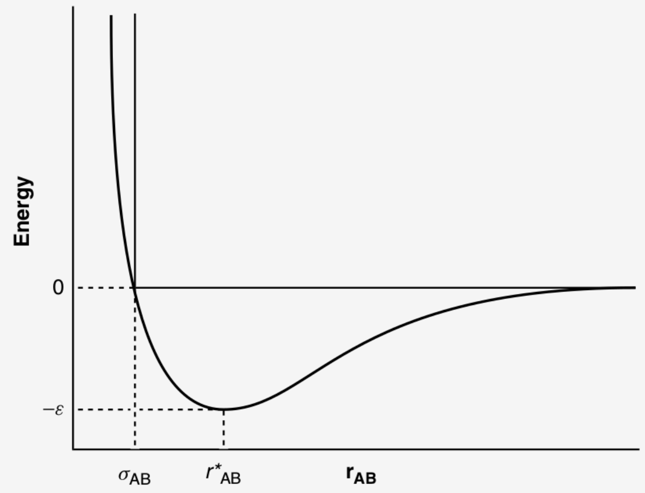

Non-attractive hard-sphere potential (straight lines) and Lennard–Jones potential (curve). Key points on the energy and bond length axes are labeled

Figure 2.10: atom-atom interaction potential (Cramer (2004))

In systems made up of molecules, single atoms interact in different manners. It is convenient to consider interactions between **bonded** and **non-bonded** atoms separately: the former include internal bond distances, angles, and torsions (dihedrals); the latter act between atoms either belonging to different molecules, or belonging to the same molecule but being placed more than 3 bonds apart. Non-bonded interactions are both of dispersive-repulsive (Van der Waals), and electrostatic nature.

The analytical expression may be, for example

$$\mathcal{V}(\mathbf{r}^N) = \sum_{\text{bonds}} \frac{k_i}{2}(l_i - l_{i,0})^2 + \sum_{\text{angles}} \frac{k_i}{2}(\theta_i - \theta_{i,0})^2 + \sum_{\text{torsions}} \frac{V_n}{2}(1 + \cos(n\omega - \gamma))$$
$$+ \sum_{i=1}^{N} \sum_{j=i+1}^{N} \left(4\varepsilon_{ij}\left[\left(\frac{\sigma_{ij}}{r_{ij}}\right)^{12} - \left(\frac{\sigma_{ij}}{r_{ij}}\right)^{6}\right] + \frac{q_i q_j}{4\pi\varepsilon_0 r_{ij}}\right)$$

where the first three terms account for bond distances, angles and torsions; the double sum in the second line is extended to all "non-bonded" atoms, and contains the Van der Waals potential (compare equation (2.8)), and the electrostatic potential.

Bond distance and angle potentials have a harmonic form. The torsional term has the following behaviour:

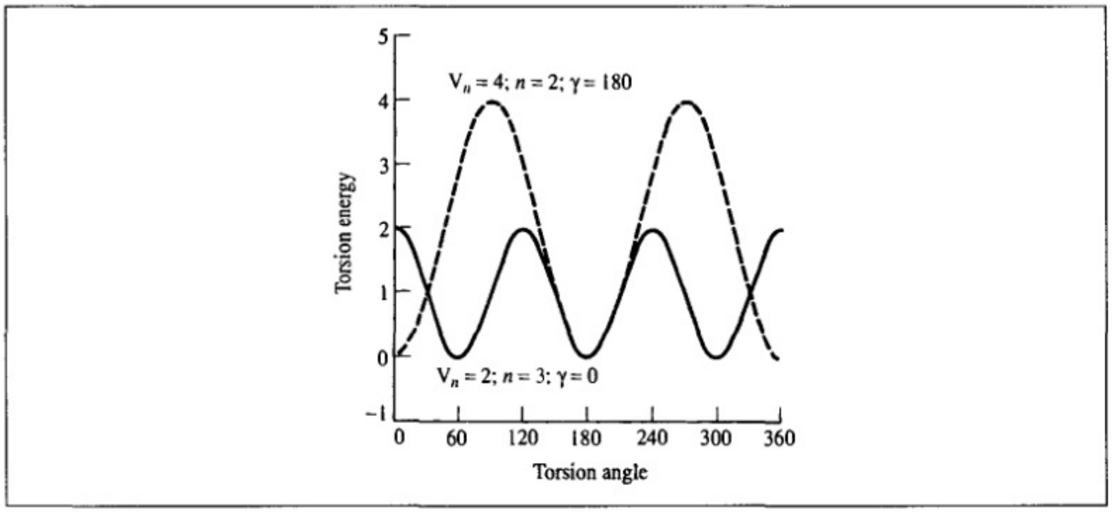

Fig. 4.7: Torsional potential varies as shown for different values of V_n, n and γ.

Many glass-forming materials (e.g. $\mathrm{AX_2}$ with $\mathrm{A = Si, Ge}$ e $\mathrm{X = O, S, Se, Te}$) do not feature separate molecules, but instead an extended network of $\mathrm{A - X}$ bonds with **mixed ionic-covalent character**.

In **purely ionic** compounds only non-bonded interactions are in effect; the potential energy contains only the three terms electrostatic, repulsive and dispersive, where the repulsive term can have an exponent $n < 12$:

$$\mathscr{V} = \sum_{i=1}^{N} \sum_{j=i+1}^{N} \left(\frac{q_i q_j}{4\pi\epsilon_0 r_{ij}} + \frac{A}{r_{ij}^n} - \frac{C}{r_{ij}^6} \right)$$

In a **purely covalent** solid, bonded interactions dominate; however in order to model such a solid with bonded interactions only, one must know *a priori* the complete, detailed map of interatomic bonds, which obviously is not available in a disordered system.

Thus, in mixed ionic-covalent glasses a non-bonded potential is used, that allows for bond forming and breaking; it may include, in addition to the pair term, a three-body term which represents the non-harmonic angle interaction:

$$\mathscr{V} = \sum_{i=1}^{N} \sum_{j=i+1}^{N} \mathscr{V}_{ij}\left(r\right) + \sum_{i=1}^{N} \sum_{j=i+1}^{N} \sum_{k=j+1}^{N} \mathscr{V}_{ijk}\left(r, r', \theta\right)$$

***Example**: simulations of* SiO_2 *in different crystal phases and in the glass phase (Vashishta et al. 1990)*

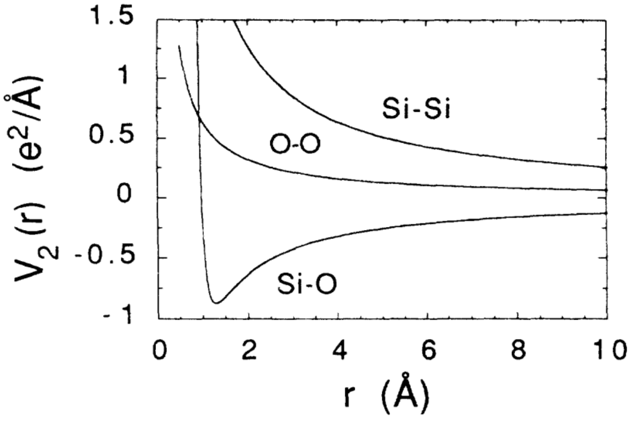

Si-Si, Si-O, and O-O contributions to the two-body part of the interaction potentials, Eq. (2), for SiO_2. Total interaction potential is a sum of two-body, Eq. (2), and three-body contributions, Eq. (3). Unit of length is Å and of energy $e^2/\text{Å} = 14.39$ eV.

$$V_2 = \frac{H_{ij}}{r^{\eta_{ij}}} + \frac{Z_i Z_j}{r} - \frac{\frac{1}{2}(\alpha_i Z_j^2 + \alpha_j Z_i^2)}{r^4} e^{-r/r_{4s}} , \qquad (2)$$

$$V_3 = B_{jik} f(r_{ij}, r_{ik}) p(\theta_{jik}, \bar{\theta}_{jik}) , \qquad (3)$$

	Z	α
Si	1.60	0.00
O	−0.80	2.40
	η	H
Si-Si	11	0.057
Si-O	9	11.387
O-O	7	51.692

	B	l	$\bar{\theta}$	r_0
A-X-A	1.40	1.0	141.00	2.60
X-A-X	0.35	1.0	109.47	2.60

As you can see from the example above, the potential parameters like q_i, σ_{ij}, ϵ_{ij}, A, C, etc., are not specific of every single atom but, in order to be physically meaningful, they are a property of an atomic species of species pair (Si, O, etc.):

As a rule, such parameters *cannot* be safely exported from a substance to another; in different substances they have similar, but not identical, values. These values are fitted to *ab initio* calculations and measured properties.

2.2.2 Monte Carlo simulation

In a Monte Carlo (MC) simulation, a statistical sample of the system's microscopic configurations is collected in accordance with the thermodynamical state of the system, in order to compute average properties.

2.2.2.1 Thermodynamical averages

The basic principle of statistical mechanics is that the observed system is an average over the statistical ensemble of all microscopically defined copies of the system that are compatible with the macroscopical variables, such as volume and temperature, that define its thermodynamical state.

For example, a closed system at constant V and T is represented by the so-called *canonical ensemble* (or "(N, V, T)" ensemble):

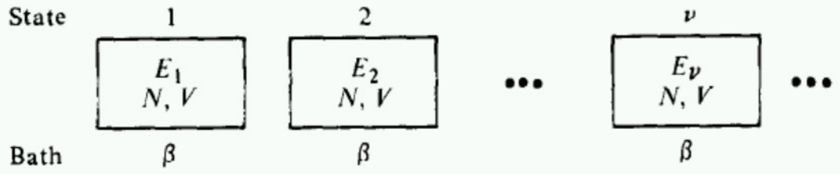

Fig. 3.2. Assembly of states for a closed system in a heat bath.

Figure 2.11: The canonical, or (N, V, T), ensemble); ($\beta = \frac{1}{k_B T}$)

In these thermodynamical conditions, the total energy of the system is *not* fixed, but is exchanged between the system and the thermostat. The probability of seeing microscopic state i with energy E_i is

$$p_i \quad \propto \quad \exp\left(-\frac{E_i}{k_B T}\right) \tag{2.9}$$

and the average of a macroscopical quantity A whose value in state i is A_i is the weighted average

$$\langle A \rangle = \frac{\sum_i p_i A_i}{\sum_i p_i} = \frac{\sum_i A_i \exp\left(-\frac{E_i}{k_B T}\right)}{\sum_i \exp\left(-\frac{E_i}{k_B T}\right)} \tag{2.10}$$

For example, in a perfect gas the total energy $\langle E \rangle = \frac{3}{2} N k_B T$

In general, $\langle A \rangle$ can be computed by correctly sampling the ensemble of states i.

2.2.2.2 How MC works

The steps in a MC simulation can be summarized as follows

1. setup:
    - prepare a conveniently sized system of N particles in a container of volume V (typically, $N \sim 10^4$ atoms), by assigning atom positions in an acceptable configuration
    - select a force field expression and parameters (for example 2.2.1)
    - compute the initial energy E_0
2. randomly generate a new configuration (new atom positions);
3. compute the energy E_i of the new configuration and compare it to the previous value of energy
4. add the new configuration to the statistical sample only if it meets a predefined criterion (usually, the Metropolis criterion), chosen so that the sample will build up the correct statistics 2.9;
5. repeat from step 2 until the desired number of steps is completed. The sample is now ready for computing averages.

A critical point in this scheme is how the new configurations are generated. Although this may be not immediately apparent to the reader, **only an extremely small fraction of the theoretically possible configurations give a nonnegligible contribution to the statistics**. To give a feeling of what this means: it can be shown (Frenkel and Smit (2002)) that in a system of 100 hard spheres near the freezing point only one out of 10^{260} configurations has a finite (that is, not infinite) energy and has a nonzero weight. Clearly, a device is needed to avoid wasting all our time in generating instances that will be discarded anyway. The technique of sampling an ensemble more efficiently in those regions that are statistically more important is called **importance sampling**.

The basic idea in MC is that, due to the fact that the potential energy is a well-behaved function of the particle positions, if one starts with an acceptable configuration, not far from the energy minimum which is the probability maximum, and then moves by a “small” step (see figure 2.12), the resulting state will probably have a finite probability too. The step should be small enough to keep the system in an acceptable zone, yet it should be large enough to ensure an efficient sampling of the configurational space.

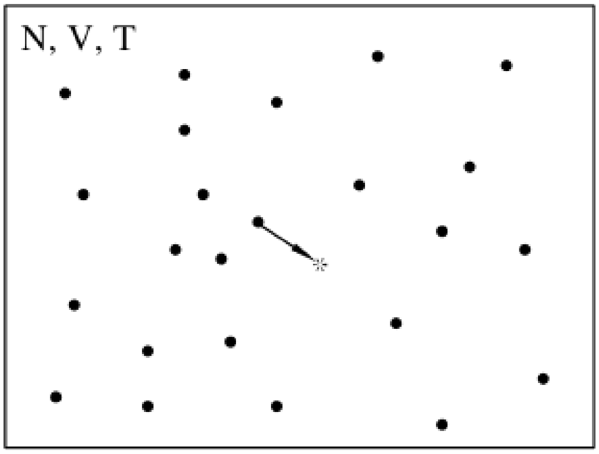

Figure 2.12: A Monte Carlo move (from Frenkel and Smit (2002))

A well-known, and very effective, representation of such ***random walk*** sampling technique is depicted in figure 2.13: if one needs to measure the average -say- pollutant content of river waters, it is best to sample it along the river, not on a regular grid!

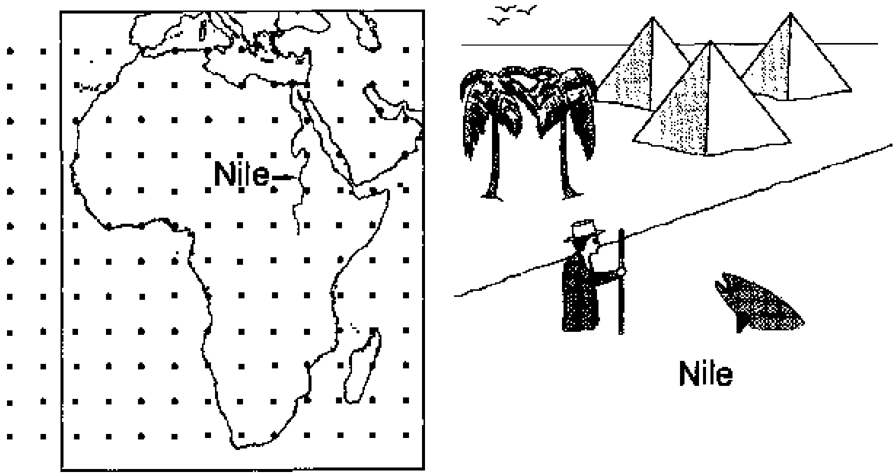

Figure 3.1: Measuring the depth of the Nile: a comparison of conventional quadrature (left), with the Metropolis scheme (right).

Figure 2.13: (from Frenkel and Smit (2002))

2.2.2.3 Energy barriers and the cooling process

The above scheme works reasonably well as long as the system is capable of exploring all the *important* configurations. A critical situation, however, is when the energy profile of the system features two minima separated by a high barrier (figure 2.14): in this case, if started from the local, as opposed to the global, minimum (the one to the left in the figure), it may not have the chance of reaching the global minimum (right), as this would involve passing through intermediate steps at high energy and low probability which will be rejected by the algorithm. Note that both the length scale of the move and the value of temperature are key elements here; the lower the T, the more unlikely it will be for the simulation to traverse the barrier (recall the probability 2.9).

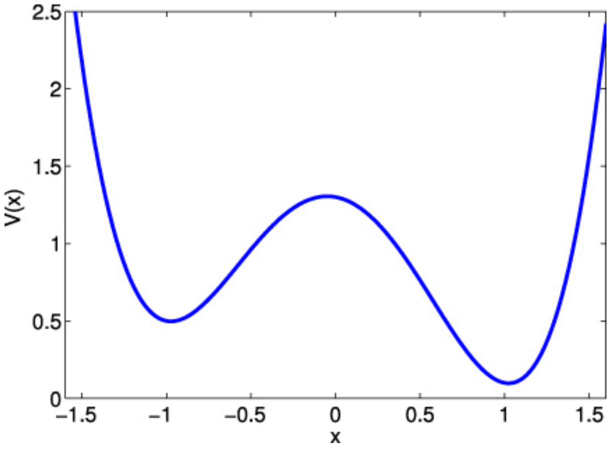

Figure 2.14: Potential energy with two wells separated by a barrier

Consider the cooling process of a liquid. One can think of the potential energy "landscape" as a roughly shaped profile crowded with local minima, with the crystal corresponding to a narrow and deep global minimum (see figure 2.15). At high temperature (left panel in the figure), the system's kinetic energy allows it to explore the whole configurational space; obviously, "high" temperature means that k_BT is large with respect to the depth of the minimum. On cooling, the system is gradually confined to the lower-energy portions of the space; until, at the melting temperature, only the crystal configuration remains accessible. If cooling is instantaneous, however, the system will get "trapped" in one local minimum close to its momentary configuration (any one of the partially filled wells in the right panel): it will then exhibit solid properties (restricted displacement), but be freezed in a liquid-like structure - that we now know is exactly the state of a glass.

C.P. Royall, S.R. Williams / Physics Reports 560 (2015) 1–75 13

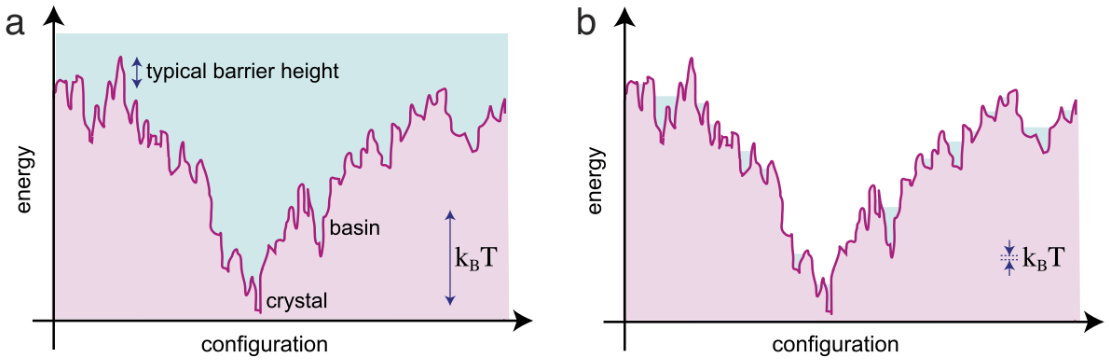

Fig. 9. A schematic illustration of the potential energy landscape. The x-axis represents configurations of all $3N$ coordinates. (a) High temperature liquid, the typical barrier height is less than the thermal energy, and all configurations can be accessed as indicated in blue. (b) Low temperature glass. The barrier height between basins is now much higher than k_BT, and the system is no longer able to explore all configurations and has become a glass but can only access local states, as indicated by the blue shading. (For interpretation of the references to colour in this figure legend, the reader is referred to the web version of this article.)

Figure 2.15: a system with a "ragged" potential profile and the regions of visited configurations at high and low temperature (from Royall and Williams (2015))

In MC, due to the dimensional limits of the simulation, configurational trapping is routine, and special techniques have been devised in order to constantly keep the system capable of exploring all of the configurational space (see for example Rauscher et al. (2009)). The bottom line is that when simulating the cooling of a liquid substance with MC it is extremely likely that it will transition to a glassy solid, although not necessarily the experimental glass.

2.2.2.4 computation of $g\left(r\right)$

As an example of how an observable quantity is computed in MC, let us consider the cross pair distribution function of a binary substance 1.4 :

$$g_{AB}\left(r\right)=\frac{\left\langle n_{AB}\left(r\right)\right\rangle}{\rho_B}$$

The two quantities are evaluated from the MC ensemble averages:

$$g_{AB}\left(r\right) = \frac{\left\langle n^{AB}\left(r,\Delta\right)\right\rangle}{n^{AB}\left(r,\Delta\right)_{unc}} = \frac{\frac{1}{T}\frac{1}{N_A}\sum_{t=1}^{T}\sum_{i=1}^{N_A}N_{it}^{AB}\left(r,\Delta\right)}{\rho_B 4\pi r^2\Delta}$$

with

$N_{it}^{AB}\left(r,\Delta\right)$ = number of type B atoms whose distance from A-type atom i is between r and $r+\Delta$, at simulation step t of T

N_A = total number of type A atoms

ρ_B = number density of type B atoms

Some typical results are shown in figure 2.16

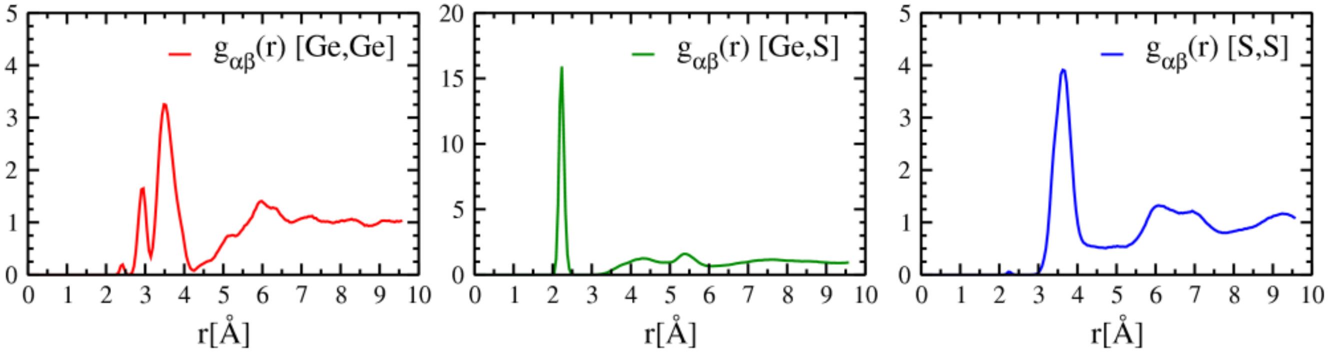

Figure 2.16: $g^{AB}(r)$ in amorphous $\mathrm{GeS_2}$ at $300\ K$, from MC simulation (ISAACS 2013)

2.2.3 Molecular Dynamics simulation

As the name suggests, with Molecular Dynamics methods the dynamical evolution of the system is simulated; this is done by numerically solving the system's equations of motion.

We will only consider MD in classical dynamics.

2.2.3.1 Phase space averages

In classical mechanics, the state of a many-body system is defined by the value of continuous variables momentum ($\boldsymbol{p}$) and position($\boldsymbol{q}$) of each particle. The domain $\{\boldsymbol{p},\boldsymbol{q}\}$ of these variables is a hyperspace called *phase space*. Energy, that in a quantum mechanical framework would take discrete values E_i, is classically a continuous function of the phase space variables:

$$E_i \rightarrow E\left(\boldsymbol{p},\boldsymbol{q}\right)$$

Accordingly, the average of some observable A (which depends on the dynamical state) in the (N,V,T) ensemble is

$$\langle A\rangle = \frac{\int A\left(\boldsymbol{p},\boldsymbol{q}\right)\exp\left(-\frac{E(\boldsymbol{p},\boldsymbol{q})}{k_BT}\right)d\boldsymbol{p}d\boldsymbol{q}}{\int \exp\left(-\frac{E(\boldsymbol{p},\boldsymbol{q})}{k_BT}\right)d\boldsymbol{p}d\boldsymbol{q}}$$

Compare the last equation to equation (2.10). More generally, if the probability of phase space point is $P\left(\boldsymbol{p},\boldsymbol{q}\right)$, the phase space average of A is

$$\langle A\rangle = \frac{\int A\left(\boldsymbol{p},\boldsymbol{q}\right)P\left(\boldsymbol{p},\boldsymbol{q}\right)d\boldsymbol{p}d\boldsymbol{q}}{\int P\left(\boldsymbol{p},\boldsymbol{q}\right)d\boldsymbol{p}d\boldsymbol{q}} \tag{2.11}$$

In MD, the aim is to follow the system's evolution, or *trajectory in phase space*, for a long enough time to allow it to explore all the accessible regions of phase space with the correct probability. System "snapshots" (positions and velocities) are recorded at some defined interval, and phase space averages (2.11) are computed from the recorded trajectory.

2.2.3.2 How MD works

In classical physics, positions and momenta (or velocities) of an *isolated* collection of particles can be known at any time t if we know their values at the initial time $\{\boldsymbol{p}_i\left(0\right),\boldsymbol{q}_i\left(0\right)\}$and the force acting on each particle i, which in turn, in conservative systems, is the gradient of the potential energy:

$$\boldsymbol{F}_i = -\boldsymbol{\nabla}_iV$$

In a Molecular Dynamics simulation the potential energy V is the sum of particle interactions, expressed with a formula like (2.10). The equations of motion, which are differential equations, are solved numerically, with the help of approximate methods in which the time differential is replaced by a small time step Δt; for example (Euler's approximation):

$$\begin{aligned}\boldsymbol{q}_i\left(t+\Delta t\right) &\approx \boldsymbol{q}_i\left(t\right)+\frac{\boldsymbol{p}_i\left(t\right)}{m_i}\cdot\Delta t\\ \boldsymbol{p}_i\left(t+\Delta t\right) &\approx \boldsymbol{p}_i\left(t\right)+m_i\boldsymbol{a}_i\left(t\right)\cdot\Delta t\end{aligned}$$

where

$$\boldsymbol{F}_i\left(t\right) = m_i\boldsymbol{a}_i\left(t\right)$$

It must be noted that in a Molecular Dynamics simulation the total energy E of the system is conserved. Thus, it may be viewed as a "Monte Carlo" simulation in which the importance sampling method is the dynamical trajectory of the system and the statistical ensemble is the (N,V,E), or *microcanonical*, ensemble.

Typical dimensions of a MD simulation are:

number of atoms	~ 1000
time step (Δt)	$\sim$ 10fs
total simulation length	1ns $\div$ 1μs

2.2.3.3 Non-ergodic systems

If the simulation is carried for a sufficiently long time, the system can be assumed to have sampled all phase space. In this case

$$\text{time average} \quad = \quad \text{statistical average}$$

where the time average is

$$\overline{A} = \frac{1}{M} \sum_{1}^{M} A\left(t_i\right)$$

or, in the limit of continuous sampling of variable t:

$$\overline{A} = \frac{1}{T} \int_{0}^{T} A\left(t\right) dt$$

Such a system is called **ergodic**.

Not all systems may be safely assumed to be ergodic. As a typical non-ergodic model, let us consider the double-well potential of figure 2.14 again. The simulation time may be not long enough for the system started from the local minimum to the left to meet a state which is capable of crossing the barrier and reach the global minimum to the right.

Glasses are non-ergodic materials.

In the complex energy landscape depicted in figure 2.15, a system possessing sufficient kinetic energy (which is to say, a high enough value of $k_B T$) will explore all the phase space in the laboratory time scale, but if cooled suddenly may get freezed in a local energy minimum, that corresponds to a liquid structure, thus becoming a glass. Again, this is what normally happens in a simulation, where cooling speeds are of the order of $10^{13} K/s$. A MD liquid, when cooled, will not crystallize, but will invariably become a glassy solid, unless specialized methods are used.

2.2.3.4 Time dependent quantities

Since a MD simulation follows the real time evolution of the system, time-dependent quantities may be computed. This is a major difference from MC simulations.

For example, the diffusion coefficient D is defined by *Fick's first law* D as the linear coefficient between the particles' flux $\boldsymbol{j}$ and the concentration gradient$\boldsymbol{\nabla} c$:

$$\boldsymbol{j} = -D \boldsymbol{\nabla} c$$

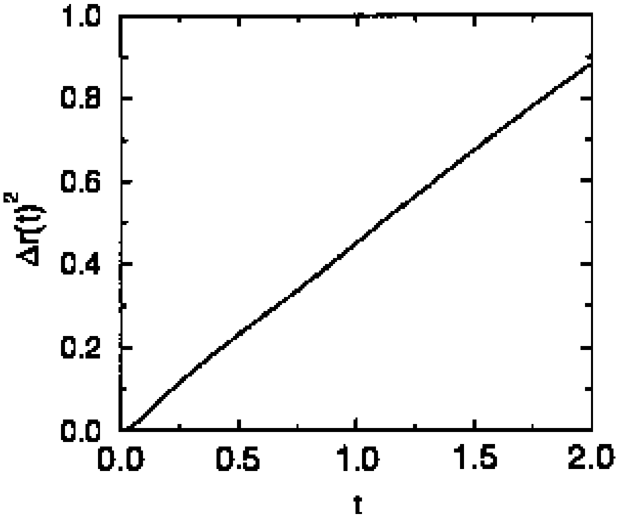

Figure 2.17: time dependence of the single particle mean squared displacement in a MD simulation (from Frenkel and Smit 2002)

From statistical mechanics we know that D is connected to the mean squared displacement of a single particle:

$$6D = \frac{\partial \left\langle \Delta^2 r\left(t\right)\right\rangle}{\partial t}$$

The function $\Delta^2 r\left(t\right)$ can be computed from a MD trajectory, and from its limiting slope (the time derivative) the diffusion coefficient is obtained.

A slightly more complicated example is offered from the time evolution of the PDF. A generalized $g\left(r\right)$ is the *particle self-correlation* (van Hove) function:

$G_s\left(\boldsymbol{r}, t\right) =$	probability of finding a particle in $\boldsymbol{r}$ at time t, if *the same particle* was in $\boldsymbol{r} = \boldsymbol{0}$ at time 0
$4\pi r^2 G_s\left(r, t\right) dr =$	probability that a particle travels a distance between r e $r + dr$ in time t

- In liquids, for $t \to \infty$, $G_s(r;t)$ tends to a gaussian of width Dt (that is, it broadens tending to the constant value 0)
- In solids, , for $t \to \infty$, $G_s(r;t)$ tends to some fixed, nonzero distribution.

2.2.4 Comparison between MC and MD

Let us now summarize the key points.

In its original definition, a Monte Carlo computation is performed at constant T and samples the (N, V, T) ensemble, while a Molecular Dynamics simulation is performed at constant E and samples the (N, V, E) ensemble. In principle, this is somehow a limitation of MD, because in a laboratory it is easier to control T than E.

However, both methods have later been extended and refined. MD simulations schemes in the (N, V, T) e (N, p, T) ensembles are quite popular now.

A major difference between the two techniques is that, as we have already remarked, time-dependent quantities can be computed from MD only.

As for structural properties, when the same force field is employed MD and MC, in the limit of infinite simulations, they should give the same results.

2.2.4.1 Computer simulation of glasses

To simulate a glassy substance, the technique of choice is Molecular Dynamics in the (N, p, T) ensemble. Through MD one can investigate all the dynamical behaviour of the system, which -as we have seen in the introduction- is a fundamental feature of liquid-to-glass transition.

A MD simulation of a glass follows this scheme:

- a high T (e.g. $3000K$) trajectory is performed for a standard amount of system time ($\sim 100ps$); the substance is liquid
- starting from the last configuration, a new trajectory is started at a lower T (e.g. $2000K$)
- this cycle is repeated at increasingly low temperatures

With this procedure the effective cooling velocity is of the order of $\frac{1000K}{10^{-10}s} = 10^{13}K/s$, much faster than any attainable in the laboratory ($\leq 100K/s$).

The transition of the simulated system to glassy state is marked by a structural "arrest" that can be followed through time-dependent quantities such as time correlation of particle positions, diffusion coefficient, etc.

As noted earlier, almost all simulated liquids form a glass when cooled, even though only few of them do so in the laboratory; they are "computer glasses". Conversely, a substance that undergoes the glass transition in experimental conditions (for example, $\mathrm{SiO_2}$) will also do so in simulation.

2.2.5 Examples of computational studies

Complete superposition of $g(r)$ computed with MC and MD, and excellent agreement of both with experimental data of liquid Ar, is seen in this early study (from Cusack 1987)

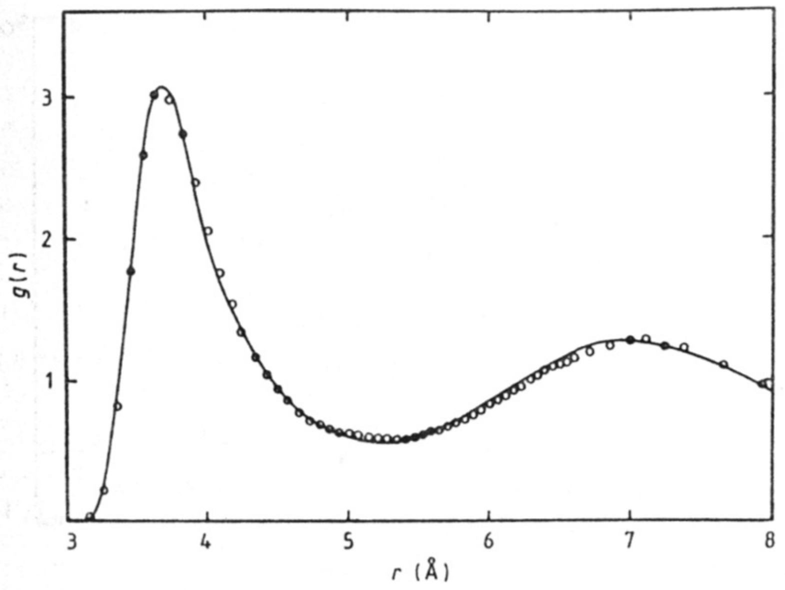

Figure 4.3 $g(r)$ for Ar at 85 K, $n_0 = 0.02125$ atoms Å^{-3}. Full curve, experimental results; circles, MC values. The MD values are indistinguishable on this scale from the MC values (see Ree and Hoover 1967, Erpenbeck and Wood 1984). (From Yarnell *et al* 1973.)

Figure 2.18: observed and computed $g\left(r\right)$ of liquid Ar

The following figures (from slides by Micoulaut (2013)) show how PDFs from simulations can (or cannot) reveal structure changes with temperature or pressure:

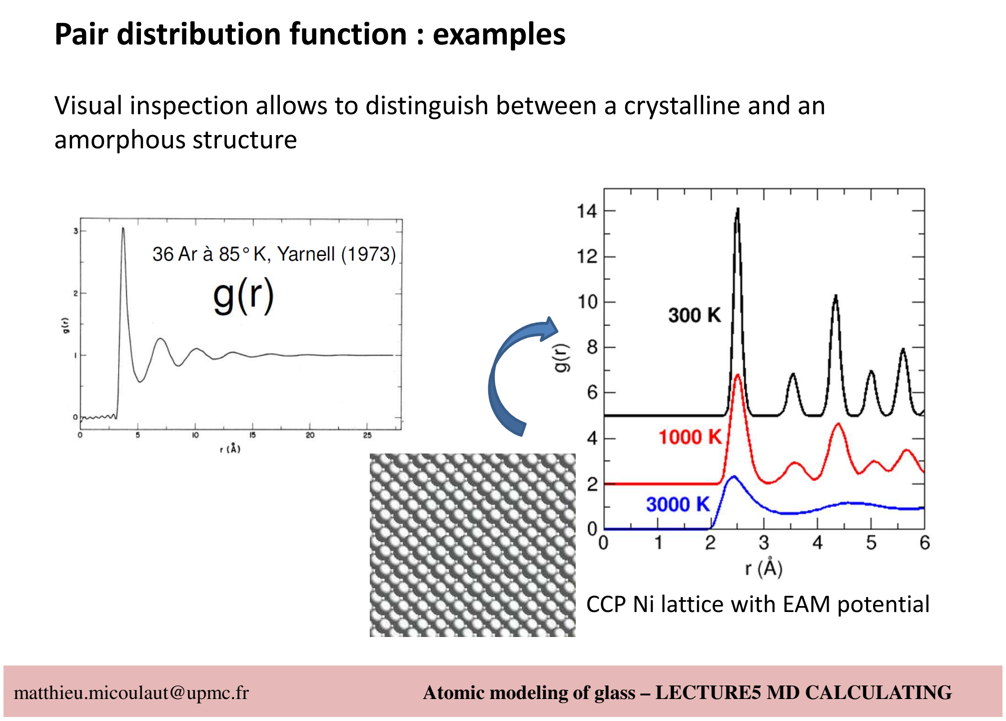

Pair distribution function : examples

Visual inspection allows to distinguish between a crystalline and an amorphous structure

CCP Ni lattice with EAM potential

matthieu.micoulaut@upmc.fr **Atomic modeling of glass – LECTURE5 MD CALCULATING**

Figure 2.19: Structure of Ni from computations (from Micoulaut (2013))

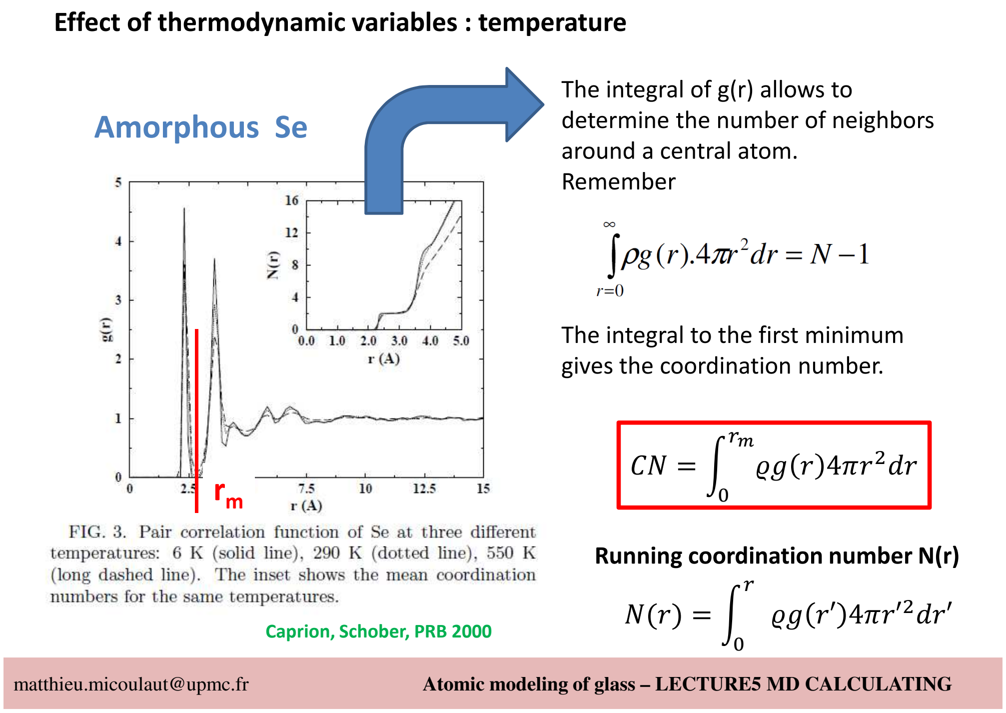

Effect of thermodynamic variables : temperature

Amorphous Se

FIG. 3. Pair correlation function of Se at three different temperatures: 6 K (solid line), 290 K (dotted line), 550 K (long dashed line). The inset shows the mean coordination numbers for the same temperatures.

Caprion, Schober, PRB 2000

The integral of g(r) allows to determine the number of neighbors around a central atom.
Remember

$$\int_{r=0}^{\infty} \rho g(r).4\pi r^2 dr = N-1$$

The integral to the first minimum gives the coordination number.

$$\boxed{CN = \int_0^{r_m} \varrho g(r) 4\pi r^2 dr}$$

Running coordination number N(r)

$$N(r) = \int_0^{r} \varrho g(r') 4\pi r'^2 dr'$$

matthieu.micoulaut@upmc.fr **Atomic modeling of glass – LECTURE5 MD CALCULATING**

Figure 2.20: temperature dependence of $g(r)$ and second-shell coordination number in amorphous Se (from Micoulaut (2013))

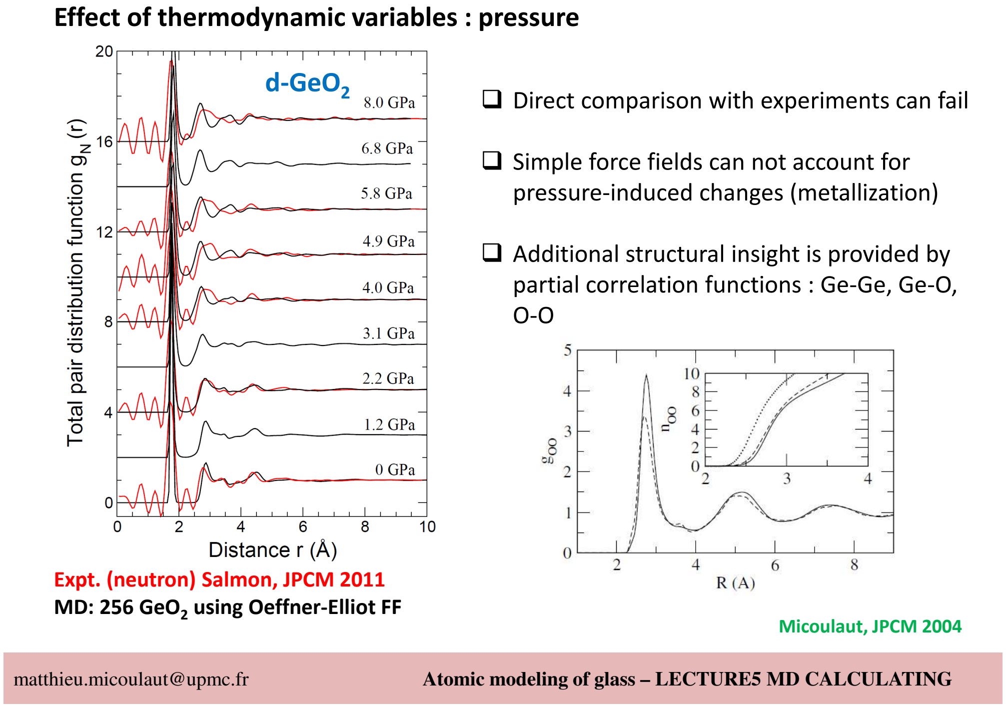

Effect of thermodynamic variables : pressure

Expt. (neutron) Salmon, JPCM 2011

MD: 256 GeO$_2$ using Oeffner-Elliot FF

- ❑ Direct comparison with experiments can fail
- ❑ Simple force fields can not account for pressure-induced changes (metallization)
- ❑ Additional structural insight is provided by partial correlation functions : Ge-Ge, Ge-O, O-O

Micoulaut, JPCM 2004

matthieu.micoulaut@upmc.fr **Atomic modeling of glass – LECTURE5 MD CALCULATING**

Figure 2.21: Pressure dependence of $g(r)$ and failure to reproduce experimental structure at high p (from Micoulaut (2013))

2.2.5.1 Computer simulation of the CKN glass

The mixture $[\mathrm{Ca}\,(\mathrm{NO}_3)_2]_{0.4}\,[\mathrm{K}\,(\mathrm{NO}_3)]_{0.6}$ is a well-known glass former ("CKN glass"), the glass transition being around $350-400K$ (see viscosity and structural relaxation in figure 2.22):

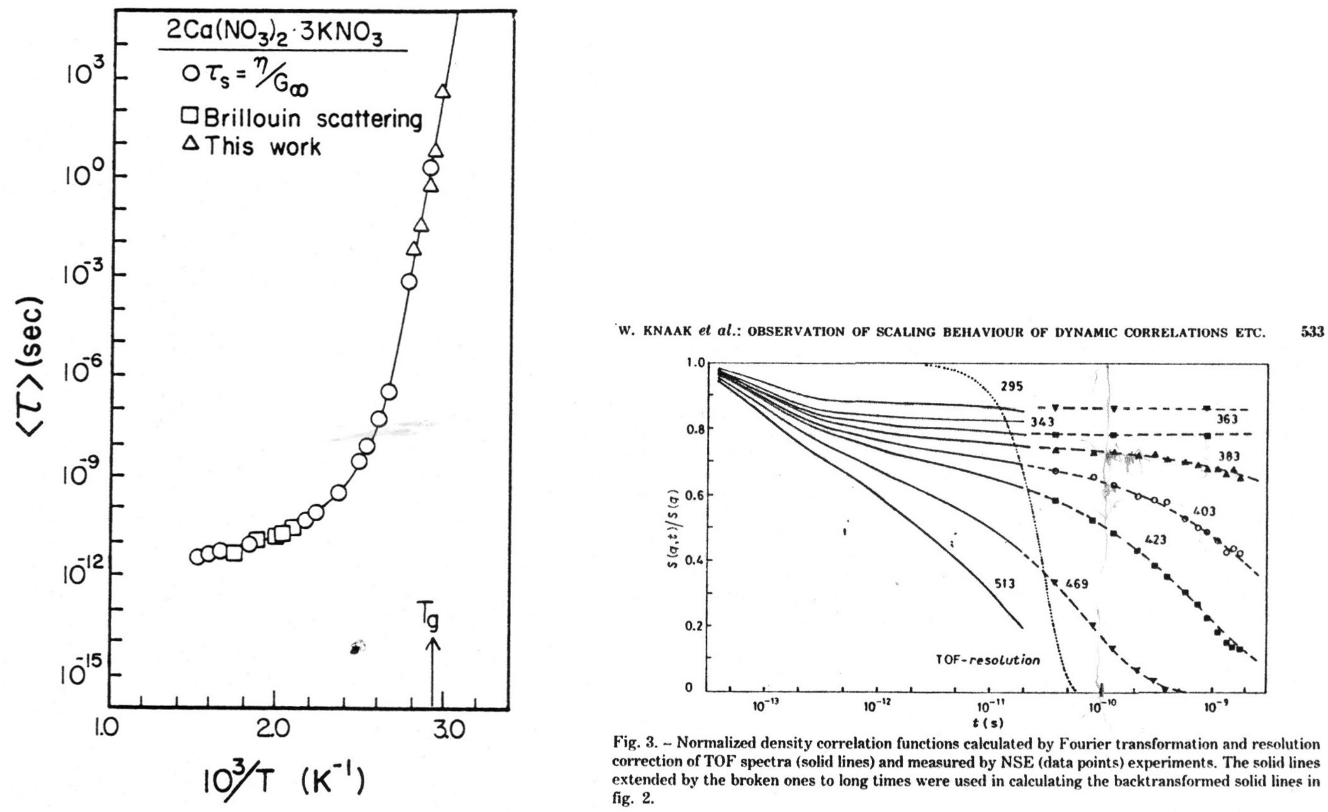

W. KNAAK *et al.*: OBSERVATION OF SCALING BEHAVIOUR OF DYNAMIC CORRELATIONS ETC. 533

Fig. 3. – Normalized density correlation functions calculated by Fourier transformation and resolution correction of TOF spectra (solid lines) and measured by NSE (data points) experiments. The solid lines extended by the broken ones to long times were used in calculating the backtransformed solid lines in fig. 2.

Figure 2.22: viscosity and density correlation in the CKN glass

In the simulation, the $\mathrm{Ca}-\mathrm{Ca}$ peak in $g\left(r\right)$ splits under a certain temperature (figure 2.23): this indicates two distinct spatial arrangements of the succession $\mathrm{Ca}^{2+}\cdots\mathrm{NO}_3^-\cdots\mathrm{Ca}^{2+}$ and is a mark of glassy phase onset. Ca^{2+} lies very close to the NO_3^- plane (consider the almost complete splitting of peaks relative to $\mathrm{Ca}-\mathrm{O}^1$, $\mathrm{Ca}-\mathrm{N}$ e $\mathrm{Ca}-\mathrm{O}^2$)

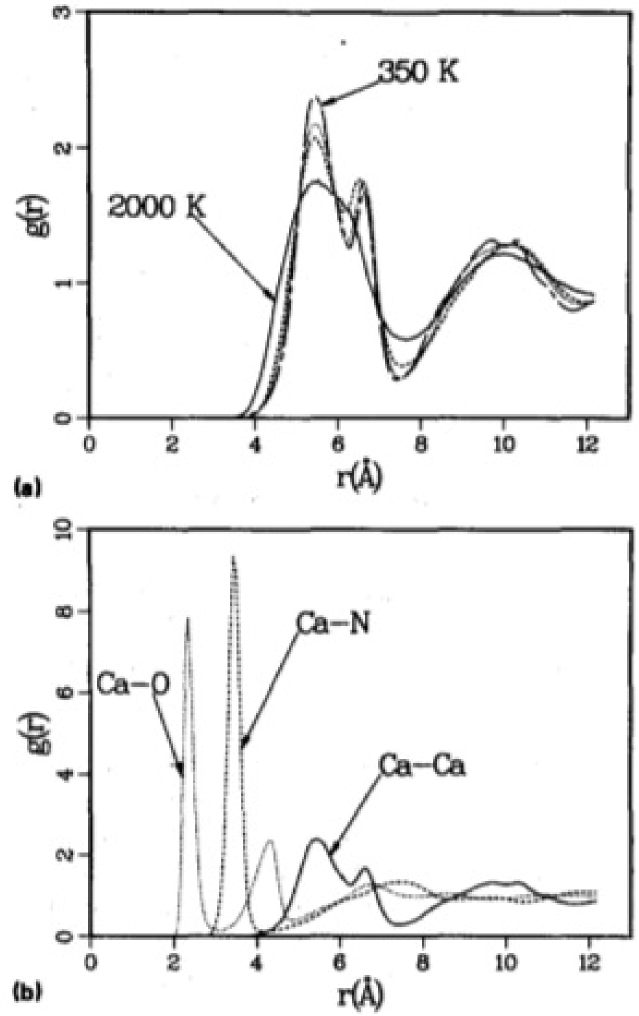

FIG. 3. (a) Radial distribution functions for Ca–Ca at various temperatures: 2000 K (full), 800 K (dashed), 550 K (dots) and 350 K (long dashes), respectively. The split first peak should be noted. (b) Atom–atom radial distribution functions for Ca–O, Ca–N, and Ca–Ca at 350 K.

Figure 2.23: $g\left(r\right)$of CKN glass (from Signorini et al. (1990))

The diffusion coefficient of Ca^{2+} (recall $6D = \frac{\partial\left\langle\Delta^2 r(t)\right\rangle}{\partial t}$) vanishes between $450K$ and $350K$ (figure 2.24)

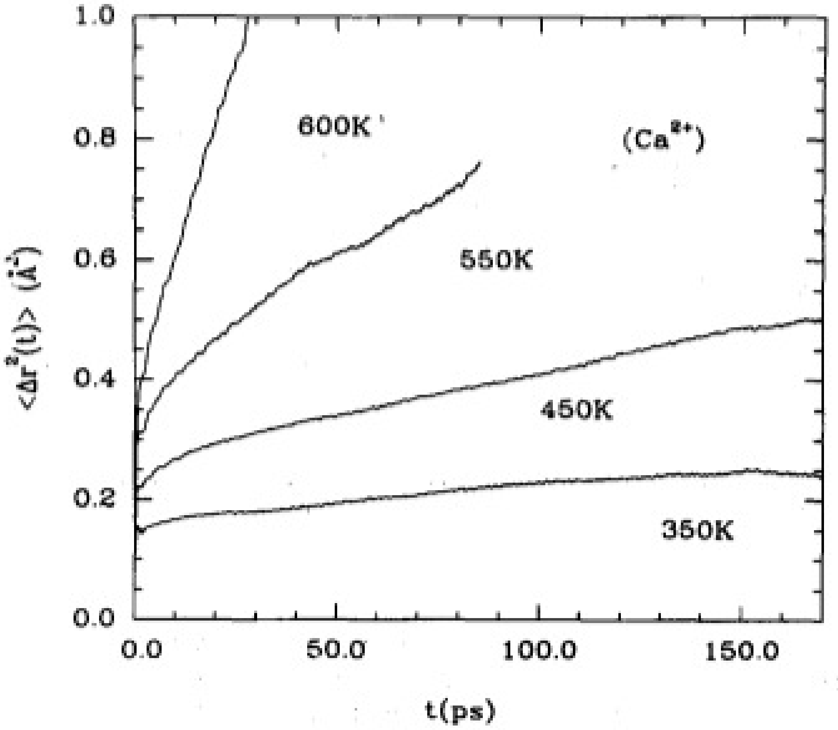

FIG. 4. Mean-square displacements of Ca^{2+} ions as a function of time at various temperatures.

Figure 2.24: (from Signorini et al. (1990))

The transition is also evident in the time-dependent PDF $G_s\left(\boldsymbol{r}, t\right)$ at various temperatures, figure 2.25. At $T = 600K$ the distribution maximum shifts to larger distances and the distribution broadens; at $T = 350K$ the ion is virtually still in this time window.

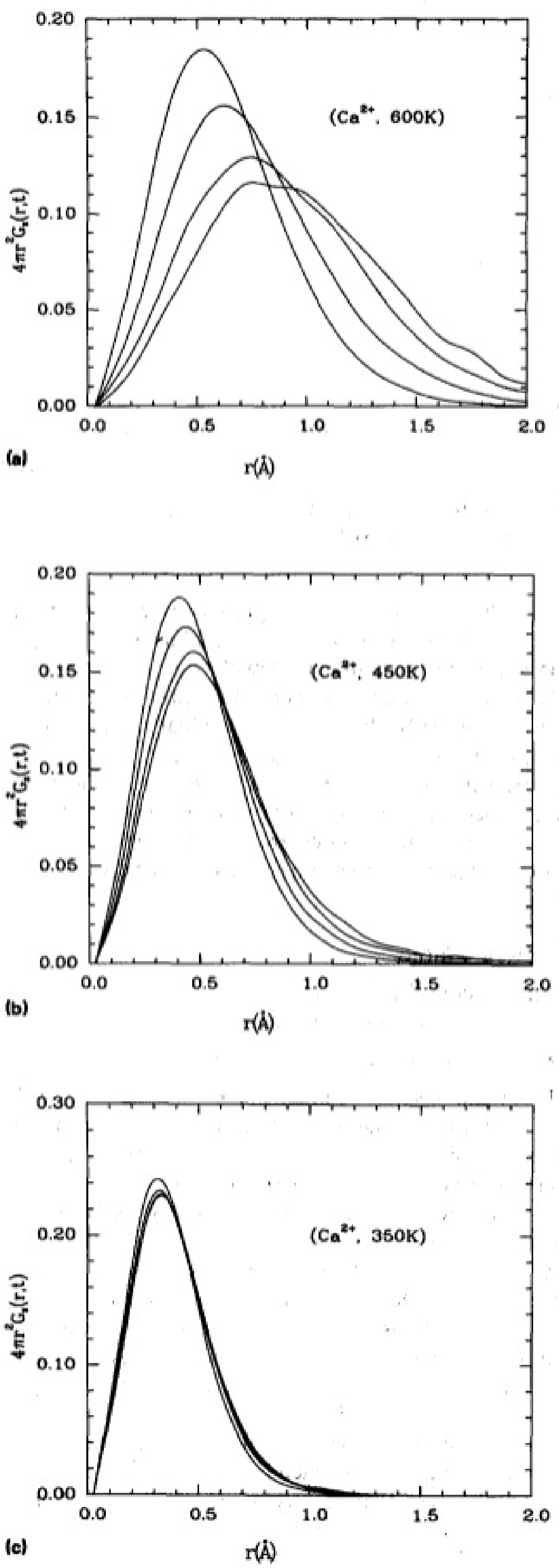

Figure 2.25: Distance travelled by Ca^{2+} at times $t = 5,\ 15,\ 30,\ 45ps$ for various temperatures

2.2.6 Reverse Monte Carlo

Reverse Monte Carlo (RMC) is a computational technique that is widely used in the investigation of disordered structures. However, it differs from the ones described above in that it is not really a simulation technique.

In MC and MD simulations, the elements of the model are the particles and the force field through which they mutually interact. These allow us to build a hopefully accurate replica of the real substance, from which observable quantities can be computed and compared to their experimental counterpart. A successful comparison has a twofold implication: it is a confirmation that the model is appropriate, and it gives us some confidence about the accuracy of the microscopic details (e.g. single particle positions) which cannot be measured.

However, our model may be *biased*, in that it may contain structural features -for example, a too stiff bond angle (see expression 2.2.1)- that is not really required to reproduce the experiments; while it may exclude other features that are equally consistent with the data.

So the question is: what structural information do measurements provide *by themselves*? Can we learn anything from them about the microscopic structure, with minimal to no assumptions about the model?

In RMC, no potential model is postulated. From randomly generated configurations (this is the “Monte Carlo” aspect) observable structural properties such as the structure factor (2.7) are computed, then compared to experimental values, and a goodness-of-fit measure such as the squared difference between the two is evaluated. The one structure that best fits the experiments is selected as the “observed” structure.

Instead of using random techniques for optimizing a model, then comparing computed properties to experimental ones, in RMC one *starts* from experimental measurements, and uses random generation of hypothetical structures to optimize agreement between computed and experimental properties (this is the “reverse” aspect).

2.2.6.1 How RMC works

In practice:

- one starts with a “reasonable” configuration and computes the observed quantity, say $S\left(Q\right)$
- the squared deviation χ^2 between computed and experimental values is evaluated:

$$\chi^2 = \sum_i^N \frac{\left[S_{exp}\left(Q_i\right) - S_{comp}\left(Q_i\right)\right]^2}{\sigma_i^2}$$

  (where N is the number of measured data, exp = experimental, $comp$ = computed, and σ_i is the error on measurement i)

- the structure of the model is perturbed with a small move (perhaps by moving one atom) and χ^2 is evaluated again; the new structure is accepted with a Metropolis-like criterion, exactly like MC
- with this procedure, a statistical sample is built with a Gaussian distribution of the deviation:

$$P\left(\chi\right) = e^{-\frac{\chi^2}{2}}$$

  which is what is expected for a random error in the measurement.

2.2.6.2 RMC Examples

Figure 2.26 reports structure factors of $\mathrm{SiO_2}$ glass computed for a system of 3000 atoms with a RMC algorithm where coordination numbers of Si and O were constrained at the known values (4 and 2)

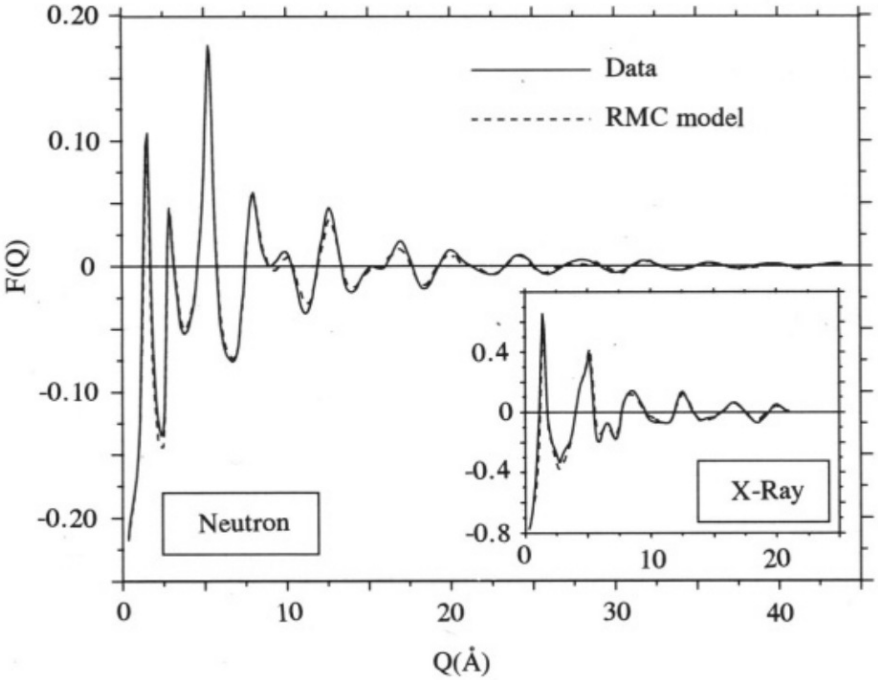

Figure 2. Structure factors for glassy silica calculated from the RMC model of Wicks[19] with co-ordination constraints (dashed lines) compared with those obtained by experiment - neutron[12] and X-ray[20] (inset).

Figure 2.26: $\mathrm{SiO_2}$ glass. Experimental and RMC fitted structure factors (from Keen 1998)

Experimental data are reproduced rather accurately; however, *local* structure (which is responsible for the peaks at medium to high Q) is slightly more disordered than expected. For example, the "tetrahedral" angle $\mathrm{O} - \mathrm{Si} - \mathrm{O}$ (dashed line in figure 2.27) is more distorted than expected (continuous line).

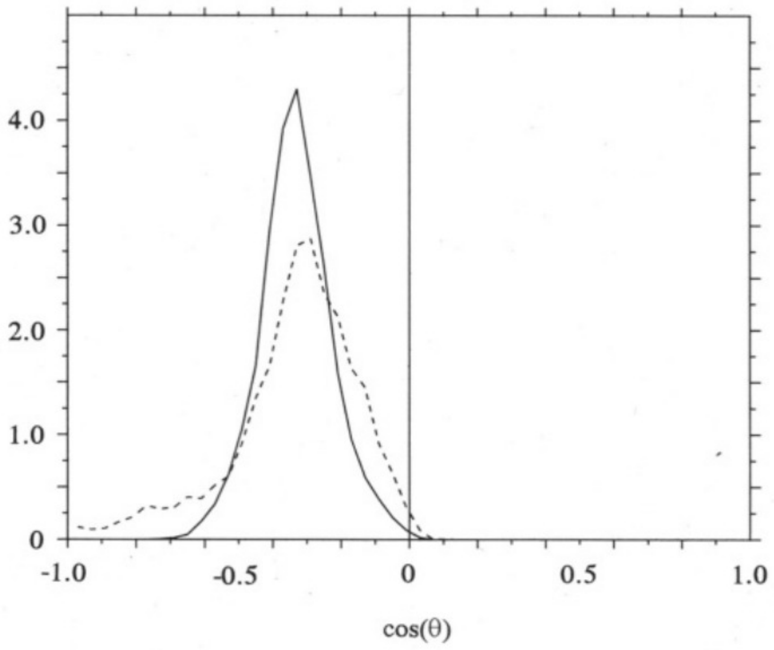

Figure 3. The intra-tetrahedral O-Si-O bond angle distribution from the RMC co-ordination constrained model of Wicks[19] (dashed line) compared with the initial model used for RMC refinement[21] (full line) (arbitrary units).

Figure 2.27: $\mathrm{SiO_2}$ glass (from Keen 1998)

The RMC procedure can be *refined* with the additional constraint that the tetrahedron must keep a regular geometry. With this requirement, while the accordance with data is maintained, the local structure is obviously respected (figure 2.27, full line), even though there is still some inaccuracy about *medium to long range structure*, as evidenced by the distribution of the angle between tetrahedra, which shows a maximum at $180°$ instead of the expected value of $\sim 140°$ (figure 2.28)

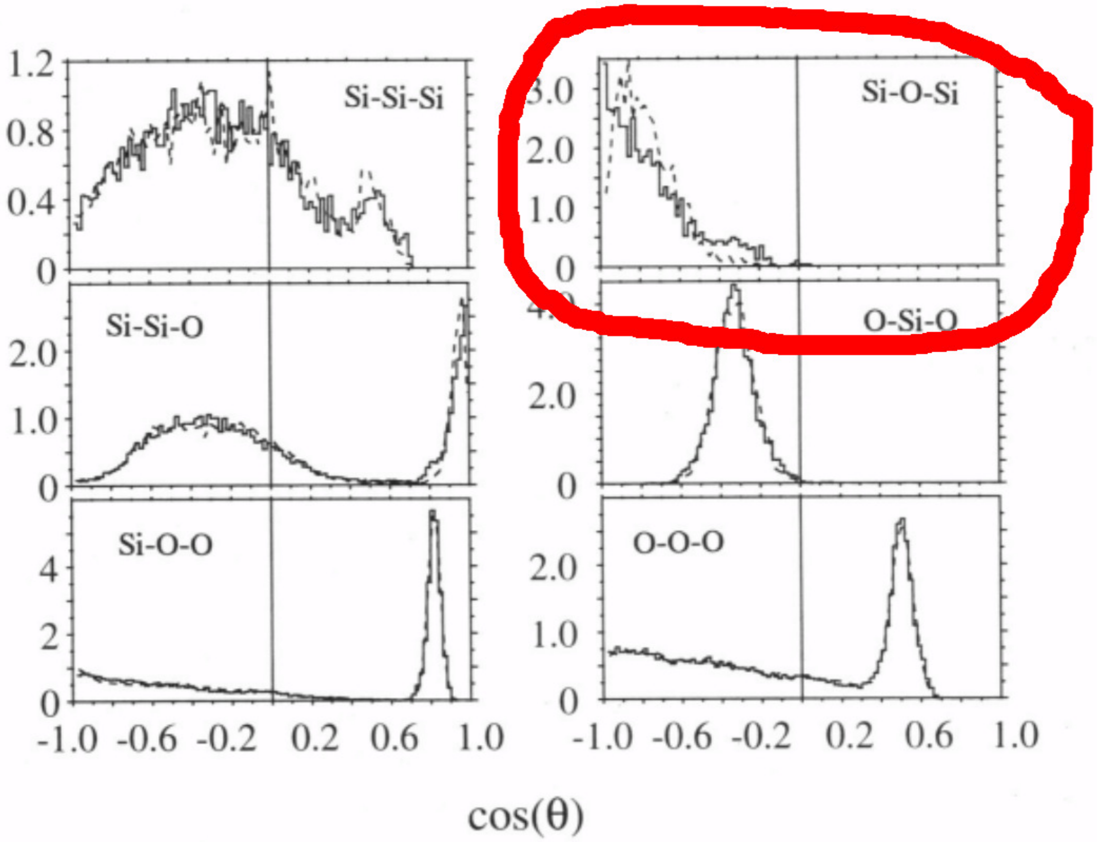

Figure 5. Bond angle distributions for glassy silica calculated from the starting model (dashed line) and the RMC refined model (full line)[21] (arbitrary units).

Figure 2.28: SiO_2 glass (from Keen 1998)

There is a simple way to test the quality of the RMC method, which is to apply RMC to a system whose structure is known with perfect accuracy: an *MD simulated system*!

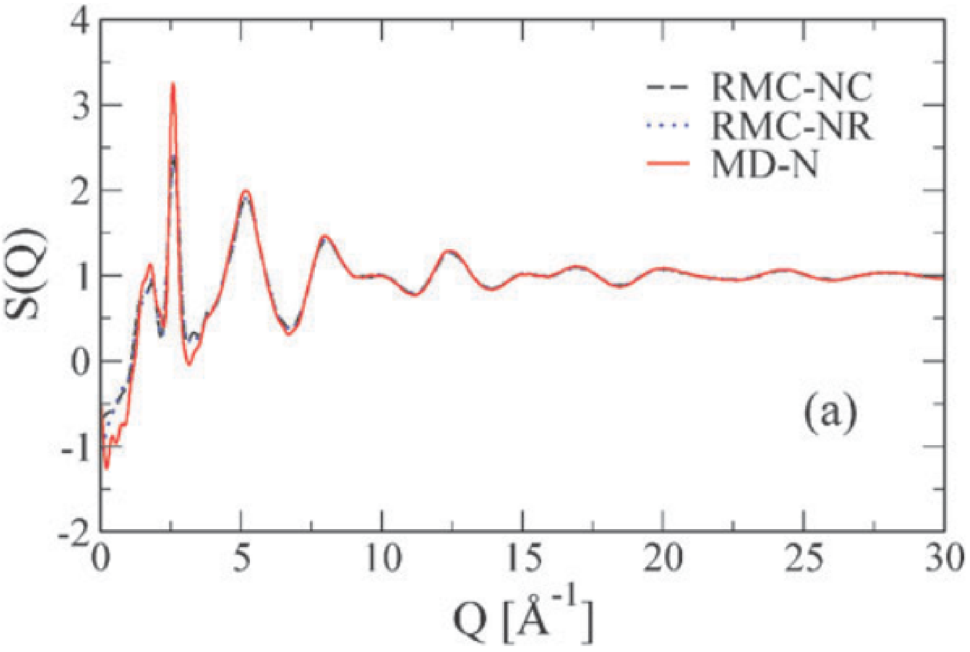

Figure 2.29: $Li_2O \cdot SiO_2$(Muller et al. 2010) Neutron Scattering simulated with MD, along with RMC fitting with two starting structures

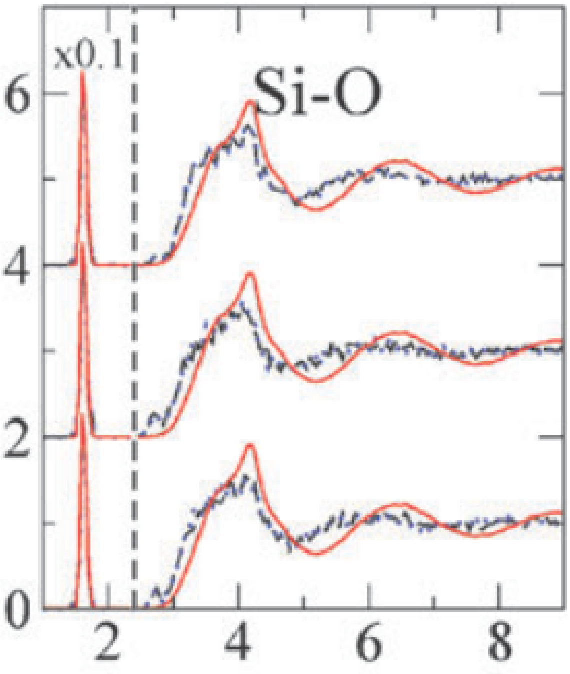

Figure 2.30: (Muller et al. 2010) Partial $g\left(r\right)$ of $Li_2O \cdot SiO_2$

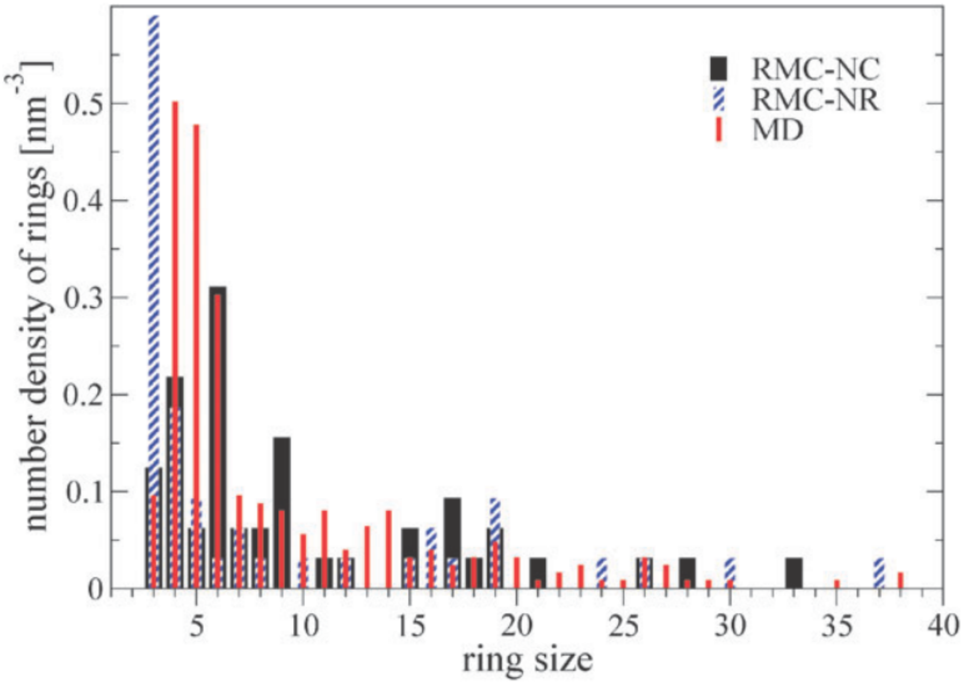

Figure 2.31: (Muller et al. 2010) Ring size distribution in $\mathrm{Li_2O \cdot SiO_2}$. See caption to figure 2.29

In a study on $\mathrm{Li_2O \cdot SiO_2}$, partial PDFs (figure 2.30) and properties on small lengths scales, such as coordination numbers and bond angles (not shown), are well reproduced by RMC, while properties in the medium range order (for example, ring size distributions, figure 2.31) are not. This may be due to the fact that the property whose value the RMC tries to fit is not so sensitive to variations in medium range structure; recall that $S(Q)$ depends on pair interactions, while medium range structure depends on multi-body interactions.

2.2.7 Reference texts for section §2.2

The subject material of this section is treated -in much more detail than here- in Cramer (2004), chapter 3 (sections 3.1-3.5). The essential reference texts for the simulation of molecular systems are Frenkel and Smit (2002) (chapters 3 and 4) and Allen and Tildesley (1987) (chapters 3 and 4). The interested reader can find a more in-depth coverage, particularly of the Monte Carlo method at Chapter 13, in the lesson notes I wrote for the "Struttura e dinamica di biomolecole" university course (Signorini (2013)). Examples are taken from Micoulaut (2013) and Signorini et al. (1990). RMC is explained rather clearly in Keen (1998).

Chapter 3

Models of glass structure

3.1 Introduction

3.1.1 Bonds in solids

The appropriate structural model for glasses is strictly correlated to the type of bonds that exist between atoms, namely whether they are true *chemical bonds* (that is, covalent, electron-pair bonds) or not.

Crystalline solids also can contain both covalent and non-covalent bonds, however the same structural model can be applied to all. Indeed, in most network-type crystal structure depictions, lines between atoms are meant to just point to geometrical coordination and do not necessarily imply the existence of covalent bonds. For example, in 3.1, of the representative compounds of the two structures, ZnS has a mixed covalent-ionic character while $\mathrm{CaF_2}$ is purely ionic.

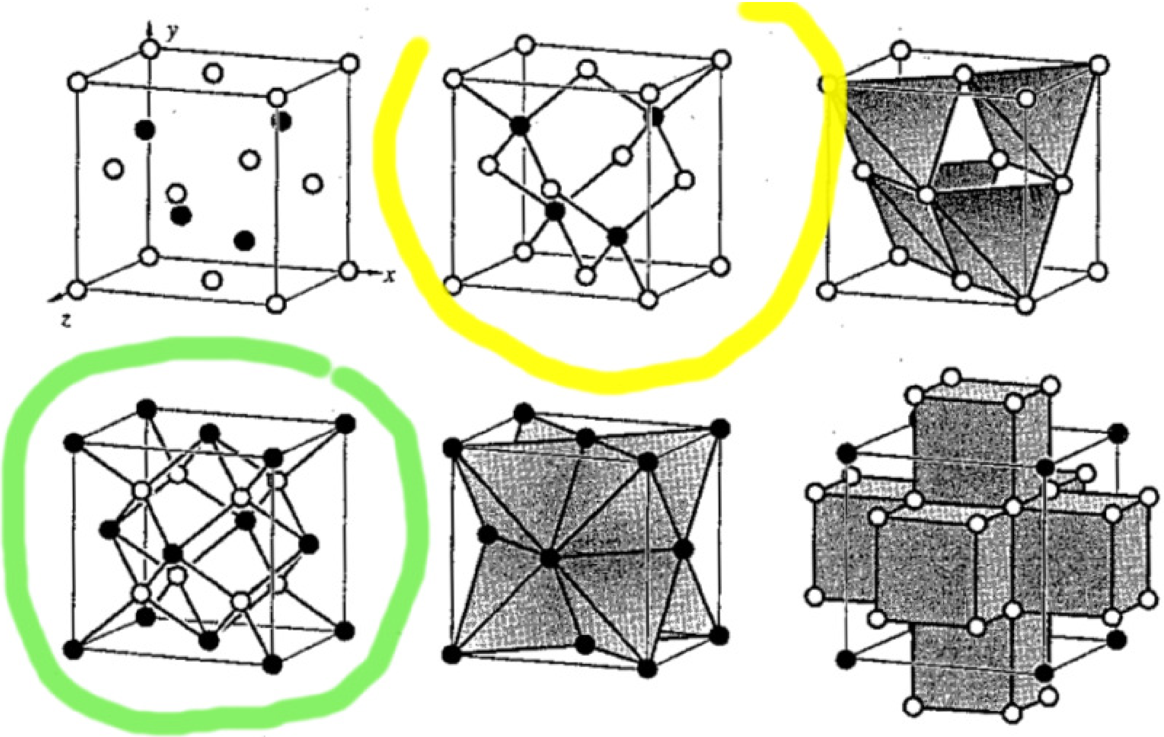

Fig. 4.8. Aspects of the structures of sphalerite, ZnS (top) and fluorite, CaF_2 (bottom). See the text for discussion.

Figure 3.1: In this figure (from O'Keeffe and Hyde 2020) lines between atoms represent chemical bonds in (mainly covalent) ZnS, but not in ionic CaF_2.

3.1.2 Classification of crystals according to bond type

In this section we briefly review how crystals can be grouped according to the *main* type of bonds:

1. **covalent crystals** (examples: C, Si; $\mathrm{SiO_2}$, GaAs; $\mathrm{PbO_2}$)
    - a network of bonds extends to the entire crystal: crystal is like a huge "macromolecule"
    - low coordination numbers (CN) (typically CN=4; sometimes CN=3 or 6); strong, directional bonds.
    - properties: hard; high melting T

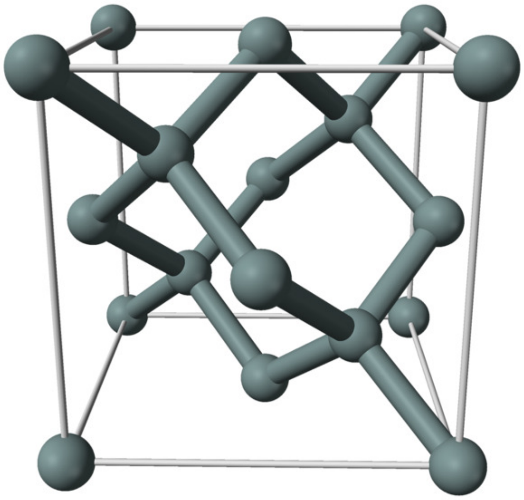

$\mathrm{C}_{(diamond)}$ (CN=4)

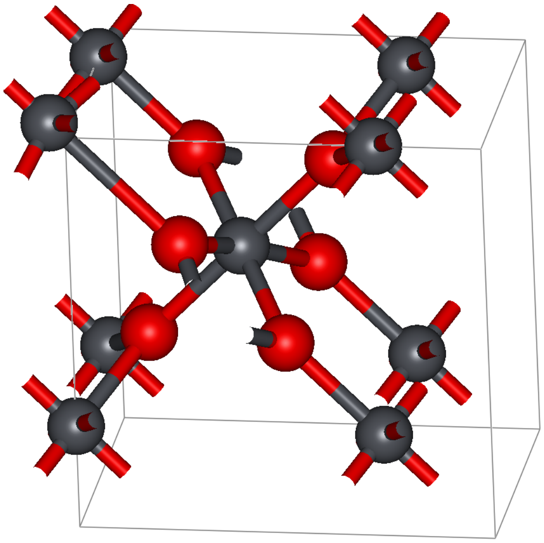

$\beta - \mathrm{PbO_2}$ (CN=6)

2. **ionic crystals**

   - formed by positive and negative ions, held together by electrostatic forces, which are spherically symmetric and long range
   - CN (*anions around a cation*) in the medium range; typically CN=6; also 4,8,9. (Smaller cation is often in *holes* of a compact structure of bigger anions).
   - properties: brittle, medium to high melting T

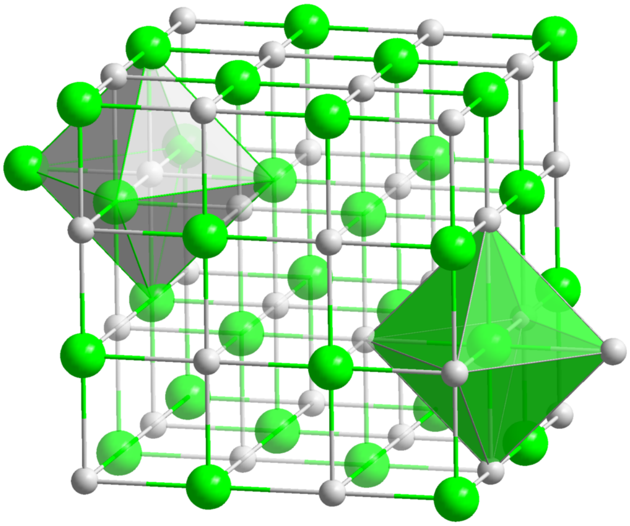

NaCl (CN=6)

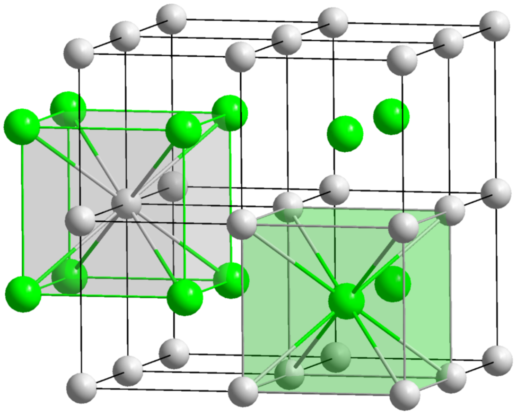

CsCl (CN=8)

3. **metals** (examples: Cu[fcc,12], Zn[hcp,12], Fe[bcc,8])

    - metallic bond, non-directional and delocalized
    - high CN (typically, CN=12; also CN=8,...).
    - properties: ductile, low melting T

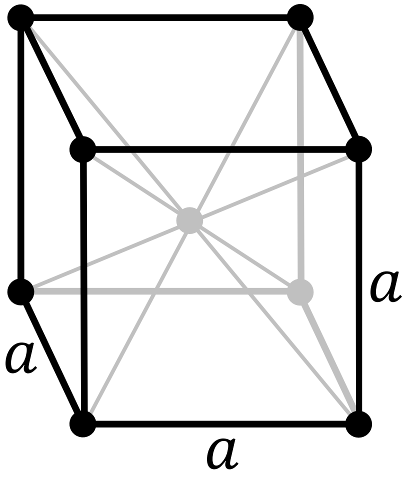

Fe (bcc, CN=8)

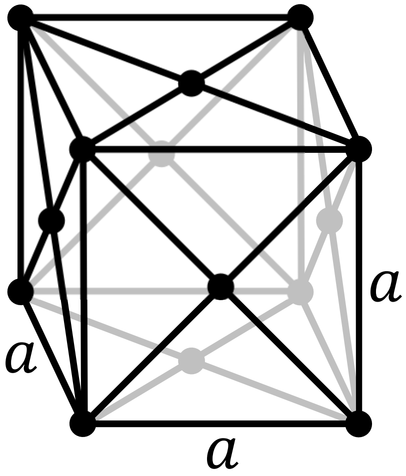

Cu, Zn (fcc,CN=12)

4. **molecular crystals**
    - isolated molecules held together by Van der Waals forces
    - CN: low within the molecule, medium to high among molecular units

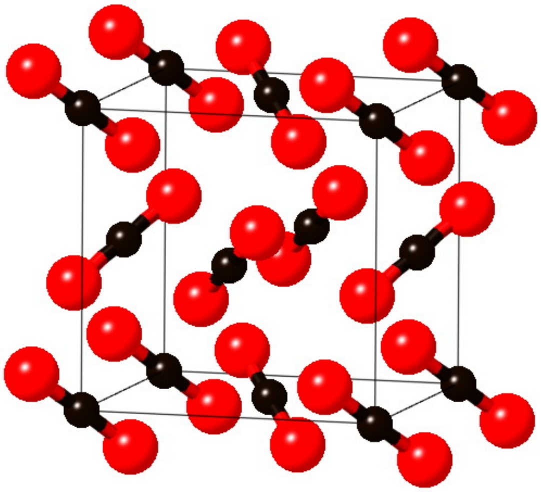

CO_2 crystal

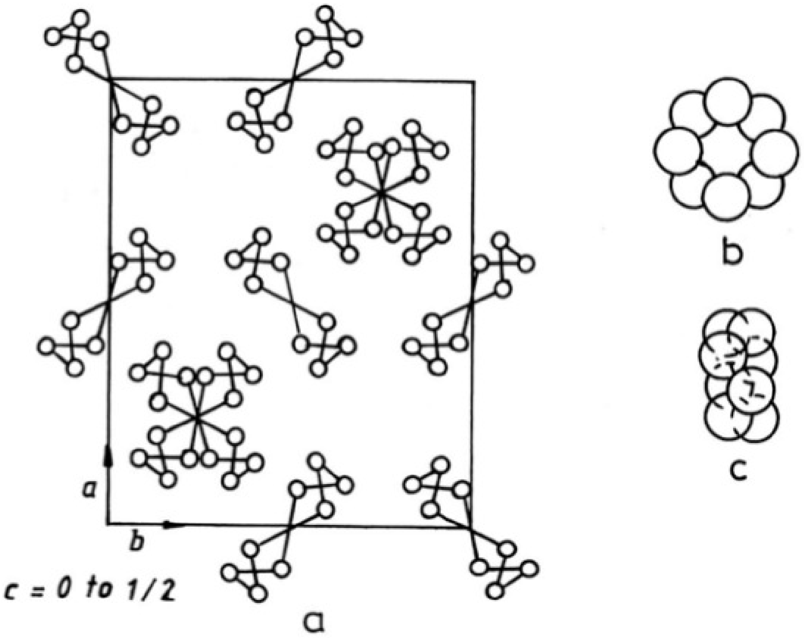

Figure 1.2. The unit cell of the orthorhombic sulphur (S_α).
a the ring packing b, c. front view and side view of the S_8 ring.

3.1.3 Structural models of glasses

While the structural model for crystals is always based on **geometry** and **symmetry**, for glasses a different model is used depending on the bond type:

- if **covalent bonds** dominate, the model is that of a **Continuous Random Network** (CRN), in which the solid is viewed as one infinite covalent compound with values for bond lengths and angles that are either fixed or restricted to a narrow range. The model involves a number of aspects, among which
  - the geometrical and topological properties of the model in itself (coordination numbers, existence and dimensions of rings, etc.)
  - structural theory of glass formation (Zachariasen rules)
  - mechanical properties: average coordination and rigidity (Phillips-Thorpe theory)
  - chemical order and concentration of partially bonded species (*bond models*)
- in **metallic** and **ionic** compounds the **Random Close Packing** (RCP) model is appropriate, where the solid is represented as a collection of hard spheres tending to be in the closest possible contact and fill the space

With the advent of computational methods (in which the “model” is the force field) traditional models have begun to lose importance; however they still have value as limiting structures whose properties are known

3.2 Continuous Random Network (CRN)

In the Continuous Random Network (CNR) model

- the system is assumed to be composed of “nodes” (the atoms) connected by node-to-node “links” (the chemical bonds).
- each node forms a fixed number of links
- the links are rigid
- the angle between two links sharing a node (the bond angles) are also rigid
- links and angles can take a limited number of given values

The last condition is not strictly required by the model, but reflects the physical fact that in a real chemical system only a few of different bond length and angle values are found. Also, the bond distances are of the order of $\sim 0.1\ nm$, and angles are always in the range $90° \div 180°$.

3.2.1 General properties of the model

The first realizations of the CRN were hand built models of a few tens or hundreds of atoms such as those of Bell and Dean for SiO_2 (1966) (figure 3.2), Polk for amorphous Si (1971) (figure 3.3), Greaves and Davis for amorphous As (1974), etc., who used plastic balls and aluminum small rods, or similar materials, and simple devices to make angles rigid. These works not only proved that the model was physically plausible, but also that the histogram of its measured atom-atom distances was remarkably consistent with the observed radial distribution function (figure 3.2).

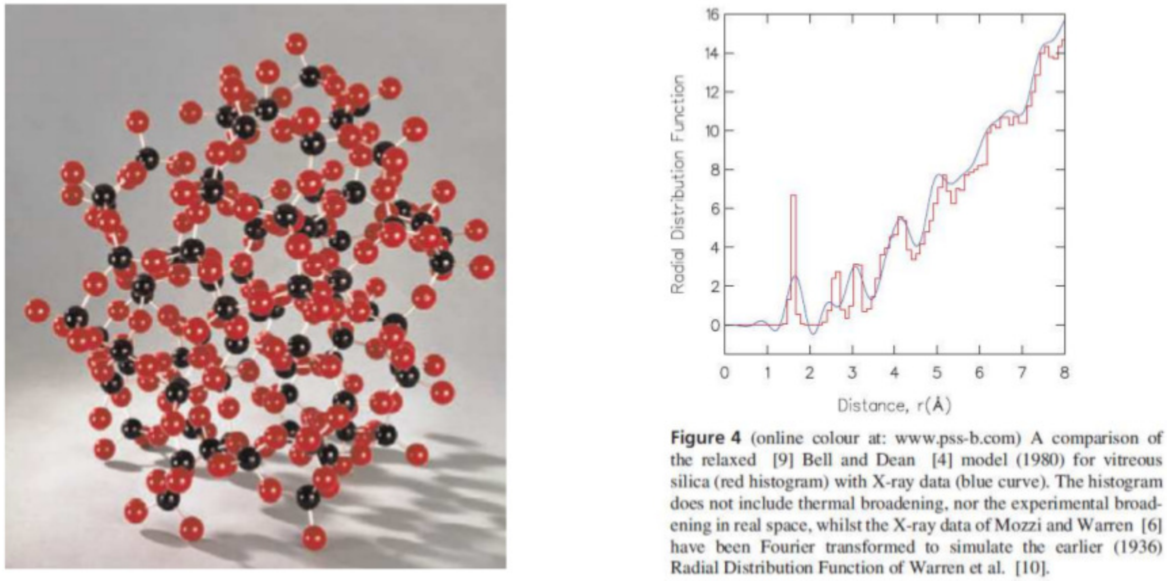

Figure 4 (online colour at: www.pss-b.com) A comparison of the relaxed [9] Bell and Dean [4] model (1980) for vitreous silica (red histogram) with X-ray data (blue curve). The histogram does not include thermal broadening, nor the experimental broadening in real space, whilst the X-ray data of Mozzi and Warren [6] have been Fourier transformed to simulate the earlier (1936) Radial Distribution Function of Warren et al. [10].

Figure 3.2:

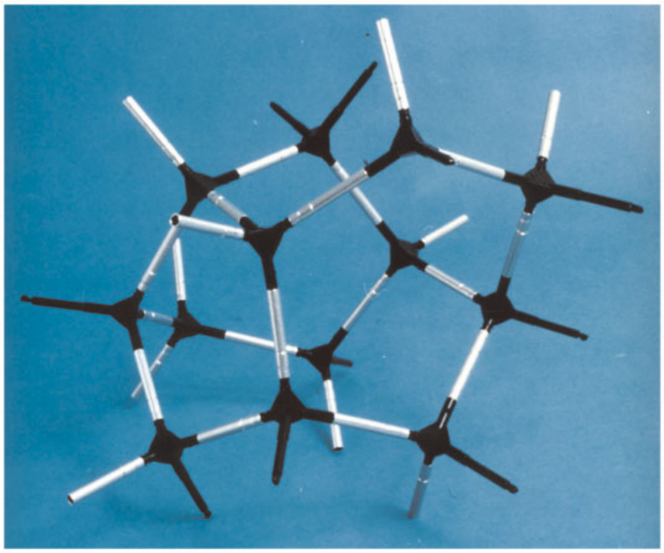

Figure 3.3:

Yet, a number of issues need to be addressed, that are best treated in a more formal approach:

1. *does the network of bonds necessarily include rings or can it also be an open structure?*
2. *is there a limit to the number of constraints (prescribed values for bonds and angles)?*
3. *is there a limit to the number of bonds one atom can form (coordination numbers)?*

To answer these questions we will consider the simplest case of a network made of N identical atoms each with a fixed number of bonds, m.

3.2.1.1 Open or closed structure?

A little analysis shows that, although in principle it is always possible to imagine an infinite structure that is open (with no rings), such structure would not be physically observable[1].

Clearly, in a totally open structure, which takes the form of a tree branching from an origin (the so-called "*Bethe lattice*"), the number of *terminal* atoms increases exponentially with the branching order k (see figure 3.4).

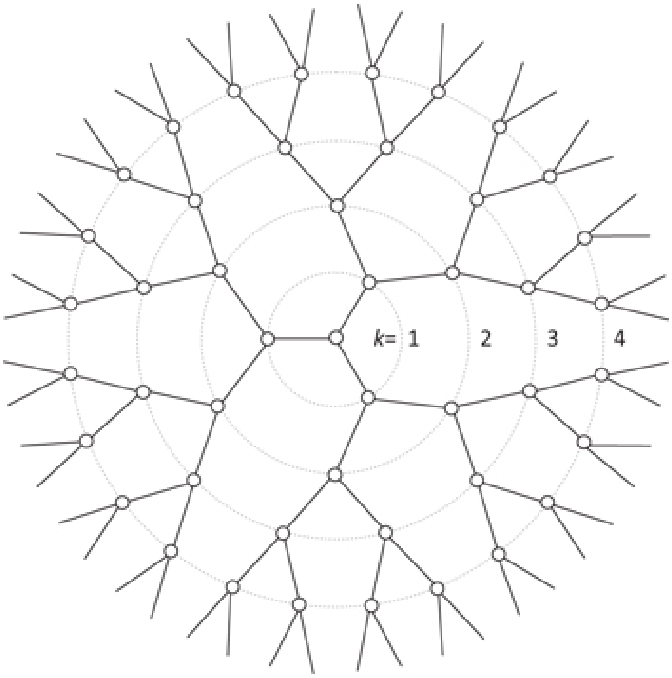

Figure 3.4:

It can be shown[2] that moving toward the exterior shell, the ratio of the number of terminal atoms N_k to that of the bulk atoms tends to a simple value

$$\lim_{k\to\infty} \frac{N_k}{N-N_k} \to m-2$$

that is, for the number of terminal atoms to be negligible with respect to the bulk atoms, as it should be in a real structure, we must have $m = 2$, which is a chain!

---

[1] Note that *finite* chemical structures with this topology exist; they are called *dendrimers* and typically have a maximum branching order $k \leq 10$ and dimensions of a few nanometers (Sapra et al. 2019)

[2] Signorini, 2019, unpublished results

Also, consider that, since angles are in the range $90° \div 180°$, the structure will curl over itself already at the first few branching orders, and rapidly become infinitely crowded.

So, **in the real world only closed structures (with rings) are observed**

3.2.1.2 Number of constraints

We next observe that **in closed structures with $m \geq 3$, it is not possible to assign a chosen value to each distance and each angle.**

Indeed, the number of constraints (assignable values for distances and angles) exceeds the number of degrees of freedom (3 per atom).

We will quantify this statement below. For now, consider the example of $m = 3$ (figure 3.5): if one chooses, for each atom, 2 distances and 2 angles (which amounts to 3 constraints per atom, because each distance is shared with the neighbour atom and counts for $\frac{1}{2}$), the rest of the constraints (1 distance and 1 angle) are determined by geometry, cannot be assigned arbitrarily.

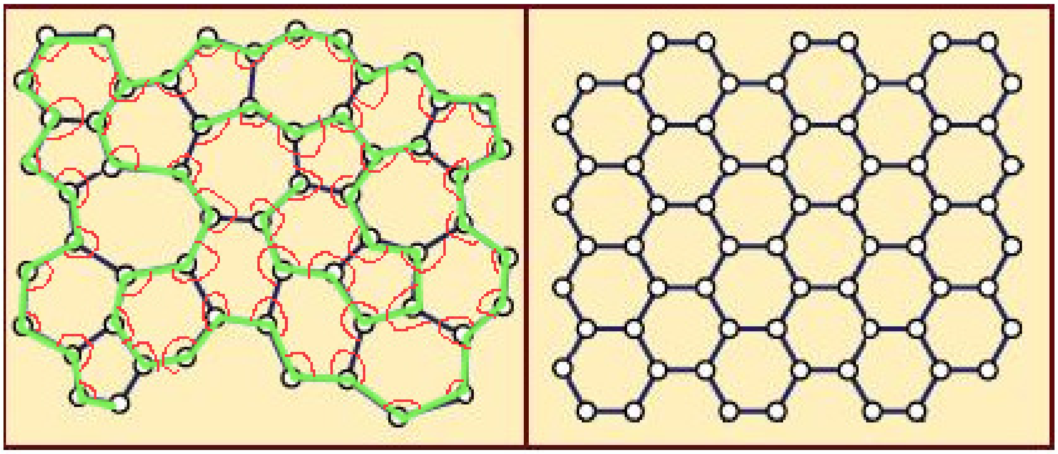

Figure 3.5: In the irregular structure of the left picture, only 2 distances (in green) and 2 angles (in red) for each atom can be assigned; the rest will be determined by geometry. The structure to the right is an example of how in some regular arrangements geometry allows bonds and angles to be all equal. Think of these pictures as in 3 dimensions.

As a special case, **it is generally not possible to assign one chosen value to all bond lengths and to all angles**. Such constraints will be only compatible with particular regular arrangements, the crystal lattices. Think for example of graphite ($m = 3$) and diamond ($m = 4$).

Important consequences of constraints being in excess is that (a) the values imposed by geometry in a random network will in general be considerably different from those those required by chemistry; and (b) that they will assume a whole spectrum of ranges instead of being fixed to the few chemically accepted values. The deviation from equilibrium values creates an excess energy, or stress, which will be higher for bond distances than for bond angles, since force constants of the latter are smaller. Consequently, bond angles values will be more broadly distributed than bond lengths.

3.2.1.3 Coordination numbers

An interesting observation is that **the number of excess constraints over degrees of freedom increases with m.**

The higher the coordination number, the higher the fraction of distances and angles that cannot be assigned arbitrarily. Again, we will quantify this statement later. For now, we note that since chemistry *does* require bond lengths and angles to assume certain values (that is, all constraints to be respected) CRNs with increasingly high coordination numbers will be increasingly difficult to form. We will see that coordination numbers 3 or 4 are most frequently found in random networks, while $m = 5$ or 6 are only compatible with regular or quasi-regular latticesfigure 3.6.

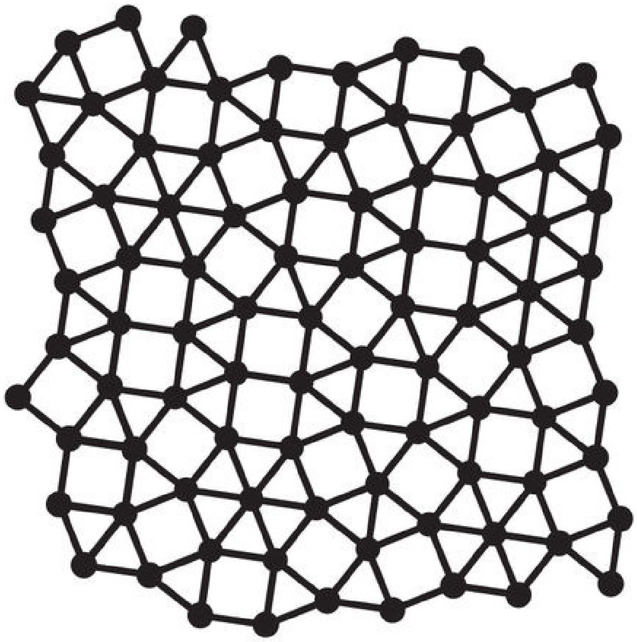

Figure 3.6: *Quasi-crystal (a somewhat ordered lattice, which however lacks translational symmetry) with coordination numbers=5, 6*

3.2.1.4 Summary

The last considerations, related both to topology and to physico-chemical requirements, can be summarized as follows.

In real random networks we expect to find

1. closed structures. with **rings**
2. **not very high coordination numbers, with typical values of 3 or 4**
3. **bond lengths and (particularly) angles distributed over a range of values**

It should be kept in mind that this model does not take into account other constraints that exist in chemical systems, although with less energy involved: torsions, nonbonded interactions, etc.

3.2.1.5 Comparison to experimental structures

Before moving on to the general case of polyatomic systems, it is interesting to compare the structural features that are obtained with the monoatomic CRN to experimental data. We have already noted that the well-known ball-and-stick model of silica glass by Bell and Dean (figure 3.2) reproduces the observed $g(r)$ to a remarkable degree. The same is quite not true for the Polk model of $a-\mathrm{Si}$ (figure 3.3), as evidenced by the following figure (figure 3.7): the fact that RDF peaks are too narrow clearly indicates that the ball-and-stick model is too rigid. The reason for the different agreement with experiments between the two models will be clearer later on, but we can anticipate that the CRN model of $a-\mathrm{Si}$ implies much more *excess constraints* than that of $\mathrm{SiO_2}$.

The agreement of the Polk model would undoubtedly improve if some degree of flexibility in constraints is introduced, something that could be implemented with simple adaptations to sticks and joints; note, in any case, that a broadening of the first peak (the first neighbours' shell) can be obtained only by allowing some tolerance in the bond *length*, not in the bond *angle*, although the force constant of the latter is certainly softer than that of the former.

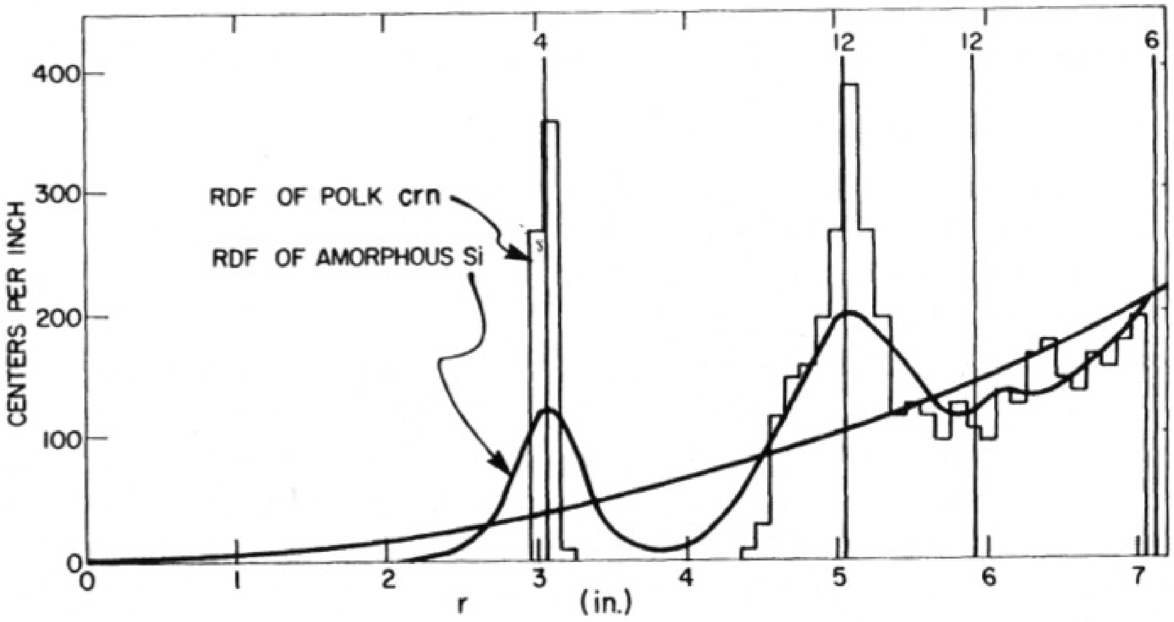

Figure 3.7: comparison of $a-\mathrm{Si}$ radial distribution function of the Polk ball-and-stick model, and experimental RDF (from Varshneya 1994)

More flexibility is allowed by simulating the CRN model in a computer program. The early (Steinhardt et al. 1974) study reported in figure 3.8, regarding $a-\mathrm{Ge}$ (isomorphous to $a-\mathrm{Si}$), used what can be considered a simplified version of a Monte Carlo simulation, consisting in a minimization of the potential energy, with no Boltzmann sampling, but with the inclusion of "structure relaxation" procedures taking into account thermal oscillations, experimental broadening and other effects. In spite of the physical inaccuracy of the computations the results appear quite satisfactory.

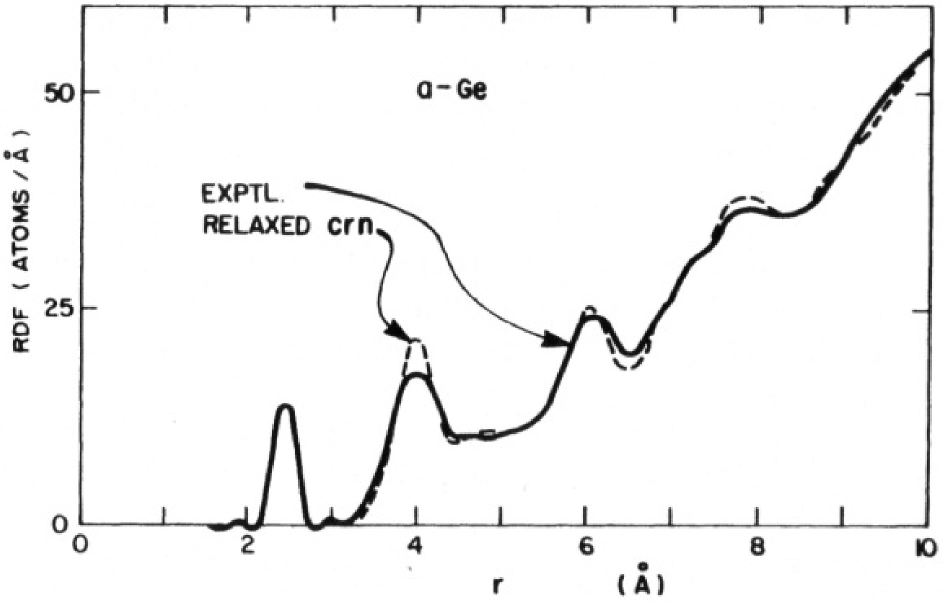

Figure 3.8: Radial distribution function of amorphous Ge (from Steinhardt et al. 1974)

3.2.2 Polyatomic CRN

Many covalent glasses contain atoms of two or more atomic species with different coordination numbers. The corresponding CRN has the same basic features as a monoatomic CRN, the main difference being that in the analysis outline above an average $\langle m \rangle$ must be considered instead of m.

Polyatomic CRN can be divided in two main classes

1. Networks with *chemical order*, where only mixed bonds $\mathrm{A-B}$ are allowed; the typical case are oxide glasses, like $\mathrm{SiO_2}$, where the metal (or nonmetal) atoms are connected by bivalent oxygen atoms acting as bridges between two metal atoms (see figure 3.9).

2. Networks without chemical order, where all types of bonds, $\mathrm{A-A}$, $\mathrm{A-B}$ and $\mathrm{B-B}$, are possible: for example, chalcogenide glasses like $\mathrm{As_2S_3}$; or fluorides, like $\mathrm{BeF_2}$; in many cases one can have non-stoichiometric compound of general formula $\mathrm{A_xB_{1-x}}$ (figure 3.10)

3.2.2.1 Oxide glasses

Oxides $\mathrm{A_xO_y}$ occupy a special place in glass theory, both because they are the glassformers which have been known for the longest time, ($\mathrm{SiO_2}$, $\mathrm{B_2O_3}$, ...), and because it is for oxide glasses that the CRN model was first developed and tested.

The network of oxide glasses is made of A atoms linked through bridging O atoms. One way to see this is that the elemental units of this CRN are, instead of atoms, identical $\mathrm{AO_m}$ ($m = 3$ or 4) polyhedral units sharing O vertices (figure 3.11). This is justified by the observation that (usually) the geometry of $\mathrm{AO_m}$ is fixed: both $\mathrm{A-O}$ distances and $\mathrm{O-A-O}$ "internal" angles are rigid. In this approach, the $\mathrm{A_xO_y}$ network can be mapped into an isomorphous monoatomic network whose nodes represent

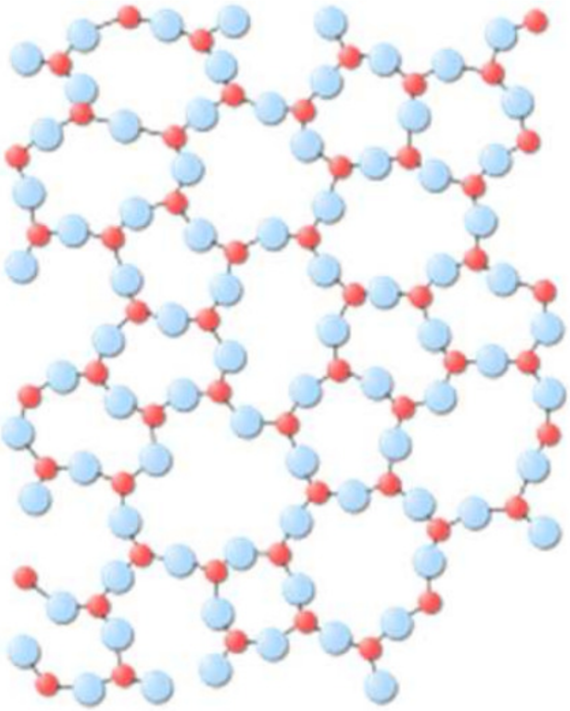

Figure 3.9: Chemically ordered AB network

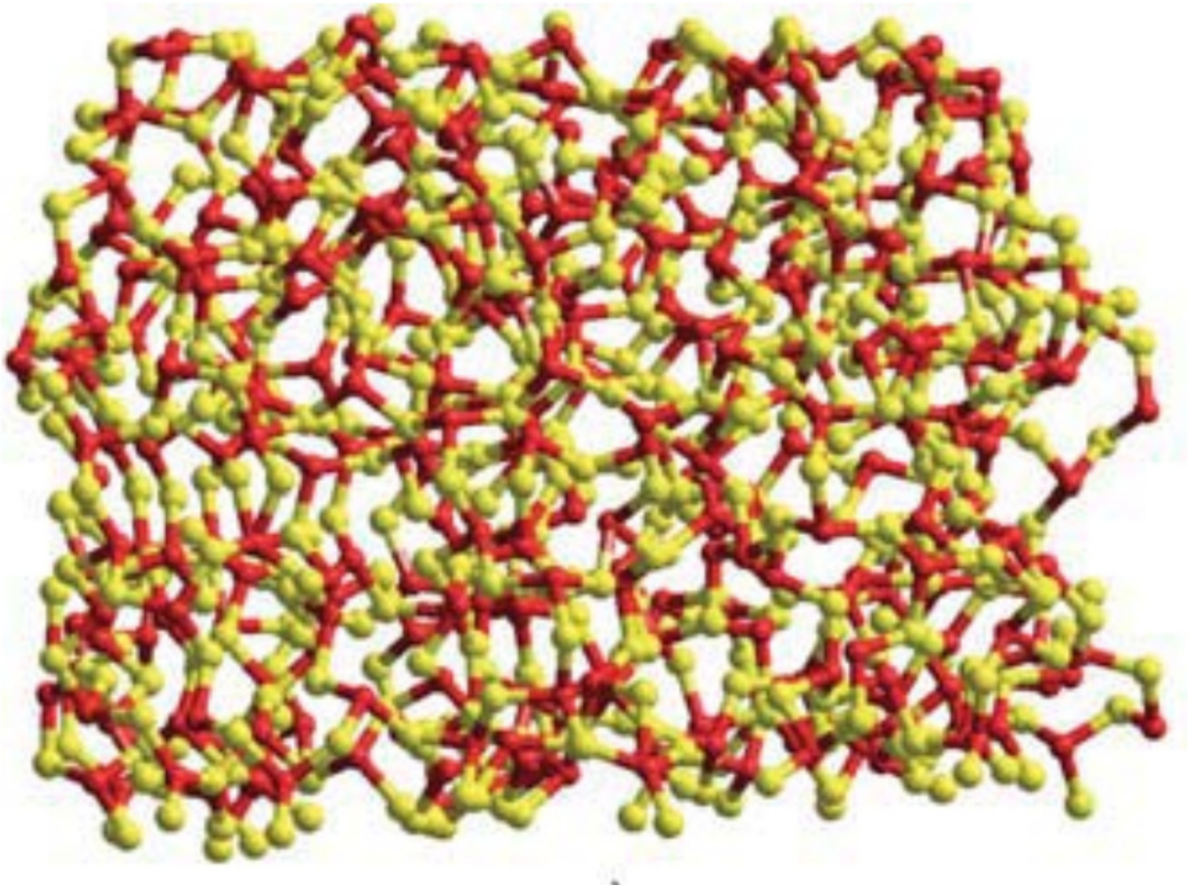

Figure 3.10: Non-chemically ordered network with tri- and bi- coordinated atoms

the polyhedron units (figure 3.12). Put differently, the polyatomic network can be obtained from the monoatomic one by substituting (“decorating”) each $\mathrm{A-A}$ link with an $\mathrm{A-O-A}$ bridge.

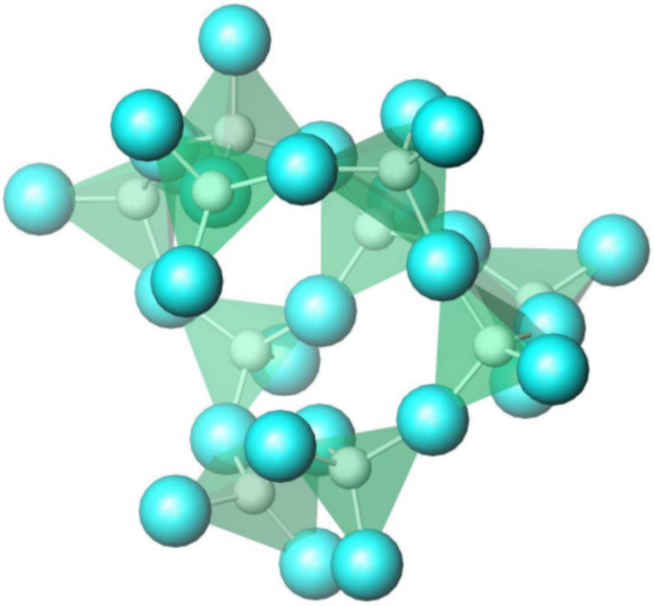

Figure 3.11: 3D vision of silica glass network as formed by $\mathrm{SiO_4}$ tetrahedra

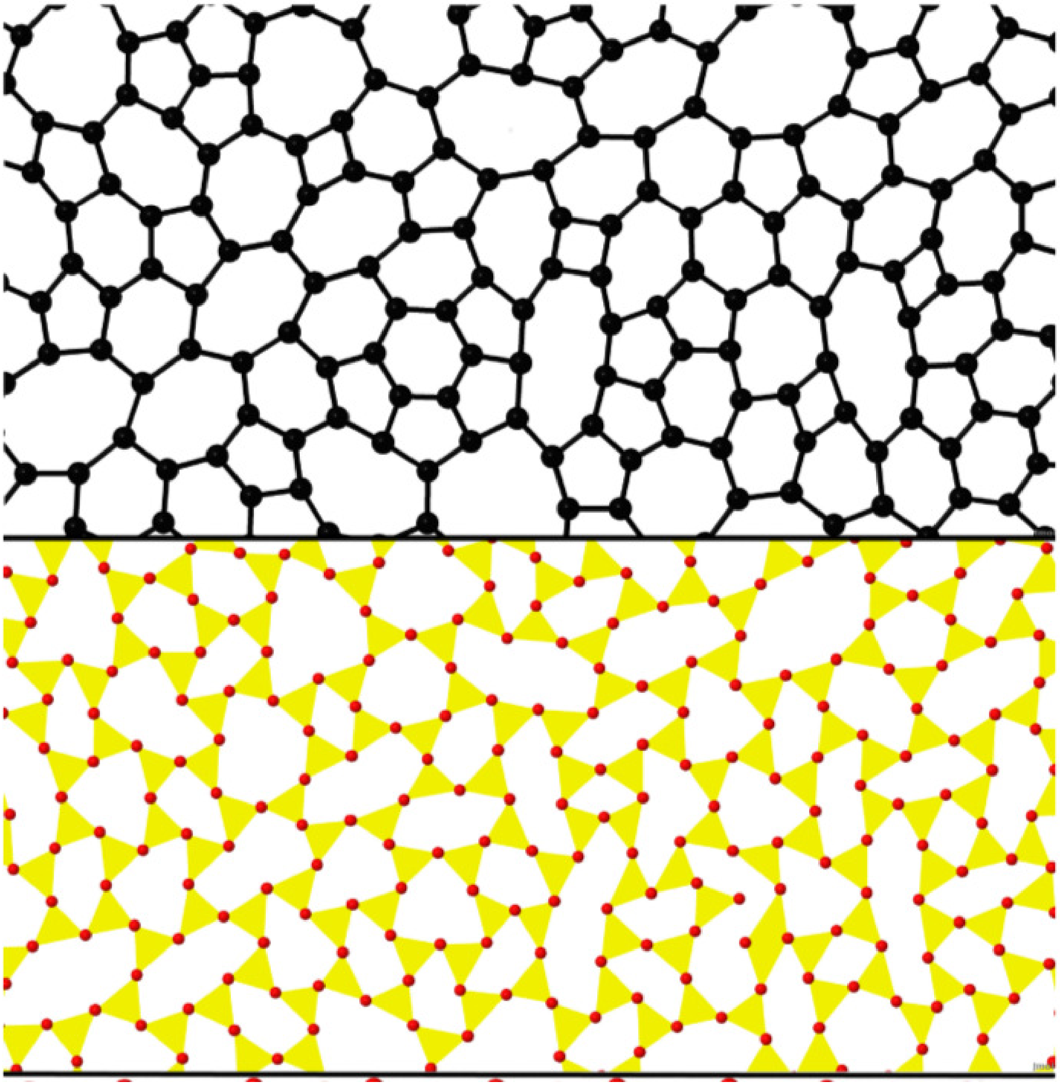

Figure 3.12: Isomorphism between a monoatomic network and a biatomic network with chemical order. Yellow tetrahedra and red bridging atoms in the bottom panel correspond to nodes and links, respectively, in the top panel

Note, however, that even if there is *topological* equivalence between the two networks, they will be *geometrically,* and *mechanically,* different if $\mathrm{A-O-A}$ (inter-polyhedra) angles are flexible. The $\mathrm{Si-O-Si}$ angle flexibility is at the origin of the broader $\mathrm{Si-Si}$ peak observed in the histogram of the $\mathrm{SiO_2}$ ball-and-stick model as compared to the first peak in the $a-\mathrm{Si}$ model (figure 3.13), and can be observed in XRD (figure 3.14).

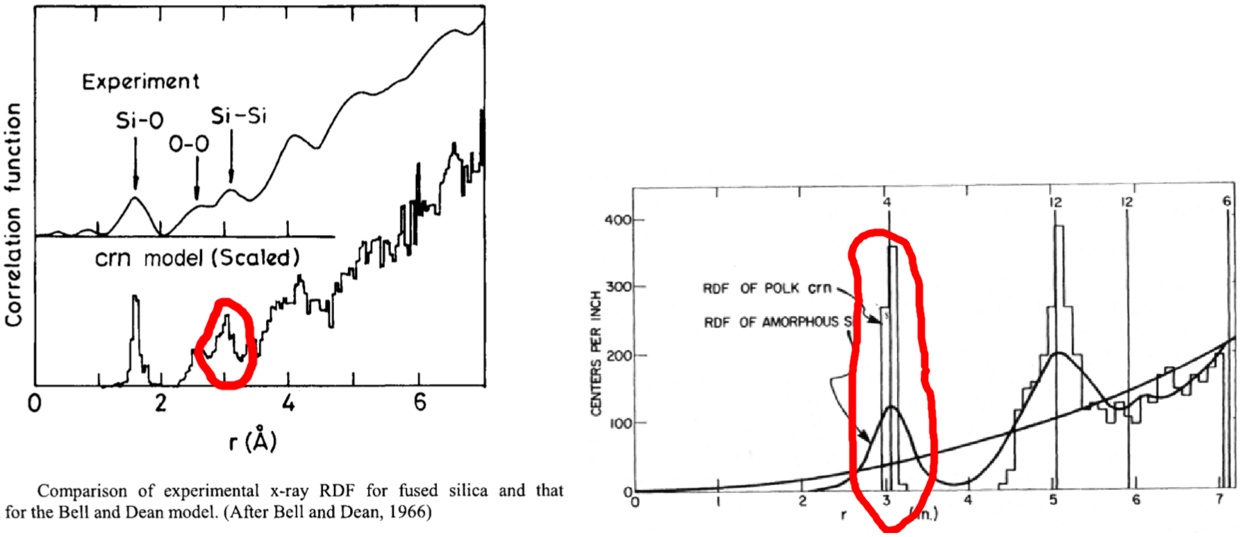

Comparison of experimental x-ray RDF for fused silica and that measured for the Bell and Dean model. (After Bell and Dean, 1966)

Figure 3.13: $\mathrm{Si-Si}$ peak in the histograms of the ball-and-stick models of $\mathrm{SiO_2}$ glass (left) and amorphous Si (right)

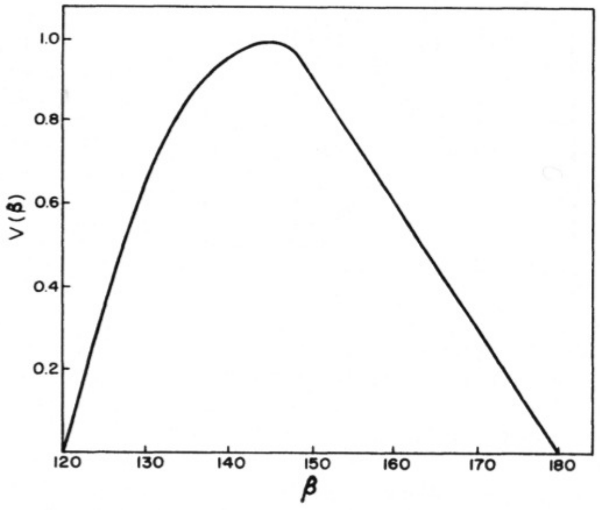

Figure 3.14: Distribution of $\mathrm{Si-O-Si}$ angle in fused silica, obtained with XRD (from Varshneya (1994))

One important property of oxide glasses is that unit polyhedra share only **vertices, not edges or faces** (figure 3.15, left).

Sharing an edge amounts to forming a 4-atom ring (figure 3.15, right), that would imply a high stress either of the intra-polyhedron $\mathrm{O-A-O}$ angle or of the inter-polyhedra $\mathrm{A-O-A}$ angle, or of both, at least some of which would have to assume values $\leq 90°$.

Also, edge sharing would reduce the amount of branching in the network, thus making the structure less rigid [3]

---

[3] rather unexpectedly: see Lucas (2014), Wilson (2012))

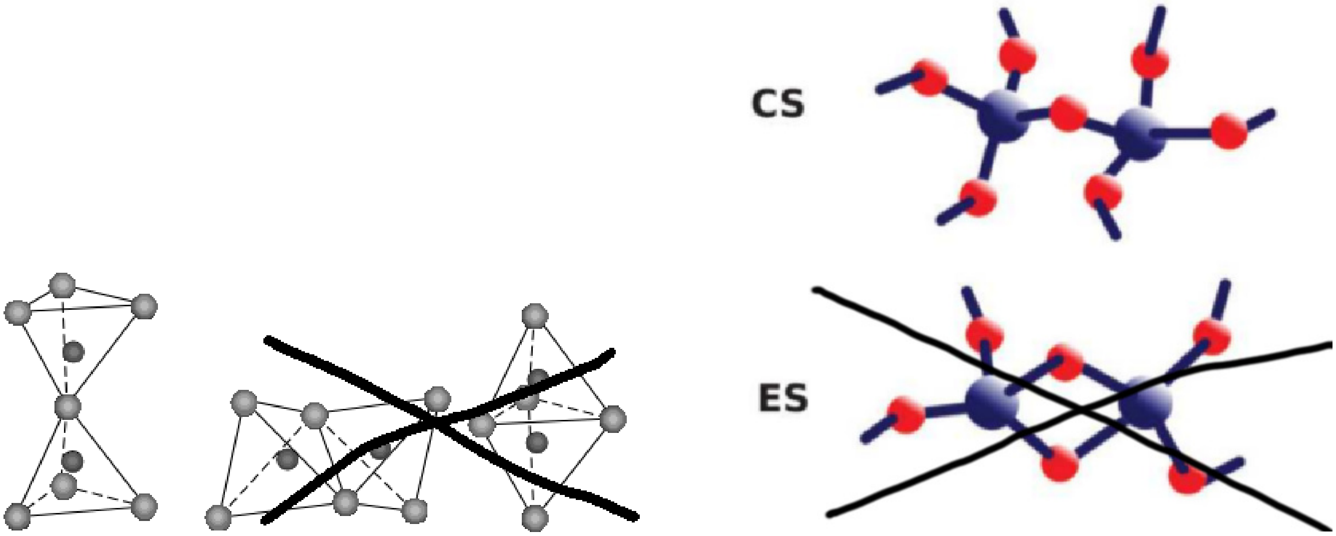

Figure 3.15: SiO_4 tetrahedra share only vertices, not edges or faces

In summary:

The CRN model of an oxide $\mathrm{A_xO_y}$ *obeys the following rules:*

- *number of bonds (coordination number)*
  - $\mathrm{O} = 2$
  - $\mathrm{A} = 3$ *or* 4
- *flexibility, in* decreasing *order:*
  - $\mathrm{A-O-A}$ *angles (external to polyhedron)* $>$
  - $\mathrm{O-A-O}$ *angles (internal)* $>$
  - $\mathrm{A-O}$ *bonds*
- *angles are always* $> 90°$*; no* 4*-atom ring, polyhedra share vertices only*

3.2.2.2 Structural theories of oxide glass formation; Zachariasen's rules

The above rules are **topological criteria for covalent oxide glass formation**.

In fact, a ***structural theory for glass formation*** -now in contrast with the ***kinetic theory*** (any substance can form a glass, provided it is cooled fast enough)- has been advanced early in the study of glasses, and has enjoyed a considerable success since.

In 1932, **Zachariasen** made an attempt to explain why some oxides can form glasses rather easily while others cannot, by considering **local structures** (coordination geometries) found in **corresponding crystals**. He took the observation that glasses exhibit mechanical properties, density, enthalpy of formation, etc., that are very similar to the crystalline form of the same substance, as an indication that local structures of crystals are conserved in the glass phase.

On this basis, he stated a set of **rules for the formation of oxide glasses** (Varshneya (1994); Rao (2002)), that were bound to have great influence on glass science.

These rules, in essence, correspond to the rules for the formation of a continuous random network such as the ones summarized above. In fact, Zachariasen described oxides as made up of ions (partly, for continuity with a previous model by Goldschmidt which considered the ratio of ionic radii, as in Pauling's analysis of crystal structures); however, his theory is based on bonds (or "coordinations") between atom pairs, which is more consistent with a covalent nature of interactions[4].

---

[4] For a more detailed discussion of the relationship between the nature of bonding and the glass-forming ability see Rao (2002), p. 36

Here are Zachariasen's rules Rao (2002):

In a glass forming oxide of the formula $\mathrm{A_mO_n}$

1. *Oxygen atom may be linked to no more than two A atoms*
2. *The number of oxygen atoms surrounding A atoms must be small (3 or 4)*
3. *The oxygen polyhedra share only corners with each other, neither edges nor faces*
4. *At least three comers in each polyhedron must be shared.*

The first three rules are consistent with the CRN rules we have found above. Rule 4 is simply the statement that for a simple network to not reduce to a chain the average number of links of each node (in this case, the polyhedron) must be $m \geq$3.

For an illustration of Zachariasen's rules with examples involving oxides of different formula, see http://www1.chim.unifi.it/u/signo/did/vetri/3-modelli-strut.pdf (in Italian).

The CRN structure of oxide glasses was first observed in real space in 2012 (Lichtenstein et al. (2012); Huang et al. (2012)), with different electron microscopy techniques, in a thin layer of glassy $\mathrm{SiO_2}$ adsorbed on a surface. An ordered domain (figure 3.16, right) and an amorphous domain can be seen, with a striking resemblance to the original drawings of 2D structures by Zachariasen.

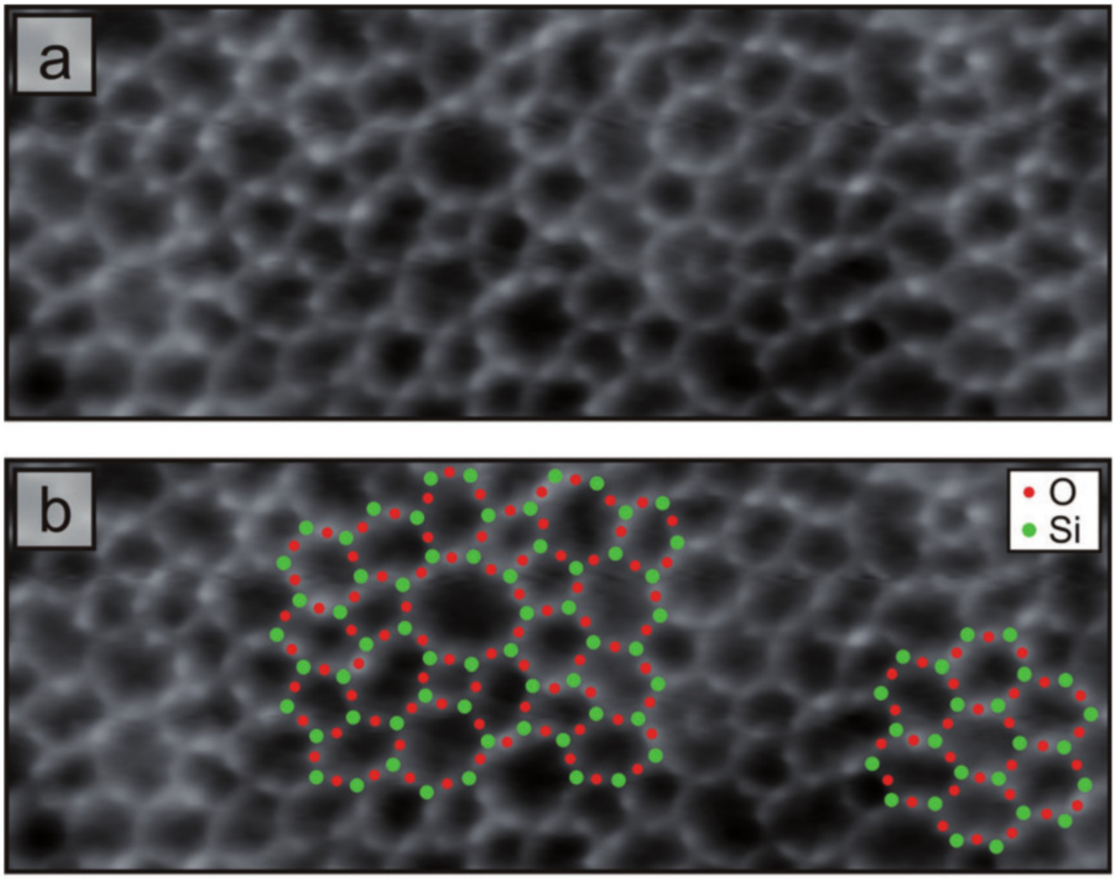

Figure 3.16: STM image of a thin layer of glassy $\mathrm{SiO_2}$ adsorbed on a Ru surface. In (b) O atoms are marked (in red) and the position of Si atoms is calculated to be in the centre of O triangles

3.2.2.3 Glasses with no chemical order

As we have seen, a binary CRN can also be formed with two elements not including O.

The reference compounds for this class are **chalcogenides**, which are formed by

- one element of group 16 (S,Se,Te) heavier than O ("chalcogens")
- and one element of groups 14 and 15 (Si,Ge; P,As)

In chalcogenides there needs to be no chemical order: **homopolar bonds** (between same-species atoms) are allowed. This opens the possibility for **non-stoichiometric compounds** such as $\mathrm{Si_xSe_{1-x}}$ (figure 3.17):

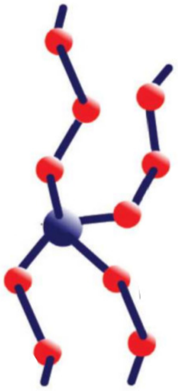

Figure 3.17: a fragment of network with homopolar bonds

In these substances Zachariasen's rules, which are based on the exclusive presence of $\mathrm{AB_m}$ units linked by their vertices, do not hold. Indeed, the $\mathrm{AB_m}$ groups, while not being the only groups that are present in the network, are also found to form edge-sharing dimers (figure 3.18)

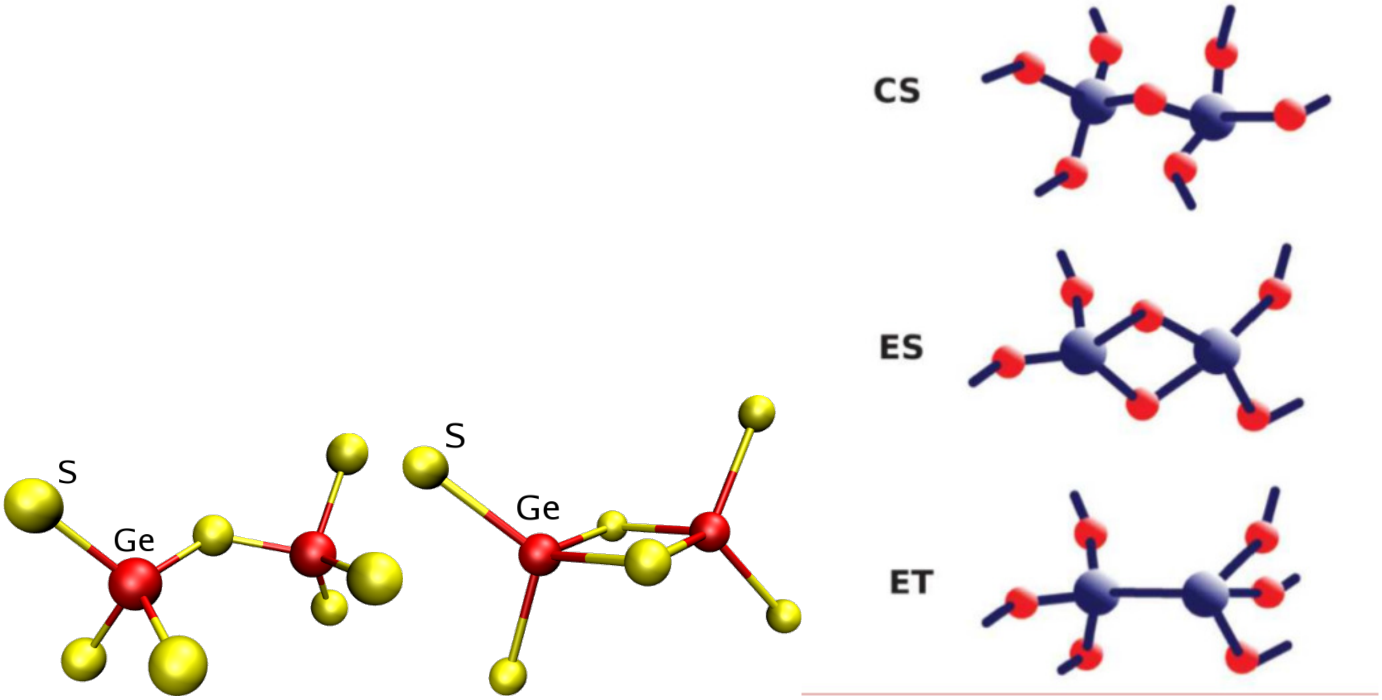

Figure 3.18: dimer structures found in chalcogenide glasses (CS, corner sharing; ES, edge sharing; ET, ethane-like)

3.2.3 Coordination number and rigidity (Phillips-Thorpe theory)

In the CRN model, the **rigidity** of a glass is connected to the degree of **connectivity** between atoms. The more bonds an atom forms, and the more rigid these bond are, the more rigid the lattice will be.

Rigidity properties depend on the **difference between the number of constraints and the number of degrees of freedom** of atoms.

We have seen above that in a monoatomic CRN like $a - \mathrm{Si}$, with a high coordination number (CN=4), not all constraints on bond lengths and angles can be satisfied, and the lattice can be built only if the constraints are relaxed, even partially.

If atoms with lower coordination (for example, O or S, with CN=2) are introduced, a less constrained CRN results. In these binary systems, **the higher the fraction of low CN atoms, the lower the rigidity** is.

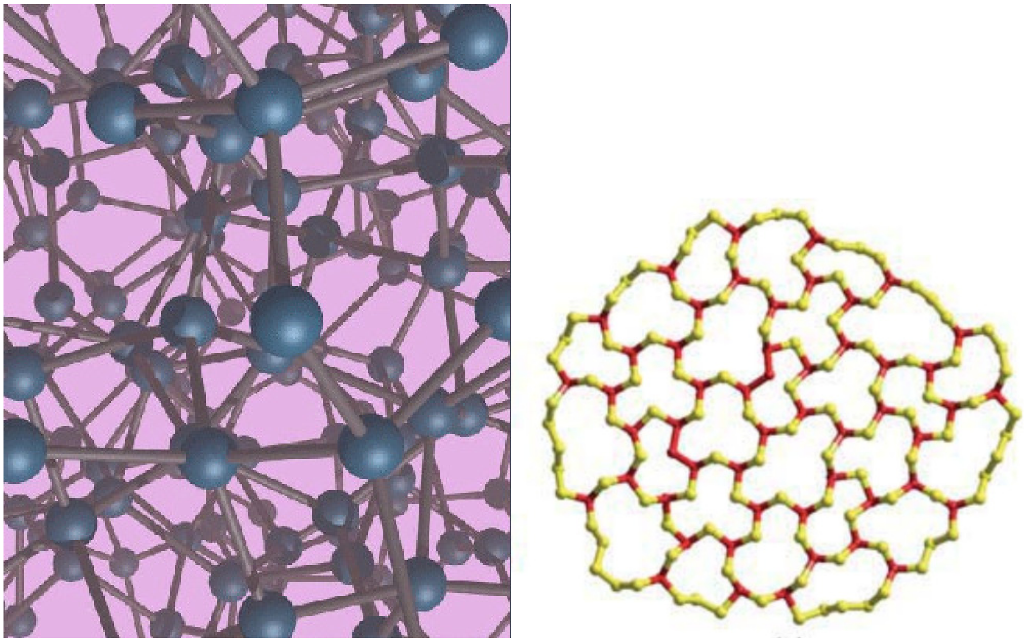

Figure 3.19: A high coordination, rigid network (left) and a low coordination, less rigid one (right)

Phillips and Thorpe (Thorpe 1983) have developed a simple theory about the rigidity of a CRN as a function of the average coordination.

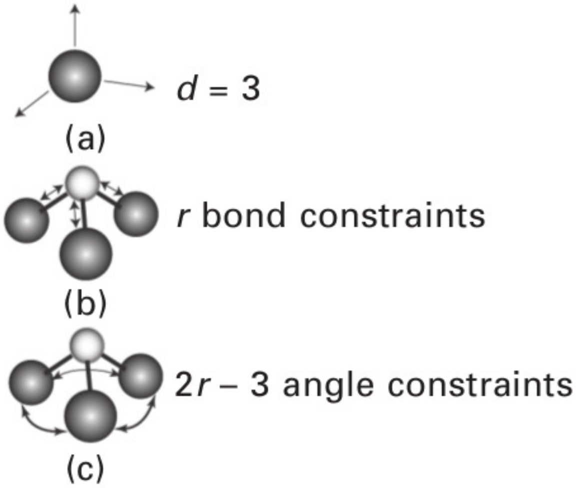

Figure 3.20: degrees of freedom (d) and constraints in a CRN with coordination r

In a CRN of atoms with coordination number r, for each atom we define (figure 3.20)

$$n_{bond} = \frac{r}{2}$$

bond distances (since each bond is shared by two atoms), and

$$n_{angle} = 2r - 3$$

bond angles (the computation of n_{angle} takes into account the fact that angles are not all independent). If distances and angles are fixed, the total number n of constraints is therefore[5]

$$n = \frac{r}{2} + 2r - 3$$

In a mixed lattice like $\mathrm{As_2S_3}$ an **average coordination number** may be defined as

$$\langle r \rangle = \sum_{species\ i} r_i x_i$$

where r_i is the CN of della species i, and x_i is its molar fraction. For example,

$$\begin{aligned} \mathrm{As_2S_3} \quad &: \quad \langle r \rangle = \frac{2 \cdot 3 + 3 \cdot 2}{2 + 3} = 2.40 \\ \mathrm{SiO_2} \quad &: \quad \langle r \rangle = \frac{1 \cdot 4 + 2 \cdot 2}{1 + 2} = 2.67 \end{aligned}$$

So the number of constraints per atom in a mixed lattice is

$$n = \frac{\langle r \rangle}{2} + 2 \langle r \rangle - 3 \tag{3.1}$$

To estimate the system's rigidity, one compares n to the number d of degrees of freedom per atom; in tri-dimensional space it is obviously$d = 3$ (the 3 cartesian coordinates)

- If $\boxed{n < d}$ → less constraints than degrees of freedom; the system is underdetermined or *floppy*
- If $\boxed{n > d}$ → more constraints than degrees of freedom; the system is overdetermined or *stressed rigid*
- If $\boxed{n = d}$ → the constraints equal all degrees of freedom; the system is optimally constrained and *isostatic*
    - for example, density has a maximum for $n = d$; more constraints would prevent the system from reaching the minimum energy configuration (Lucas (2014))

In tridimensional space the value of $\langle r \rangle$ for which the critical value $n = d$ is reached is given by substituting $n = d = 3$ in equation (3.1)

$$\begin{aligned} 3 &= \frac{\langle r \rangle}{2} + 2 \langle r \rangle - 3 \\ \langle r \rangle &= 2.40 \end{aligned} \tag{3.2}$$

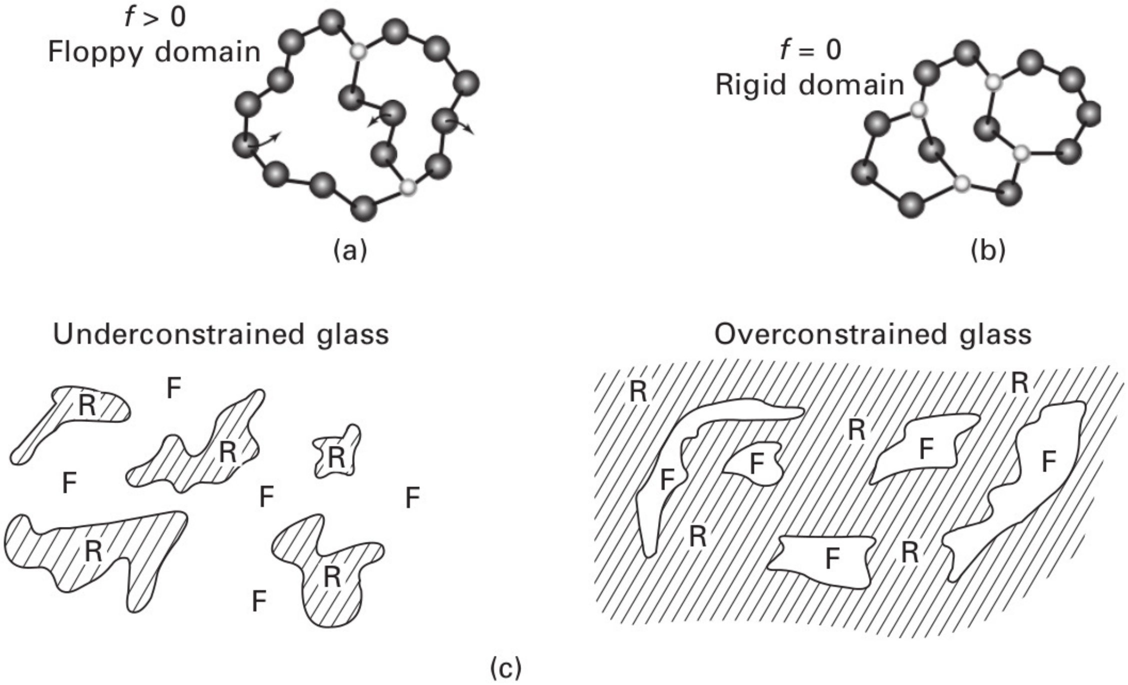

Figure 3.21: Rigidity percolation (from Lucas 2014). f is the fraction of free modes ($f \sim (d-n)$ or $f=0$ if $(d-n)<0$)

Now, in non-stoichiometric systems $\langle r\rangle$ depends on the relative concentration of the species with different CN. By increasing the fraction of the species with higher CN, $\langle r\rangle$ is increased: starting from an underdetermined system composed of a floppy (F) matrix with isolated rigid (R) domains, when these domains eventually interconnect the system transitions to a rigid matrix with isolated floppy regions; this transition, which occurs in a narrow interval of composition, is called **rigidity percolation** (figure 3.21)

The rigidity of the disordered network is found to be also connected to the *difficulty* in forming a glass. For example, in the system $\mathrm{Ge_xSe_{1-x}}$ one has

$$\begin{aligned}\langle r\rangle &= 4x+2(1-x)\\ &= 2x+2\end{aligned}$$

so the critical value $\langle r\rangle = 2.40$ (equation (3.2)) is reached for $x = 0.20.$ Indeed, this composition corresponds to minimum *difficulty* in forming the glass, as measured by the cooling rate required for glass formation.

The main merit of Phillips-Thorpe theory is in linking the mechanical properties of a series of glasses to a single parameter, the average coordination number $\langle r\rangle$.

This is clearly illustrated in the data for $\mathrm{Ge-As-Se}$ mixtures with varying composition(Halfpap and Lindsay 1986). Two series were prepared with variable $\langle r\rangle$, one at high- and one at low-As content (squares and circles in the ternary phase diagram). In spite of the large difference in the composition (and

---

[5] it is assumed that rings are formed by 6 or more atoms, otherwise there are additional dependencies between distances and angles (see Thorpe (1983),Lucas (2014))

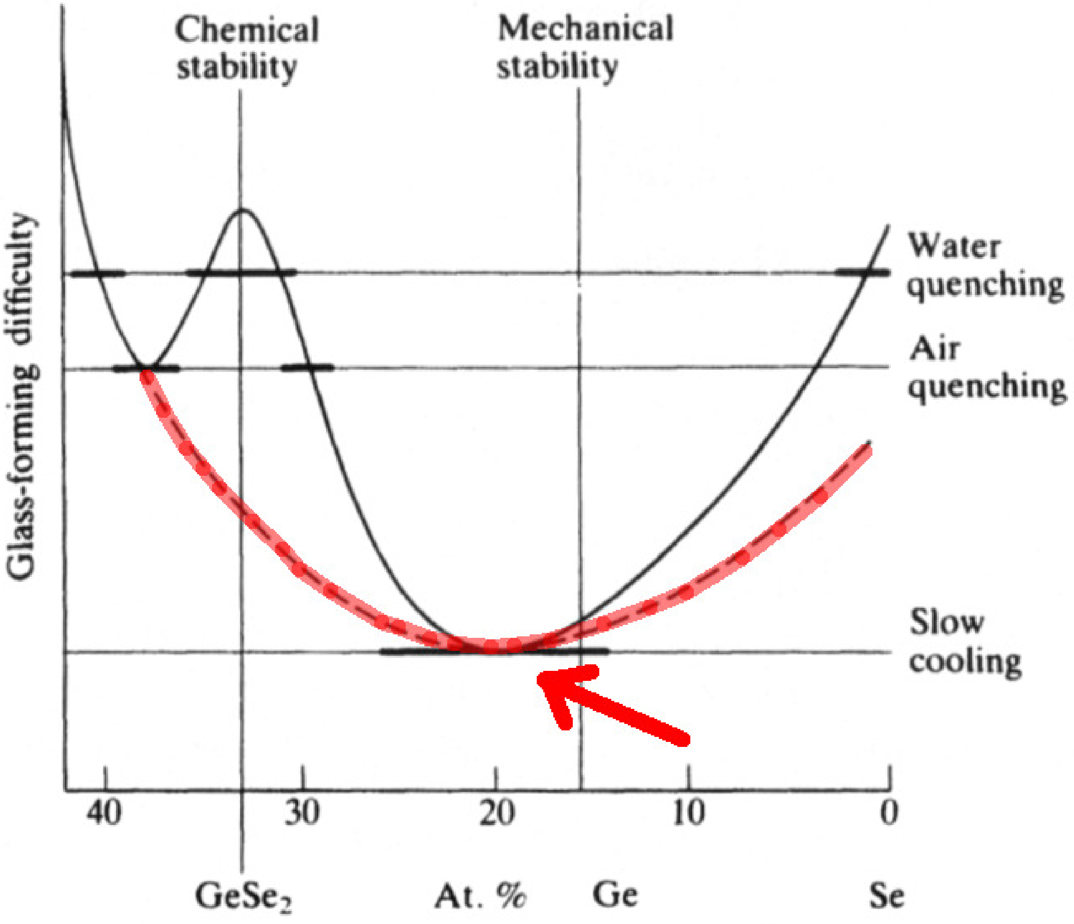

Figure 3-3. Glass-forming difficulty versus composition in the Ge–Se system. Solid horizontal bars are experimental data for the three cooling rates employed (rapid using water, medium using air, and slow cooling). Solid curve is drawn to guide the eye. Dashed curve is the prediction from Phillips' constraint theory. (After J. C. Phillips, *J. Non-cryst. Sol.* **34**, 153 (1979). Reproduced with permission of Elsevier Science Publishers.)

Figure 3.22: Glass forming difficulty as a function of composition in Ge_xSe_{1-x} (from Varshneya 1994 - including caption)

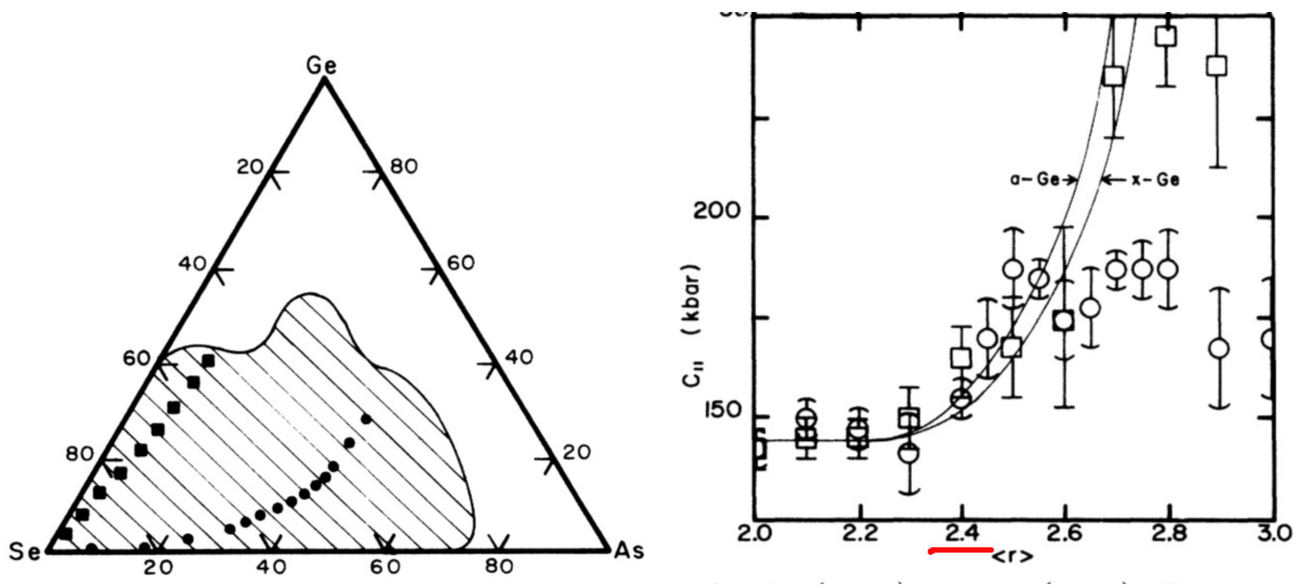

Figure 3.23: Composition (left) and elastic constant C_{11} as a function of average coordination number $\langle r \rangle$ (right) in two series of $\mathrm{Ge-As-Se}$ mixtures

so in the microscopic structure) between the two series, it is found that the elastic constant C_{11} begins to rise around $\langle r \rangle \sim 2.40$ **for both series** (figure 3.23).

Obviously the original approach of Phillips and Thorpe, that we have presented here, suffers from oversimplification. Points that have been addressed by later research include: accounting for rings with < 6 elements and for systems with dangling bonds or atoms with varying r (such as silicon $Q^{(n)}$ species in alkali silicate glasses).

3.2.4 Bond models

Another topological approach to the structure of network glasses investigates the role of the nature and number of bonds formed by an atom. We will delineate the approach here while leaving a more detailed discussion to specific sections below.

One issue regards the relative amount of heteropolar (AB) and homopolar (AA, BB) bonds in a binary non-stoichiometric compound $\mathrm{A_xB_{1-x}}$. Can this relative amount be predicted from composition only?

Chalcogenide glasses ($\mathrm{As-Se}$, $\mathrm{Ge-Se}$), figure 3.24, are an example of such systems.

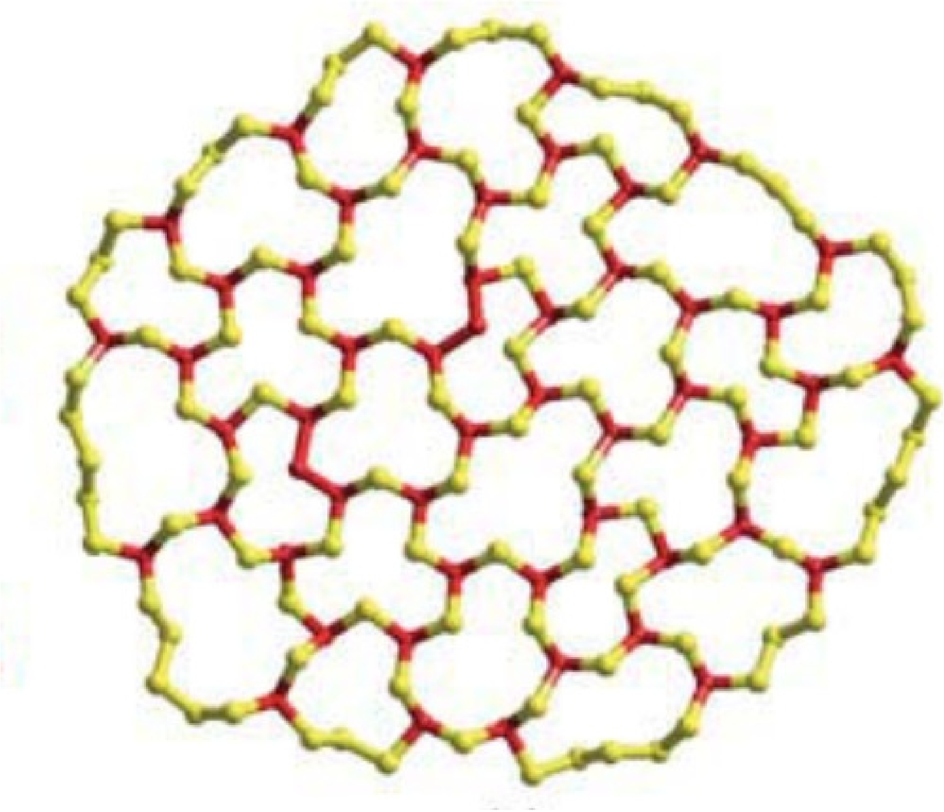

Figure 3.24: A possible configuration of As (red)-S (yellow) system

Chalcogenides can be studied with a topological model where

- each atom species forms a fixed number of bonds
- no dangling bonds are present

This topological model is then integrated with considerations about bond energies and their influence on bond type distributions. The subject is treated in a later section.

A second field of investigation is systems where the same unit can have different number of bonds, with the total number of bonds being constrained by the system's overall composition.

In mixed oxides containing a "network former" (Si or B) and a "network modifier" (alkali metal) such as

$$(\mathrm{M_2O})_\mathrm{x} \cdot (\mathrm{SiO_2})_{1-\mathrm{x}}$$

anionic groups are formed with **Non-Bridging Oxygen, NBO**). Formally, they can be thought as derived from a pure $\mathrm{SiO_2}$ network upon addition of the alkali oxide:

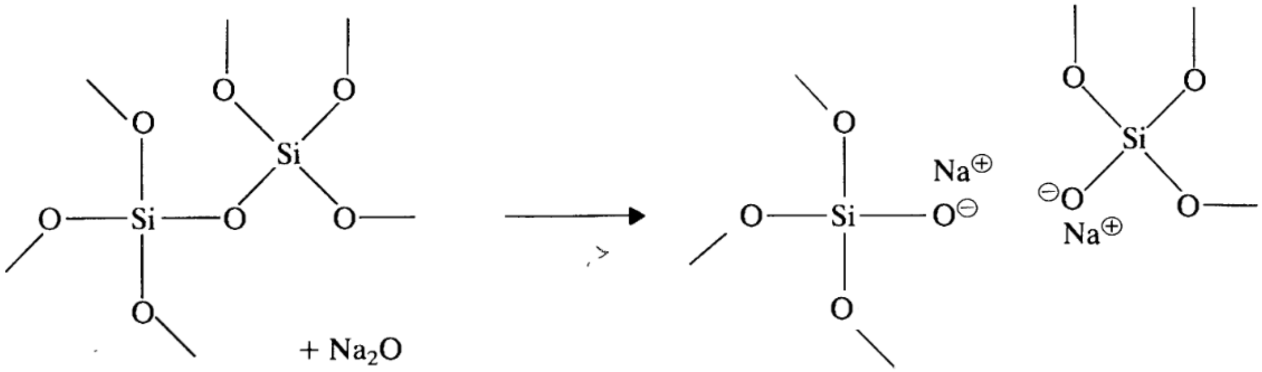

At high $\mathrm{M_2O}$ concentrations several groups can be formed with different number of NBO:

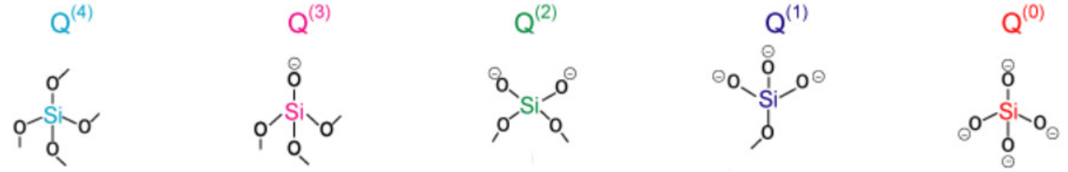

Clearly, there is no *a priori* way of knowing if (say) one $\mathrm{M_2O}$ unit produces two $Q^{(3)}$ units, as in the reaction above, or one $Q^{(2)}$unit.

A similar scenario is encountered in alkali-borate glasses

$$(\mathrm{M_2O})_\mathrm{x} \cdot (\mathrm{B_2O_3})_{1-\mathrm{x}}$$

where different boron units exist:

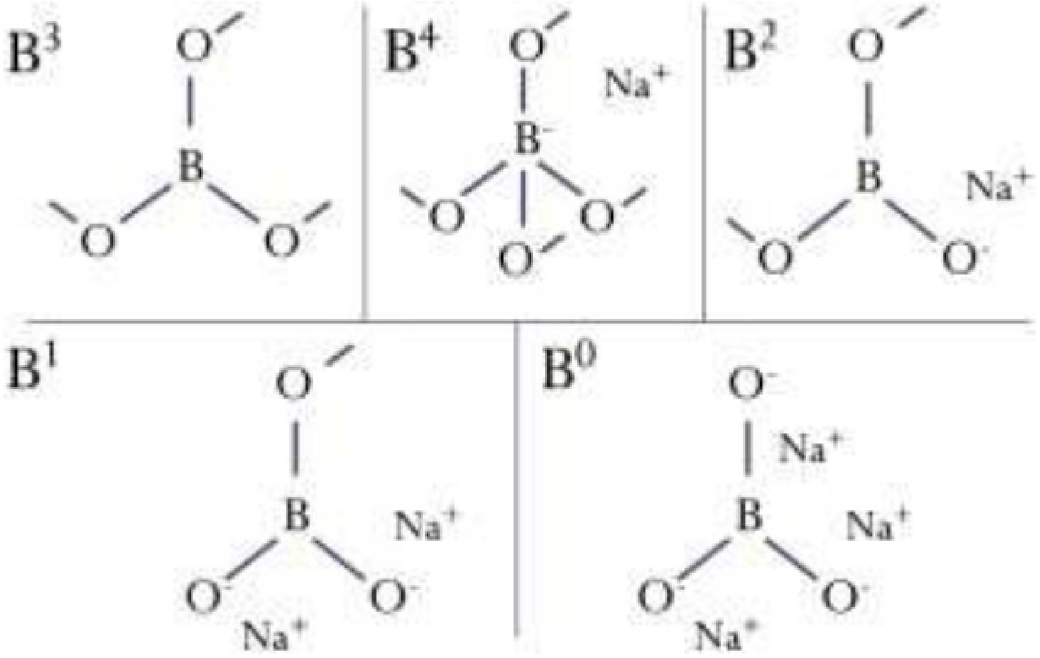

Note that in this case, in contrast to the previous one, besides all the tri-coordinate boron groups with all the possible number of NBO, B^2, B^1 e B^0, at low M^+ concentration also the tetracoordinate group B^4 carrying a negative charge is found.

In systems like alkali silicate or alkali borate glasses the relative abundance of the various groups (or species) is determined

- by quantitative relations originating from the fixed molar fractions of atoms (composition constraints)

  In general, these constraints are not sufficient to determine the abundance of the various species. For example in $(\mathrm{M_2O})_\mathrm{x} \cdot (\mathrm{SiO_2})_{1-\mathrm{x}}$ we have the following system of equations

  $$\begin{aligned} \sum_i Q_i &= 1 - x \\ (4Q_0 + 3.5Q_1 + 3Q_2 + 2.5Q_3 + 2Q_4) &= 2 - x \end{aligned}$$

  that is, for each composition x, **2 equations with 5 unknowns** ($Q_0, \dots, Q_4$).

- from simplified models based on some additional hypotheses and/or parameters

- from thermodynamical data such as equilibrium constants

As anticipated, these bond models will be treated in more detail when discussing specific applications below.

3.3 Random Close Packing (RCP)

In systems where atom pair attractive forces are long-range and non-directional (like metallic, Coulombic or van der Waals interactions) we expect the structure to be driven only by the tendency toward minimization of atom-atom *distances* (and thus, of total energy), with no role being played by the *direction* of atom-atom links. Obviously, distances cannot go to zero: there is some minimum value, the sum of neighbour atoms' radii, below which they cannot be reduced.

In fact, most elemental metals in the solid state assume **dense packing** crystalline structures, like **Hexagonal Close Packing (HCP)** or **Face Centered Cubic (FCC)**, suggesting that their potential energy is lowest in these arrangements. Note that some metals, and especially alloys, can form also **amorphous** solids.

The simplest way to model isotropic force systems is thinking of them as a collection of hard spheres that are compressed to maximum density.

Historically, researchers have started with physical models. It is an experimentally reproducible result that if a container (preferably one with irregular shape and rough inner surfaces) is filled with hard spheres of equal dimensions, and shaken until the volume occupied by the spheres cannot be further reduced, then the density reaches a well defined limiting value: if expressed as the fraction of the total volume occupied by the spheres this value is

$$\phi_{RCP} = \frac{V_{spheres}}{V_{total}} \simeq 0.637 \tag{3.3}$$

Note that the spheres, although packed to the maximum, do not assume a regular arrangement. This type of packing is therefore called **Random Close Packing (RCP)**. Other names are Dense Random Packing (DRP), or, more specifically, Dense Random Packing of Hard Spheres (DRPHS).

Other procedures aimed at reducing the total space occupied by the spheres, such as putting hard balls in a rubber balloon which is then kneaded, or settling them in oil, also give the limit value of equation (3.3). The same result is obtained by simulating the system in a computer.

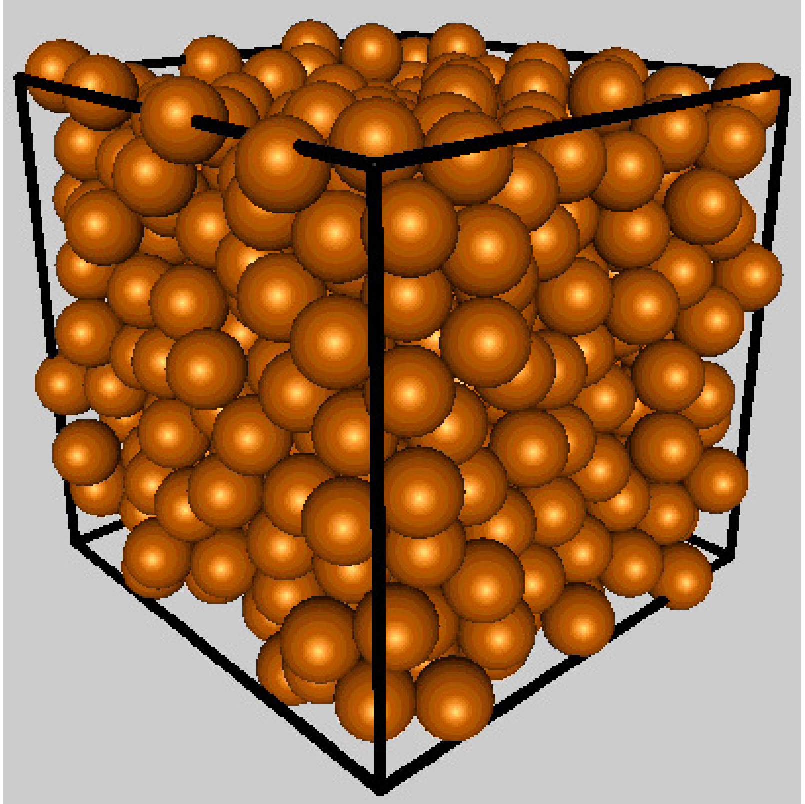

Figure 3.25: Random Close Packing of equal hard spheres

This reproducibility suggests that such systems have a rather well-defined structure. Indeed, structural elements of RCP, such as coordination numbers, have a characteristic distribution; figure 3.26 shows the $g(r)$ of a steel ball model and of a computer simulated system.

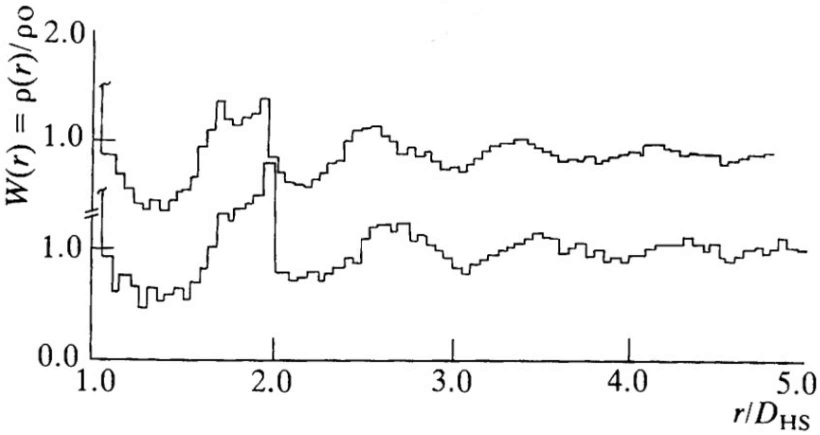

Fig. 7.8 Distribution functions for dense random packed models plotted versus hard-sphere diameter D_{HS}:
(a) DRP of single-sized balls (Finney 1970);
(b) computer generated single-sized sphere DRP (Bennett 1972).

Figure 3.26: Pair distribution function $g(r)$ of RCP in a physical model and in a computer simulation

There has long been a general consensus about the view that RCP “provides the most satisfactory model for the structure of amorphous metals” (Zallen 1998) and, to some extent, also of “metallic glasses” (which in fact may contain also nonmetals, like $\mathrm{Ni}_{76}\mathrm{P}_{24}$; see table in figure 3.27).

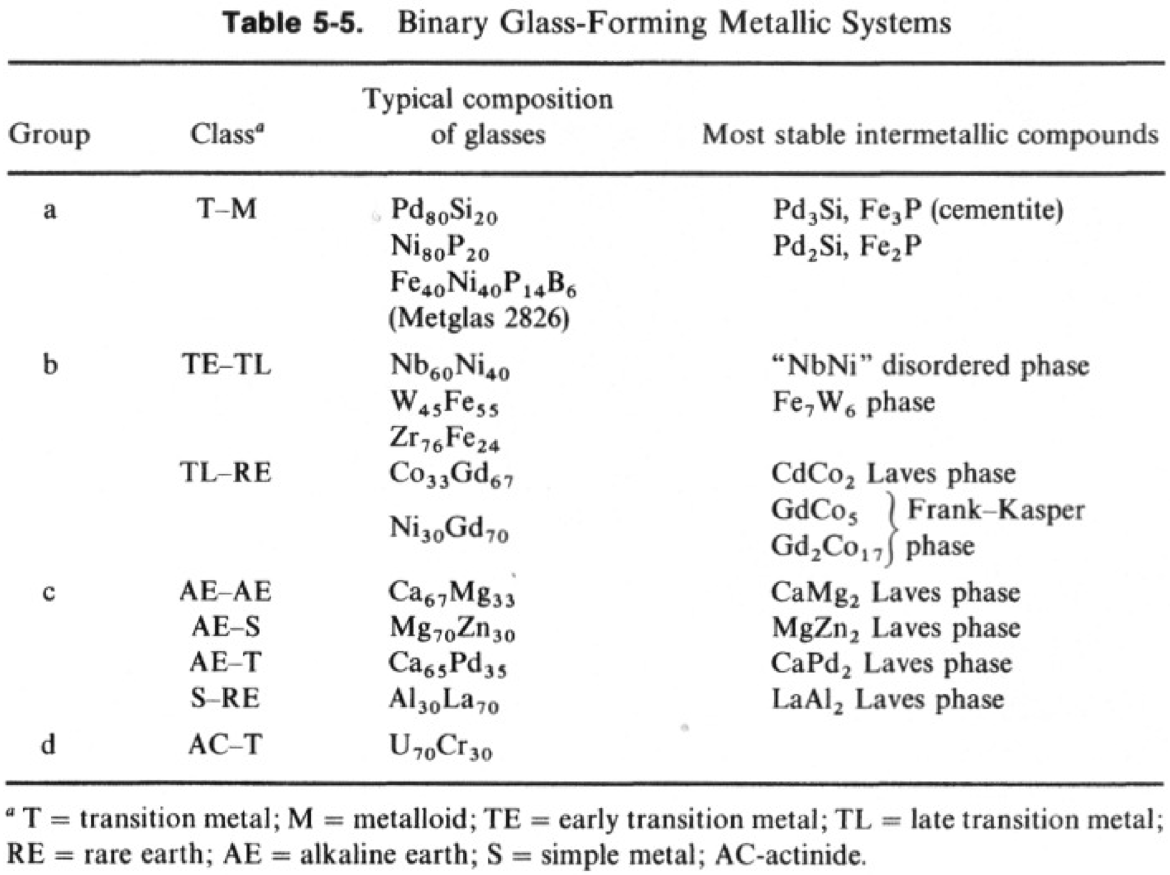

Table 5-5. Binary Glass-Forming Metallic Systems

Group	Class[a]	Typical composition of glasses	Most stable intermetallic compounds
a	T–M	$Pd_{80}Si_{20}$ $Ni_{80}P_{20}$ $Fe_{40}Ni_{40}P_{14}B_6$ (Metglas 2826)	Pd_3Si, Fe_3P (cementite) Pd_2Si, Fe_2P
b	TE–TL	$Nb_{60}Ni_{40}$ $W_{45}Fe_{55}$ $Zr_{76}Fe_{24}$	“NbNi” disordered phase Fe_7W_6 phase
	TL–RE	$Co_{33}Gd_{67}$	$CdCo_2$ Laves phase
		$Ni_{30}Gd_{70}$	$GdCo_5$ Gd_2Co_{17} Frank–Kasper phase
c	AE–AE	$Ca_{67}Mg_{33}$	$CaMg_2$ Laves phase
	AE–S	$Mg_{70}Zn_{30}$	$MgZn_2$ Laves phase
	AE–T	$Ca_{65}Pd_{35}$	$CaPd_2$ Laves phase
	S–RE	$Al_{30}La_{70}$	$LaAl_2$ Laves phase
d	AC–T	$U_{70}Cr_{30}$	

[a] T = transition metal; M = metalloid; TE = early transition metal; TL = late transition metal; RE = rare earth; AE = alkaline earth; S = simple metal; AC-actinide.

Figure 3.27:

In figure 3.28 the $g(r)$ of RCP is compared to the observed (XRD) $g(r)$ of the metallic glass $\mathrm{Ni}_{76}\mathrm{P}_{24}$. Single-sized balls RCP is only partially appropriate for this system, as the atomic radii of Ni and P are similar, but not equal ($\frac{r(\mathrm{P})}{r(\mathrm{Ni})} = 0.78$[6]).

---

[6] Sheng et al. (2006)

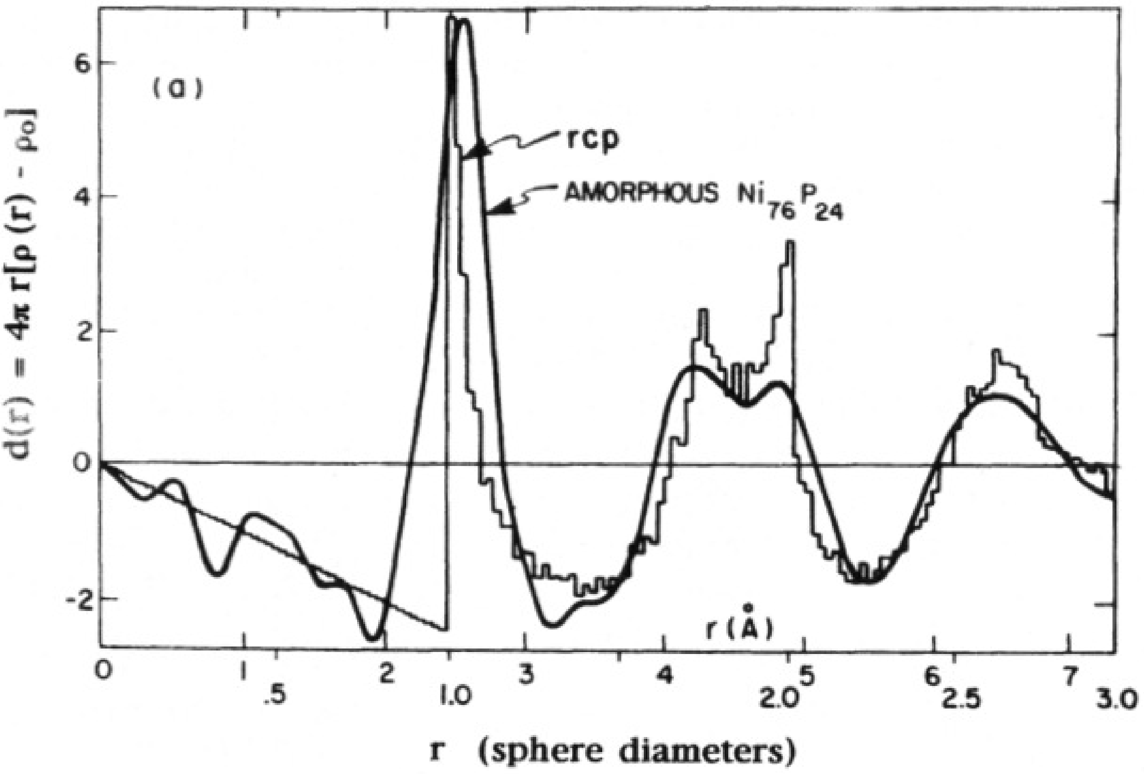

Figure 3.28: Comparison of atom-atom contacts distribution of RCP and of $\mathrm{Ni}_{76}\mathrm{P}_{24}$ (from Varshneya 1994); the quantity plotted on the y axis is the "reduced RDF" $4\pi r\left[\rho\left(r\right)-\rho_0\right]=4\pi r\rho_0\left[g\left(r\right)-1\right]$

The definition of RCP that we have given above is, clearly, totally *empiric*. In a more formal way, RCP can be expressed as "the densest, non-regular arrangement of spheres, such that no empty space remains where another sphere could fit". However, RCP is still not well-defined *mathematically*. One reason for this is that one can always make a *closer*-packed structure that is less *random* (Torquato et al. 2000) - since, as we will see shortly, there are some regular structures that have a higher packing fraction ϕ than RCP. In any case, there are a number of theoretical frameworks about the subject of the so-called "jammed matter" where RCP appears as a special case. In one of these theories (Song et al. 2008) a value is found for the packing fraction of RCP that is very close to the empirically determined value (equation (3.3)):

$$\phi_{RCP}=\frac{6}{6+2\sqrt{3}}=0.63397$$

3.3.1 Comparison of RCP to crystal close-packed structures

It should be stressed that *RCP is not the most efficient packing of spheres in space*.

The problem of finding the densest packing of spheres has been addressed in the past, motivated by practical purposes, such as how to efficiently store cannonballs in a ship. Back in 1611, Kepler hypothesized that the densest packing was a regular one, namely that of the regular close-packed structures with hexagonal symmetry, HCP and FCC, which is

$$\phi_{HCP}=\frac{\pi}{\sqrt{18}}=0.74048$$

	packing fraction $\phi = \frac{V_{spheres}}{V_{total}}$
FCC/HCP	0.740
RCP	$\simeq 0.64$

Table 3.1: Packing fraction of crystal close-packed structures and RCP

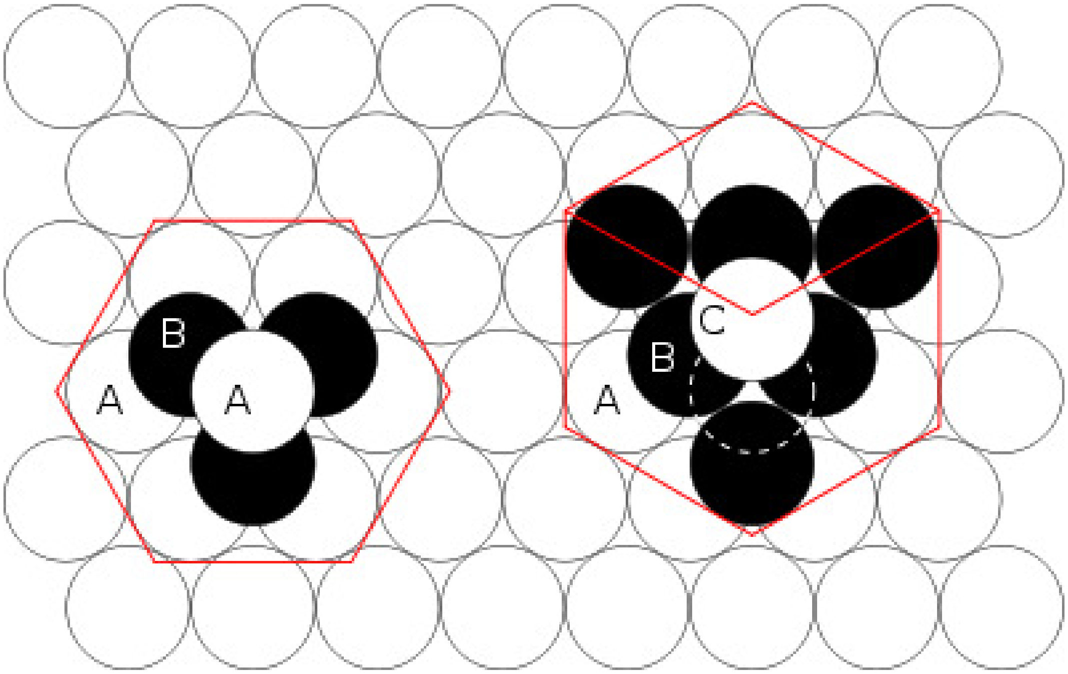

Figure 3.29: Crystal close packed structures: left, Hexagonal Close Packing (HCP); right, Face Centered Cubic (FCC)

It was later proved that HCP/FCC are the densest *regular* packings, while the mathematical proof of Kepler's conjecture, that this is the highest *absolute* packing, either regular or irregular, was first found only in 1998 (Hales 2005).

As is well known, HCP and FCC can be generated by superimposing layers of hexagonally arranged spheres with the spheres of the next layer occupying positions above the center of the triangles formed by the spheres of the previous one; the third layer is placed in the same position as the first one, with an $ABABAB...$ sequence, in HCP, or in a third possible position with an $ABCABC...$ sequence, in FCC (see figure 3.29). Although this is not usually noted, any non-periodic alternation of planes A, B, C (such as $ABCBABACB...$), called "Barlow packing", gives a quasi-lattice with the same packing fraction.

Packing fractions of regular and random close packing are summarized in Table 3.1.

3.3.2 Icosahedral geometry and local versus long-range packing

What, then, makes disordered metal structures possible, if packing is more efficient in ordered ones?

There are a number of possible explanations for this, including the role of differently sized atoms and the fact that the atom-atom potential is not well reproduced by a hard sphere approximation.

However, the main reason is of geometrical nature, and lies in what can been seen as a competition between *local* and *long-range* packing.

To understand this, let us first consider dense packing of hard disks in 2D. One way to find the arrangement of maximum density is to start with one disk, then add one disk at a time in the closest position to the other disks. Obviously, the closest that two disks can go is to be in contact; the third disk can be in contact to both the first two, with centers forming an equilateral triangle. We can now place a new disk in contact with two existing ones, forming a triangle that shares one side with the first triangle. If this procedure is iterated, a hexagonal arrangement is built, that *fills up* the whole plane. We can describe this by saying that the densest-packing elementary figure in the plane, the equilateral triangle, can tile the plane exactly, without leaving empty areas.

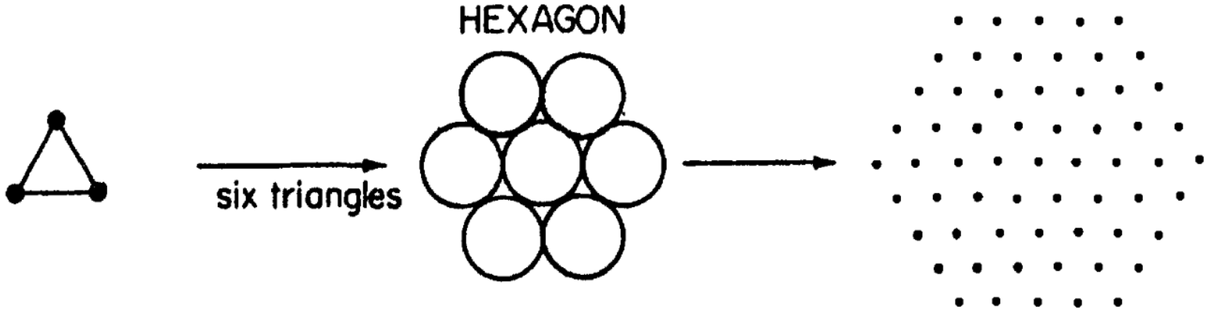

Figure 3.30:

Now let us turn to 3D. Analogous to 2D, three spheres are best packed in a triangular arrangement. The fourth sphere can be laid just over the center of the three, thus forming a regular tetrahedron, where each sphere is in contact with the other three. The **regular tetrahedron** is the densest elementary packing figure in space; however, it **cannot completely fill the space** without leaving empty holes. We see this in figure 3.31: up to five tetrahedra can be stacked sharing one face, leaving a small dihedral of $\delta_5 = 7.4°$ empty. This means that if we follow the same procedure as in 2D, adding one sphere upon the face of an existing tetrahedron, and we iterate, we will end up with empty cavities (and, additionally, with an atom pattern that has no symmetry).

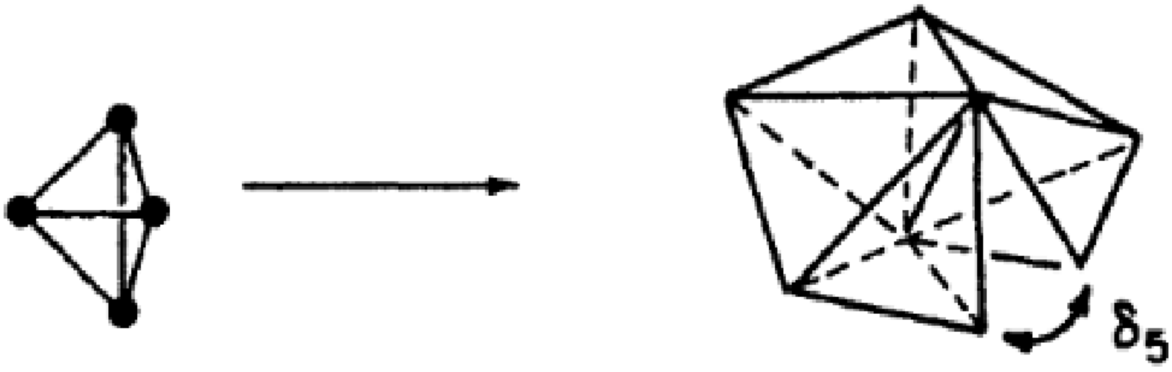

Figure 3.31: Five adjacent regular tetrahedra leave an empty segment

A more efficient filling of space can be accomplished by *distorting tetrahedra slightly*: for example, if the three spheres on one face are moved away from each other by about 5%, still being in contact with the fourth one, such modified tetrahedra can be joined to form a regular *icosahedron* around a center sphere (figure 3.32) where all spheres on the vertices are in contact with the center sphere.

Figure 3.32: Slightly distorted tetrahedra form a regular icosahedron

With the icosahedral geometry a good *local* packing is accomplished: there are **12 spheres** in contact with a central sphere and *almost* in contract with each other.

This however turns out to be only a partial success on a larger scale, because, again, **icosahedra cannot fill space**.

In the HCP structure (see for example O'Keeffe and Hyde 2020) each sphere, like in the icosahedron, is surrounded by **12 atoms** (or spheres) at distance d. Here, tetrahedra are regular, but share edges, not faces; and the coordination polyhedron has also square faces, where only two atoms are in contact (figure 3.33). As a result, the average distance between outer atoms is larger than in the icosahedron. The same holds for FCC.

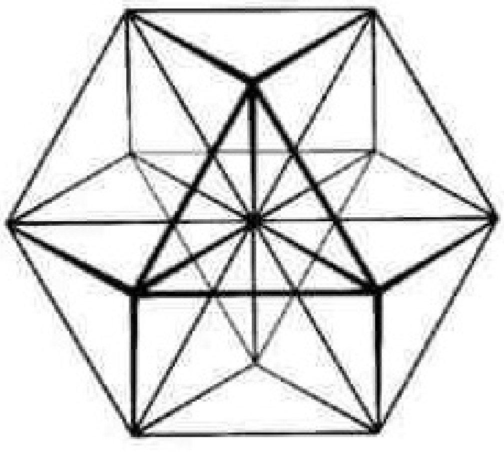

Figure 3.33: HCP structure contains both regular tetrahedra and square pyramids

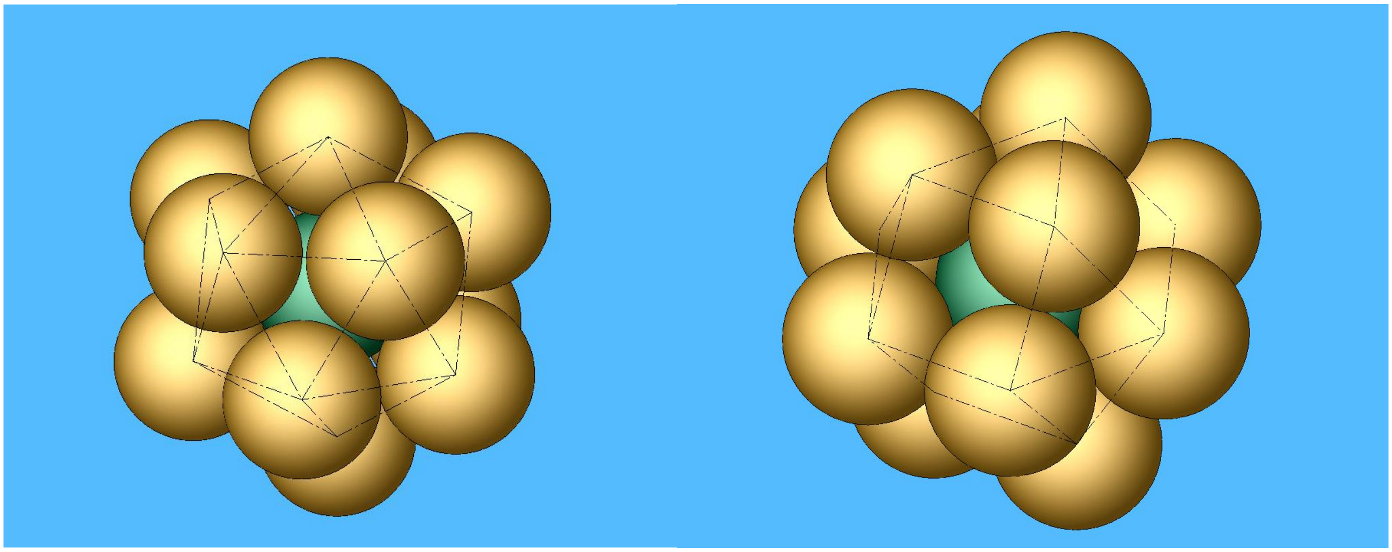

Figure 3.34: Direct comparison of icosahedral (left) and HCP (right) arrangements of 12 atoms around a central atom

The 13-atom cluster in the icosahedron has a higher (local) packing fraction ($\phi_{icos} = 0.766^7$) than HCP, and has a lower energy (De Graef and McHenry 2007). But, unlike the icosahedron, the 13-atom cluster in **HCP can be repeated indefinitely**, because it **can fill up space** [8].

Thus, by sequentially adding up tetrahedra to an icosahedral seed, the resulting structure will increasingly include empty regions, until (at around 5000 atoms, (Cheng and Ma 2011, p 404)) its density becomes lower than that of HCP.

One way to put this is that **FCC/HCP structures,** as compared to icosahedron-based arrangements, **renounce optimal short-range packing in favour of optimal long-range packing**.

The conceptual map of building the densest packing at each range level, with “frustration” steps where the geometrical element cannot be propagated, is illustrated in figure 3.35.

---

[7] Hermann et al. (2007)

[8] together with regular octahedra https://mathworld.wolfram.com/TriangularOrthobicupola.html

402 *Y.Q. Cheng, E. Ma / Progress in Materials Science 56 (2011) 379–473*

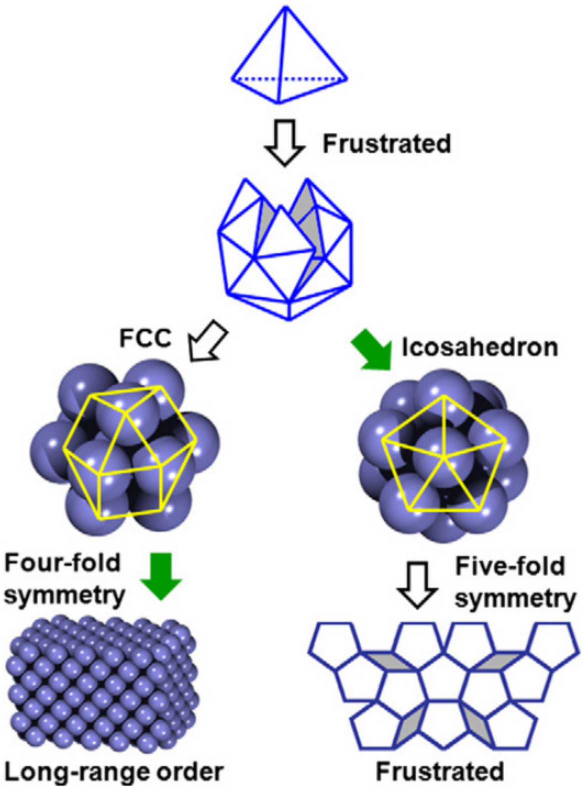

Fig. 16. Frustration map of the polytetrahedral packing of identical hard spheres. Green solid arrow points to the optimal choice at each stage.

Figure 3.35:

Icosahedral-type (nonregular) clusters are found in RCP, in monoatomic liquids or in metallic glasses of similar-sized atoms, although in these contexts clusters with higher CN (e.g. 13 or 14, see below) prevail.

In this perspective, one may say that a glass is formed, in place of a crystal, when an isotropic liquid is cooled so fast that there is not enough time (probability) for the locally disfavoured FCC/HCP structures to form and grow in competition with the locally favoured clusters.

3.3.3 More on comparing RCP to crystal close-packed structures

A more detailed comparison of close-packed structures, disordered (RCP) and regular (HCP/FCC), can be made by looking at either their lattice polyhedra or Voronoi polyhedra.

3.3.3.1 lattice polyhedra

In crystal close-packed structures, we can consider those lattice polyhedra[9] whose vertices are atoms in close contact and such that they can host one smaller sphere; these are often called "holes" or "cavities". There are two types of holes in a crystal of N atoms:

---

[9] we do *not* refer here to *Delauney* lattice, which is formed only by tetrahedra

- regular tetrahedra ($2N = \frac{2}{3}$)
- regular octahedra ($N = \frac{1}{3}$)

These two types of polyhedra make up a *complete tiling of space*. Note that euclidean space cannot be completely tiled with either tetrahedra alone, or octahedra alone.

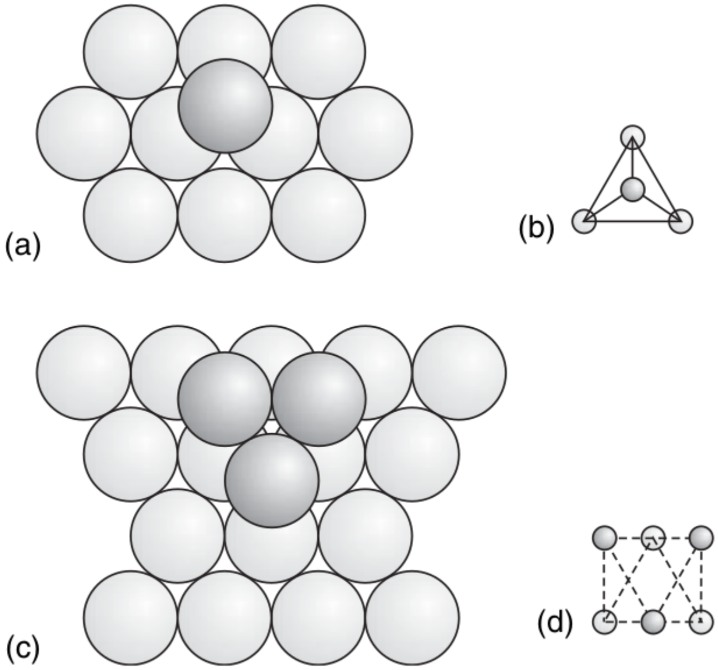

Figure 7.12 Tetrahedral and octahedral sites in closest-packed arrays of spheres: (a) a tetrahedral site between two layers and (b) the same site drawn as a tetrahedron; (c) an octahedral site between two layers and (d) the same site drawn as an octahedron

Figure 3.36: Tetrahedral and octahedral holes in FCC/HCP

In the RCP, one can similarly define polyhedra or holes, including, besides atoms in "close contact", also atoms in "near-close contact", separated by a distance less than 5% longer than one diameter (compare the geometry of the icosahedron, above). In his seminal work of the 1960s, J. D. Bernal (see for example Bernal 1960; a complete review of his work is in found in Finney 2013) showed that the RCP structure can be completely tiled with only five different, slightly distorted polyhedra whose faces are equilateral triangles.

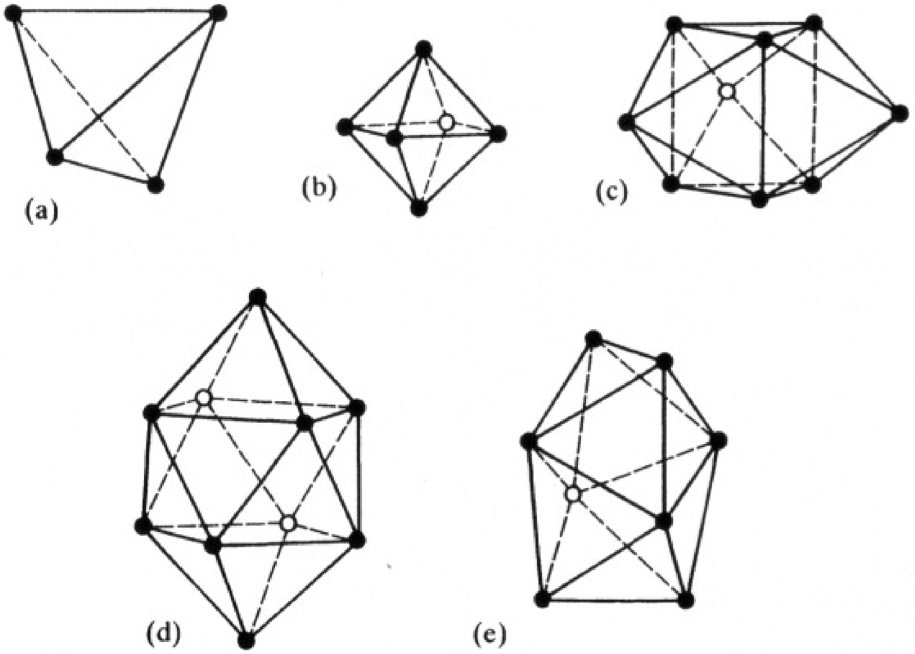

Figure 5-38. The "canonical holes" of Bernal. (a) Tetrahedron. (b) Octahedron. (c) Trigonal prism (shown capped with half-octahedra at each of the three rectangular faces). (d) Archimedean anti-prism (shown capped with half-octahedra on the bottom and the top faces). (e) Tetragonal dodecahedron.

Figure 3.37: Bernal canonical holes

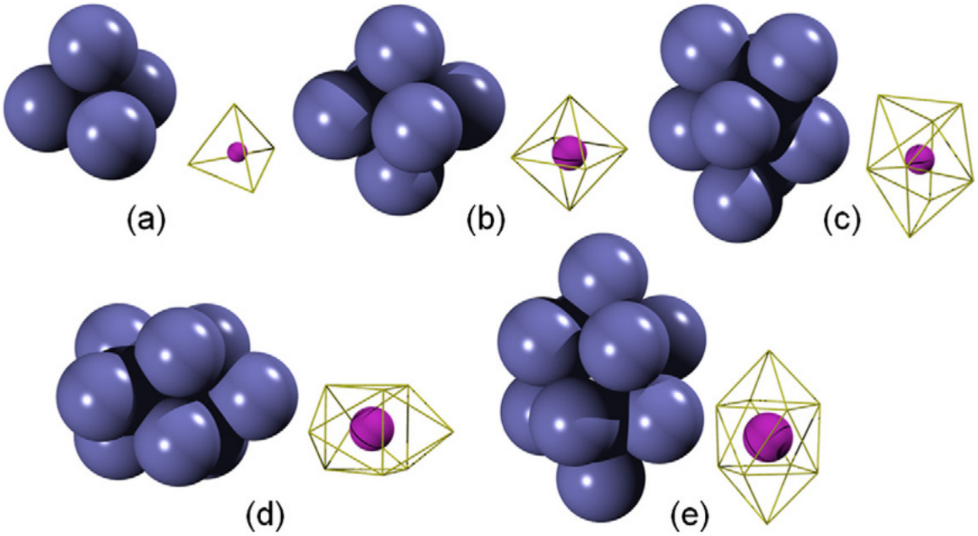

Fig. 15. Bernal's canonical holes: (a) tetrahedron (b) octahedron (c) tetragonal dodecahedron (d) trigonal prism capped with three half octahedra (e) Archimedean antiprism capped with two half octahedra. In each panel, the left figure shows the hard sphere packing surrounding the hole, and the right figure shows the hole in the center (the radius of the pink sphere corresponds to the size of the hole).

Figure 3.38: Another representation of Bernal holes

These “**Bernal canonical holes**” have different occurrences in RCP than their counterparts in FCC/HCP: tetrahedra (a) are $\sim 80\%$; octahedra (b) $\sim 10\%$[10]

3.3.3.2 Voronoi polyhedra

In **crystal close-packed** structures the Voronoi polyhedra are

- HCP: rhombic dodecahedron, (a) in figure 3.39 [11];
- FCC: Trapezo-rhombic dodecahedron (coloured in figure 3.39)

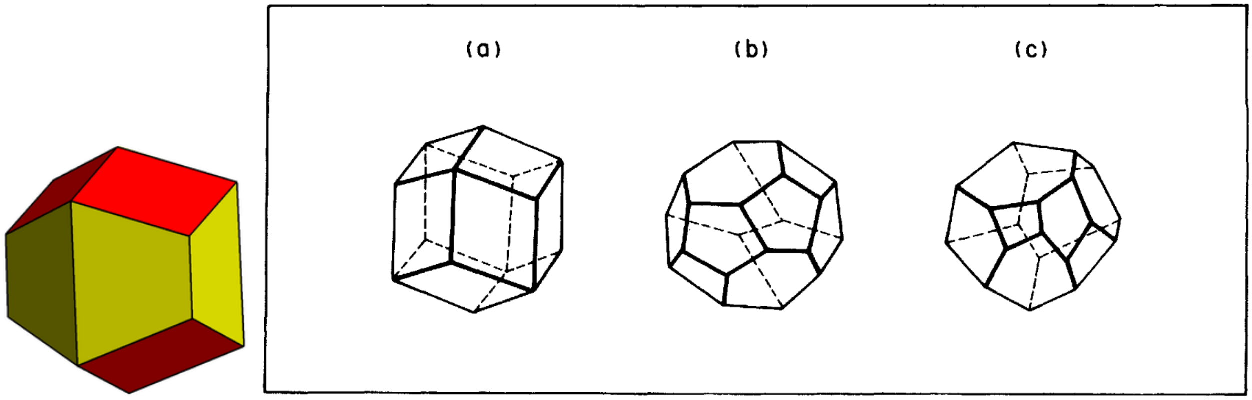

Figure 3.39:

In the **RCP**, on the other hand, there many types of VP, e.g. (b) e (c) in figure 3.39, with number of faces $= 12 \div 17$

The distribution of Voronoi polyhedra in RCP is reported in figure 1.15. For comparison, in FCC/HCP structures

- the number of faces per cell is 12
- the number of edges per face is 4 in FCC, and 4 or 5 in HCP

The following table summarizes properties of crystal and random close-packed structures:

		FCC	HCP	RCP
packing fraction ϕ		0.74048		0.637
lattice polyhedra (holes)	*tetrahedra*	$\frac{2}{3}$		$\sim 80\%$
	octahedra	$\frac{1}{3}$		$\sim 10\%$
	other (Bernal)	0		$\sim 10\%$
Voronoi polyhedra	*faces*	12		$12 \div 17$ (max at 14)
	edges / face	4	4 or 5	$3 \div 8$ (max at 5)

---

[10] Bernal (1964); (Chaudhari and Turnbull (1978) has 84% and 5%)

[11] this is the VP corresponding to the $CN = 12$ arrangement of neighbours of figure 3.34 (right)

3.3.4 close-packed structures of binary systems

As already mentioned, most metal glasses are formed by binary **mixtures** of metals, or metal/metalloid pairs. More precisely, by the term "metallic glass" we mean (Elliott 1984) an amorphous material that (a) contains (although not exclusively) metal elements, and (b) exhibits metallic properties (electrical, magnetic, optical). This definition **excludes,** for example, $a-\mathrm{Sb}$ o $a-\mathrm{As}$, that are semiconductors, not metallic; or $a-\mathrm{Si}:\mathrm{H}$ which has metallic properties but does not contain metal elements.

The structure of binary systems equivalent to RCP is determined by the atomic radii ratio R^*. If $R^* \approx 1$, as in $\mathrm{Ni_{63}Nb_{37}}$ the structure is similar to monoatomic RCP, with a prevalence of CN>12. If R^* is lower, and the smaller atom has a lower molar fraction than the bigger one ("solute" and "solvent", respectively), clusters of solvent atoms around one solute atom tend to assume lower CNs. In a study that makes use of experimental data and calculations, many local packing clusters were found with a distribution that depends on R^*

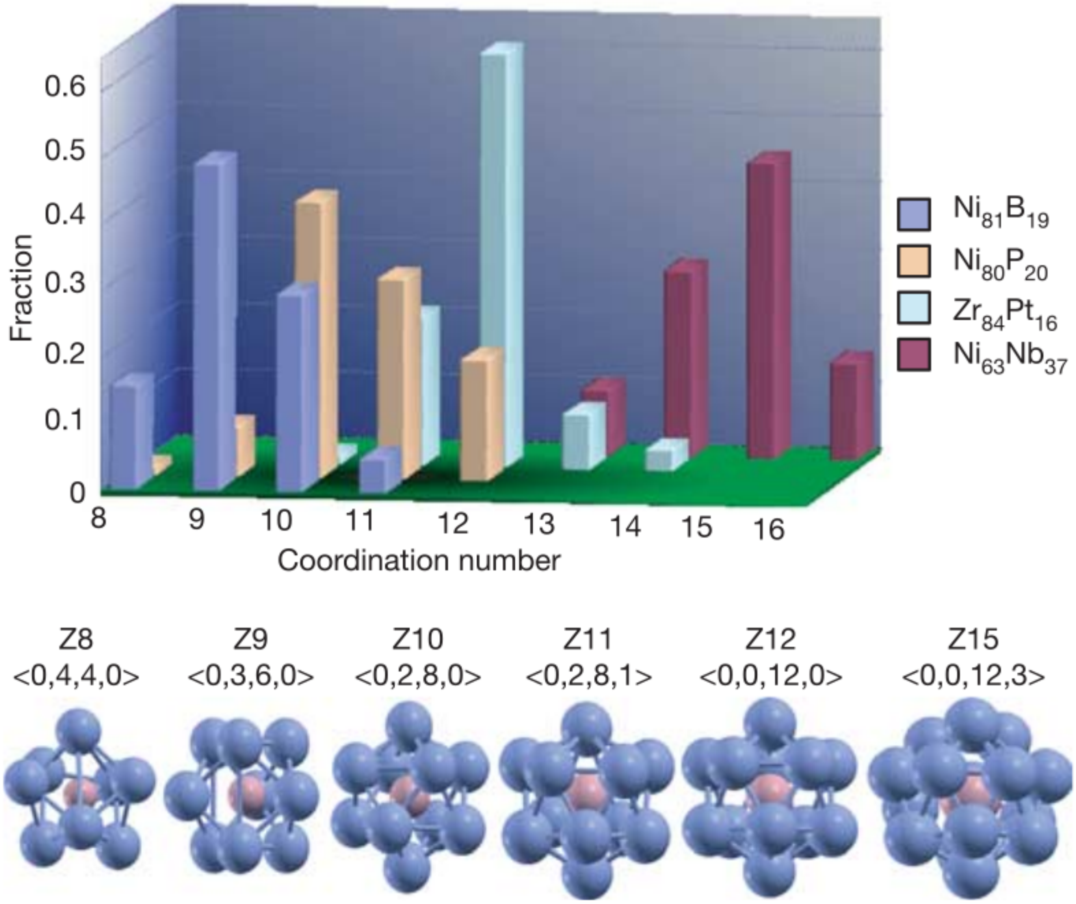

Figure 3 | CN distribution of the solute atoms in several representative MGs, obtained from *ab initio* calculations. The average CN changes with the effective atomic size ratio, and for each glass the majority of the solute atoms (>75% of total) have two dominant CNs. Also shown are the Kasper polyhedra corresponding to the different CNs. The Kasper polyhedra are the dominant coordination polyhedra in the relaxed MGs.

Figure 3.40: (from Sheng et al. (2006))

Chapter 4

Glass structures

4.0.1 Oxide glasses: simple

4.0.2 Oxide glasses: multi-component

4.0.3 Non-oxide glasses with CRN structure

4.0.4 Other non-oxide glasses: metal, ionic

Bibliography

M. P. Allen and D. J. Tildesley. *Computer simulation of liquids*. Oxford University Press, New York, 1987. ISBN 0-19-855645-4.

M. Alonso and E. J. Finn. *Elementi di fisica per l'universita, vol II: campi e onde*. Masson-Addison Wesley, 1982.

JD Bernal. Geometry of the structure of monatomic liquids. *Nature*, 185(4706):68–70, 1960.

John Desmond Bernal. The bakerian lecture, 1962. the structure of liquids. *Proceedings of the Royal Society of London. Series A, Mathematical and Physical Sciences*, 280(1382):299–322, 1964.

Ronald Newbold Bracewell. *The Fourier transform and its applications*, volume 31999. McGraw-Hill New York, 1986.

P Chaudhari and D Turnbull. Structure and properties of metallic glasses. *Science*, 199(4324):11–21, 1978.

Y.Q. Cheng and E. Ma. Atomic-level structure and structure-property relationship in metallic glasses. *Progress in Materials Science*, 56(4):379 – 473, 2011. ISSN 0079-6425. doi: https://doi.org/10.1016/j.pmatsci.2010.12.002. URL `http://www.sciencedirect.com/science/article/pii/S0079642510000691`.

C. J. Cramer. *Essentials of Computational Chemistry: Theories and Models, 2nd ed.* Wiley, 2004. ISBN 0-470-09182-7.

N. E. Cusack. *The Physics of Structurally Disordered Matter: An Introduction.* IOP Publishing Ltd, 1987. ISBN 0-85274-591-5.

Marc De Graef and Michael E McHenry. *Structure of materials: an introduction to crystallography, diffraction and symmetry*. Cambridge University Press, 2007.

S. R. Elliott. *Physics of amorphous materials*. Longman London ; New York, 1984. ISBN 0582446368.

John L. Finney. Bernal's road to random packing and the structure of liquids. *Philosophical Magazine*, 93(31-33):3940–3969, 2013. doi: 10.1080/14786435.2013.770179. URL `http://dx.doi.org/10.1080/14786435.2013.770179`.

D. Frenkel and B. Smit. *Understanding molecular simulation*. Academic Press, London and San Diego, California, 2002. ISBN 0-12-267351-4.

Thomas C Hales. A proof of the kepler conjecture. *Annals of mathematics*, pages 1065–1185, 2005.

B L Halfpap and S M Lindsay. Rigidity percolation in the germanium-arsenic-selenium alloy system. *Physical Review Letters*, 57(7):847, 1986.

Helmut Hermann, Antje Elsner, and Dietrich Stoyan. Behavior of icosahedral clusters in computer simulated hard sphere systems. *Journal of non-crystalline solids*, 353(32-40):3693–3697, 2007.

Pei-Yin Huang, Robert Hovden, Qingyun Mao, D. Muller, S. Kurasch, U. Kaiser, J. Kotakoski, A.V. Krasheninnikov, Anchal Srivastava, Viera SkÃ¡kalovÃ¡, J. Smet, and J.C. Meyer. Quantitative atomic-resolution imaging and spectroscopy of a 2d silica glass. *Microscopy and Microanalysis*, 18:340–341, 07 2012. doi: 10.1017/S1431927612003558.

ISAACS. The radial distribution functions, 2013. URL `http://people.cst.cmich.edu/petko1vg/isaacs/phys/rdfs.html`.

DA Keen. Reverse Monte Carlo refinement of disordered silica phases. In Billinge, SJL and Thorpe, MF, editor, *LOCAL STRUCTURE FROM DIFFRACTION*, FUNDAMENTAL MATERIALS RESEARCH, pages 101–119. PLENUM PRESS DIV PLENUM PUBLISHING CORP, 1998. ISBN 0-306-45827-6.

E. Leonova. *Structural investigation of Complex Glasses by Solid-state NMR*. PhD thesis, Stockholm University, 2009.

Leonid Lichtenstein, Christin Buechner, Bing Yang, Shamil Shaikhutdinov, Markus Heyde, Marek Sierka, Radoslaw Wlodarczyk, Joachim Sauer, and Hans-Joachim Freund. The atomic structure of a metal-supported vitreous thin silica film. *Angewandte Chemie International Edition*, 51(2):404–407, 2012. ISSN 1521-3773. doi: 10.1002/anie.201107097. URL `http://dx.doi.org/10.1002/anie.201107097`.

P. Lucas. Mean coordination and topological constraints in chalcogenide network glasses. In Jean-Luc Adam and Xianghua Zhang, editors, *Chalcogenide Glasses*, pages 58 – 81. Woodhead Publishing, 2014. ISBN 978-0-85709-345-5. doi: http://dx.doi.org/10.1533/9780857093561.1.58. URL `http://www.sciencedirect.com/science/article/pii/B9780857093455500039`.

M. Micoulaut. "Atomistic Modeling of Glass Structure and Glass Properties", 2013. URL `http://www.lptl.jussieu.fr/user/mmi/IMI.html`.

Jcg Montoro and Jlf Abascal. The Voronoi Polyhedra as tools for structure determination in simple disordered-systems. *JOURNAL OF PHYSICAL CHEMISTRY*, 97(16):4211–4215, APR 22 1993. ISSN 0022-3654. doi: {10.1021/j100118a044}.

Christian R. Muller, Vindu Kathriarachchi, Michael Schuch, Philipp Maass, and Valeri G. Petkov. Reverse monte carlo modeling of ion conducting network glasses: An evaluation based on molecular dynamics simulations. *Phys. Chem. Chem. Phys.*, 12:10444–10451, 2010. doi: 10.1039/C003472J. URL `http://dx.doi.org/10.1039/C003472J`.

Michael O'Keeffe and Bruce G Hyde. *Crystal structures*. Courier Dover Publications, 2020.

K. J. Rao. *Structural Chemistry of Glasses*. Elsevier Science and Technology Books, 2002. ISBN 0080439586.

N Ramesh Rao, PSR Krishna, Saibal Basu, BA Dasannacharya, KS Sangunni, and ESR Gopal. Structural correlations in gexse1- x glasses–a neutron diffraction study. *Journal of non-crystalline solids*, 240(1-3):221–231, 1998.

Sarah Rauscher, Chris Neale, and Régis Pomes. Simulated tempering distributed replica sampling, virtual replica exchange, and other generalized-ensemble methods for conformational sampling. *Journal of chemical theory and computation*, 5(10):2640–2662, 2009.

C Patrick Royall and Stephen R Williams. The role of local structure in dynamical arrest. *Physics Reports*, 560:1–75, 2015.

Rachit Sapra, Ram P Verma, Govind P Maurya, Sameer Dhawan, Jisha Babu, and V Haridas. Designer peptide and protein dendrimers: A cross-sectional analysis. *Chemical reviews*, 119(21):11391–11441, 2019.

J. E. Shelby. *Introduction to Glass Science and Technology, 2nd edition*. The Royal Society of Chemistry, 2005. ISBN 0-85404-639-9.

HW Sheng, WK Luo, FM Alamgir, JM Bai, and E Ma. Atomic packing and short-to-medium-range order in metallic glasses. *NATURE*, 439(7075):419–425, JAN 26 2006. ISSN 0028-0836. doi: {10.1038/nature04421}.

Giorgio F. Signorini. "Simulazione di molecole di interesse biologico", 2013. URL `http://www1.chim.unifi.it/u/signo/did/biomol/lezioni.pdf`.

Giorgio F. Signorini, J.L. Barrat, and M.L. Klein. Structural relaxation and dynamical correlations in a molten salt near the liquid-glass transition: a molecular dynamics study. *J. Chem. Phys.*, 92:1294–1303, 1990. URL `http://citeseerx.ist.psu.edu/viewdoc/download?doi=10.1.1.1050.1201&rep=rep1&type=pdf`.

C. Song, P. Wang, and H. A. Makse. A phase diagram for jammed matter. *Nature*, 453:629–632, May 2008. doi: 10.1038/nature06981.

P Steinhardt, R Alben, and D Weaire. Relaxed continuous random network models:(i). structural characteristics. *Journal of Non-Crystalline Solids*, 15(2):199–214, 1974.

M.F. Thorpe. Continuous deformations in random networks. *Journal of Non-Crystalline Solids*, 57(3): 355 – 370, 1983. ISSN 0022-3093. doi: http://dx.doi.org/10.1016/0022-3093(83)90424-6. URL `http://www.sciencedirect.com/science/article/pii/0022309383904246`.

Salvatore Torquato, Thomas M Truskett, and Pablo G Debenedetti. Is random close packing of spheres well defined? *Physical review letters*, 84(10):2064, 2000.

A. K. Varshneya. *Fundamentals of Inorganic Glasses*. Academic Press, 1994. ISBN 0-12-714970-8.

P. Vashishta, R. K. Kalia, J. P. Rino, and I. Ebbsjö. Interaction potential for SiO_2: A molecular-dynamics study of structural correlations. *Phys. Rev. B*, 41:12197–12209, Jun 1990. doi: 10.1103/PhysRevB.41.12197. URL `http://link.aps.org/doi/10.1103/PhysRevB.41.12197`.

Mark Wilson. Model investigations of network-forming materials. *Phys. Chem. Chem. Phys.*, 14:12701–12714, 2012. doi: 10.1039/C2CP41644A. URL `http://dx.doi.org/10.1039/C2CP41644A`.

R. Zallen. *The Physics of Amorphous Solids*. A Wiley-Interscience publication. Wiley, 1998. ISBN 9780471299417. URL `https://books.google.it/books?id=V0jr74rPdUIC`.